The Geochemical Behavior of Metalloids and Their Effect on the Highly Siderophile Elements During the Crystallization of a Magmatic Sulfide Liquid in Relation to the Formation of Ni-Cu-PGE Magmatic Sulfide Deposits

by

Fabio Cafagna

A thesis submitted in partial fulfillment
of the requirements for the degree of
Doctor of Philosophy (Ph.D.) in Mineral Deposits and Precambrian Geology

The Faculty of Graduate Studies
Laurentian University
Sudbury, Ontario, Canada

THESIS DEFENCE COMMITTEE/COMITÉ DE SOUTENANCE DE THÈSE
Laurentian Université/Université Laurentienne
Faculty of Graduate Studies/Faculté des études supérieures

Title of Thesis
Titre de la thèse The Geochemical Behavior of Metalloids and Their Effect on the Highly Siderophile Elements During the Crystallization of a Magmatic Sulfide Liquid in Relation to the Formation of Ni-Cu-PGE Magmatic Sulfide Deposits

Name of Candidate
Nom du candidat Cafagna, Fabio

Degree
Diplôme Doctor of Philosophy

Department/Program
Département/Programme Mineral Deposits and Precambrian Geology

Date of Defence
Date de la soutenance April 9, 2015

APPROVED/APPROUVÉ

Thesis Examiners/Examinateurs de thèse:

Dr. Pedro Jugo
(Co-supervisor/Co-directeur de thèse)

Dr. Andrew McDonald
(Co-supervisor/Co-directeur de thèse)

Dr. Doug Tinkham
(Committee member/Membre du comité)

Approved for the Faculty of Graduate Studies
Approuvé pour la Faculté des études supérieures
Dr. David Lesbarrères
M. David Lesbarrères
Acting Dean, Faculty of Graduate Studies
Doyen intérimaire, Faculté des études supérieures

Dr. James Brenan
(External Examiner/Examinateur externe)

Dr. Nelson Belzile
(Internal Examiner/Examinateur interne)

ACCESSIBILITY CLAUSE AND PERMISSION TO USE

Ai miei Genitori

To my Parents

Abstract

The highly siderophile elements (HSE), which include Re, Au and the platinum-group elements (PGE: Ru, Rh, Pd, Os, Ir, Pt) are of scientific and economic interest because they are tracers of geological processes (e.g., planetary differentiation) or have industrial or investment value. In most ore deposits, HSE are usually mined as by-products of Ni-Cu mineralization, such as those of the Sudbury district (Canada). Although at high temperature HSE are expected to be in lattice of sulfides they are usually found as discrete phases or platinum-group minerals (PGM). Many of PGM have metalloids (As, Se, Sb, Te and Bi) as essential constituents but, despite this relationship, the role of metalloids on HSE mineralization is still unclear. This dissertation documents the results of three experimental studies undertaken to investigate the effect of metalloids on the geochemistry of HSE. The first study examined whether the metalloids can mobilize HSE in an anhydrous environment. The results show that metalloids do not transport the HSE but also that Au, Pd and Pt can be efficiently fractionated from the other HSE and transported away from a sulfide assemblage through a relatively low-porosity, low-permeability medium in absence of hydrothermal fluids. The second study investigated the solubility of metalloids in monosulfide solid solution (mss) and intermediate solid solution (iss), to asses the conditions required for the formation of immiscible metalloid liquids and their effect on HSE partitioning. The results show that the metalloids form two separate phases, one that is As-rich and strongly sequestered Pt from the sulfides and another that is Bi-Te rich and affected mostly Pd and Au. The results also show that the other HSE (Ru, Rh, Re, Os, Ir) are largely unaffected by the presence of metalloids. In addition the results show that mss can dissolve significant amounts of metalloids (hundreds of ppm) before metalloid

saturation can occur. The third study constrained the geochemical behavior of metalloids and HSE in a pyrite-bearing sulfide system. The results show that Co-Ni-rich and HSE bearing pyrite can form during cooling of a sulfide melt and also that the HSE partition roughly equally between mss and pyrite, whereas Pd that partitions preferentially into mss and Au partitions preferentially into iss. Moreover, pyrite showed compositional zonation of many elements similar to that documented in natural pyrite samples that are also Co-rich and HSE-bearing. Thus, identification of such pyrite in natural assemblages is consistent with a magmatic origin.

Keywords

Platinum-group elements, PGE, highly siderophile elements, HSE, metalloids, As, Se, Sb, Te, Bi, platinum-group minerals, PGM, magmatic sulfides, ore deposits, Sudbury Igneous Complex, footwall, experimental study, transport of PGE, HSE fractionation, solubility of metalloids, partitioning of HSE, partitioning of PGE, monosulfide solid solution, mss, intermediate solid solution, iss, pyrite.

Statement of co-authorship

The initial design of the first study was done when the project was conceived by Dr. Pedro Jugo. However, the execution of the experiments, the analyses of the results and the conclusions reached are entirely my work, executed under the supervision of Dr. Jugo. The second and third studies were conceived and carried out by me, after discussing and confronting ideas with Dr. Jugo, who constantly offered advice and supervised all the steps of the work.

Acknowledgements

This thesis was a long and complex work. Several problems and obstacles slowed down the work. I would not have been able to complete the project without the help and support of several people along the way. It is difficult, if not impossible, to thank everybody. If someone is forgotten from this list, I sincerely apologize.

A special thank to my supervisor, Dr. Pedro Jugo. He always believed in me and in the project, even when I did not. He kept me on the project even when I had to interrupt for a long period of time. Not many other people would have had his patience.

Furthermore, I would like to thank my advisory committee, composed by my co-supervisor Dr. Andy McDonald and by Dr. Doug Tinkham, for their advices and inputs.

This thesis would not have been completed without the help of some outstanding technicians who helped me through analytical techniques. Therefore, thanks to Willard Desjardins for teaching me how to make epoxy “pucks” and how to polish samples; to Sandra Clarke for teaching me how to use an SEM and to Dave Crabtree for the help with the microprobe; finally, thanks to Joe Petrus, for the hours spent on the LA-ICP-MS and for guiding me through Iolite.

I would like to thank my mother, Luisanna, who always encouraged me to look beyond the horizon, supported me and never had a doubt I would have made it. Together with her, I would like to thank the rest of my family, in Italy; it was hard for them to know me so far away.

I will never thank enough my love, Zsuzsanna, whom I met here in Canada. She is always by my side, no matter what. She taught me that working hard is rewarding, that I can reach any goal if I want. We made it, together, Szerelmem.

I also want to thank all my friends, in Canada and in Italy. In my years here in Canada, I had the chance to meet people from literally all around the world. They made a better person of me and I had the chance to learn the beauty of multiculturalism and diversity. This is something that few lucky people have the luxury to experience.

Table of contents

Abstract ..... **IV**

Keywords V

Statement of co-authorship ..... **VI**

Acknowledgements ..... **VII**

Table of contents ..... **IX**

Index of tables ..... **XIII**

Index of figures ..... **XV**

Index of appendices ..... **XIX**

Introduction **20**

Structure of the thesis **23**

An Experimental Study on the Role of Te, Bi and As in the Mobilization of Highly Siderophile Elements (HSE): Implications for the Formation of the Footwall Deposits of the Sudbury Igneous Complex (Ontario, Canada) **26**

Abstract **27**

2.1. Introduction **29**

2.2. Regional Geology of the Sudbury District **31**

2.3. Sulfide melts, metalloids and HSE **33**

2.4. Experimental methods and analytical techniques **35**

2.4.1 Starting materials 35

2.4.2 Initial experimental protocol 36

2.4.3 Modified experimental protocol 39

2.4.4 Analytical techniques 40

2.5. Results **41**

2.5.1. The sample chamber 41
2.5.2. Dispersion ‘halo’ through the graphite capsule 44
2.6. Discussion 46
2.6.1. Transport mechanisms 46
2.6.2. Equilibrium 48
2.6.3. Implications for sulfide and PGE mineralization within the footwall of the SIC 50
2.7. Conclusions 53
Acknowledgements 54
References 54
Tables 64
Figures 69
Exsolution of Immiscible Metalloid-bearing Liquids from Sulfides and the Role of Metalloids in the Behavior of Highly Siderophile Elements: Constraints from Experiments Synthesized Between 1050 °C and 600 °C 82
Abstract 83
3.1. Introduction 85
3.2. Experimental methods 87
3.2.1. First set of experiments (K-series) 88
3.2.2. Second set of experiments (KN-series) 90
3.3. Analytical techniques 92
3.4. Results 95
3.4.1. First set of experiments (K-series) 95
Phases present and textural relationships 95
Sulfide composition 96
Metalloid phases present 97

Trace element content in mss *98*

Trace element content in Cu-rich domains *99*

3.4.2. Second set of experiments (KN-series) 99

3.5. Discussion 103

3.5.1. Nature of metalloid phases 103

3.5.2. Metalloid content required to produce metalloid-bearing phases 104

3.5.3. Effects of metalloids on HSE 106

3.5.3. Behavior of other trace elements 107

3.6. Conclusions 107

Acknowledgments 109

References 109

Tables 117

Magmatic Origin of Co-rich, PGE-bearing Pyrite: An Experimental Study on the Geochemical Behavior of Highly Siderophile Elements (HSE) and Metalloids in a mss-iss-pyrite System at 650 °C 147

Abstract 148

4.1. Introduction 150

4.2. Experimental methods and analytical techniques 152

4.3. Results 157

4.4. Discussion 163

4.5. Conclusions 167

Acknowledgements 168

References 169

Tables 175

Figures 182

General conclusions 197

Appendices..... 200

Index of tables

Table 1. Composition of the sulfide mixture used as starting materials. 64

Table 2. Composition of the highly siderophile element mixtures. 65

Table 3. Summary of the experimental conditions. 66

Table 4. Summary of the main distinguishing features observed in experimental products. 67

Table 5. Average composition of synthesized sulfides (semi-quantitative EDS, normalized to 100 at. %). 68

Table 6. Correction factors for argide interferences. 117

Table 7. Summary of experimental conditions and results. 118

Table 8. Major element composition of sulfides synthesized in experiments of the K-series.... 119

Table 9. Trace element content in monosulfide solid solution synthesized in experiments of the K-series (in ppm). 121

Table 10. Trace element content in the multiphase upper domain and in the intermediate solid solution synthesized in experiments of the K-series (in ppm). 123

Table 11. Major element composition of the sulfides synthesized in experiments of the KN-series. 125

Table 12. Trace element content in sulfides synthesized in experiments of the KN-series (in ppm). 126

Table 13. Partitioning coefficients between mss and iss for KN-series experiments. 127

Table 14. Composition of the natural sulfides used as starting material. 175

Table 15. Bulk composition (in wt.%) of preliminary experiments performed to obtain pyrite as a primary phase. 176

Table 16. Nominal composition of starting mixtures. 177

Table 17. Composition of run products. 178

Table 18. Calculated partition coefficients per indicated sulfide pairs. 180

Index of figures

Figure 1. Schematic drawing of the experimental assembly used in the piston-cylinder experiments. 69

Figure 2. Back-scattered electron image (BSE) of the products of a failed experiment. 70

Figure 3. BSE image of the longitudinal section of a typical experimental product. 71

Figure 4. BSE images of the sample chamber of a Te-Bi-bearing experiment run at 900 °C. 72

Figure 5. BSE images of Pt-bearing minerals in FC-79 and FC-92. 73

Figure 6. BSE images of four representative experiments showing variations of internal textures with decreasing temperature. 75

Figure 7. BSE images of the 900 °C experimental products. 76

Figure 8. BSE detail of particles in the halo of the 900 °C Bi-bearing experiment (FC-62)..... 78

Figure 9. Comparison of experimental products at decreasing temperature. 80

Figure 10. Proposed model for the influence of a thermal aureole on the mobility of Pd, Pt, and Au and the origin of the footwall deposits..... 81

Figure 11. Sample holder used to run several experiments simultaneously. 128

Figure 12. Examples of time-resolved spectra of metalloids signal intensity (from LA-ICP-MS analyses) used to detect the presence of metalloid-bearing nuggets. 129

Figure 13. Images showing the run products of an experiment of the K series containing a mixture of As, Bi, Te and equilibrated at 1050 °C. 131

Figure 14. Images showing the results of an experiment containing As, Bi, and Te (K-series) and equilibrated at 900 °C. 132

Figure 15. BSE images of experimental products equilibrated at 750 °C. 133

Figure 16. Example of Te-bearing run, equilibrated at 600 °C. 134

Figure 17. Composition of gersdorffite-cobaltite group minerals observed in run products. Cobalt was added only to the experiments of the KN-series..... 135

Figure 18. Metalloid content in mss (by LA-ICP-MS) equilibrated at different temperatures from experiments of the K-series. 136

Figure 19. Concentration of HSE in mss (by LA-ICP-MS) from experiments of the K-series.. 137

Figure 20. Time resolved spectra obtained from a line scan ablation through the part of the lower (mss) and the upper (mss-b, Cu-rich liquid and metalloid phases) domains of the metalloid mixture-bearing experiment equilibrated at 1050 °C. 138

Figure 21. Example of run products from experiments of the KN-series..... 139

Figure 22. Examples of synthesized phases from experiments of the KN-series that contained 2 wt.% of a mixture of metalloids..... 140

Figure 23. BSE image showing details of the run products obtained from experiments of the KN-series bearing 2 wt.% metalloid mixture and quenched at 650 °C. 141

Figure 24. Images showing details of a metalloid-rich domain obtained from an experiment containing 2 wt.% of a metalloid mixture and quenched at 650 °C. 142

Figure 25. Partition coefficients between mss and iss obtained from experiments of the KN-series. 143

Figure 26. Comparison of partitioning coefficients of metalloids and HSE between mss and iss. 144

Figure 27. Partitioning coefficients of metalloids between mss and iss from KN-series plotted against the concentration of metalloids in mss to evaluate the Henryan behavior of metalloids at different concentrations. 145

Figure 28. Fugacity of S (fS_2) estimated for the experiments of the K-series as a function of temperature. 146

Figure 29. Example of time resolved spectra of the metalloids. 182

Figure 30. Reflected light images of preliminary run products. 183

Figure 31. Composition of preliminary and main experiments on a modified phase diagram of the Fe-Ni-S system. 184

Figure 32. Reflected light and back-scattered electron images of run products. 185

Figure 33. Detailed images of the metalloid-rich domain in experiment P-13. 186

Figure 34. Concentration of metalloids and HSE in each sulfide phase. 187

Figure 35. Nernst partitioning coefficients of metalloids and HSE. 188

Figure 36. Nernst partitioning coefficients of metalloid and HSE between sulfides and the core or the rim of pyrite from experiment P-07. 189

Figure 37. Confrontation of the partitioning coefficients of metalloids and HSE between mss and iss obtained from the KN-series and the P-series experiments. 190

Figure 38. Evaluation of Henryan behavior of metalloids. 191

Figure 39. Ternary diagrams showing the bulk composition of the starting materials and of the experimental products. 192

Figure 40. Element distribution maps of the sulfide assemblage from experiment P-12. 193

Figure 41. Element distribution maps of a euhedral pyrite grain surrounded by iss and mss from P-07 run. 194

Figure 42. Time-resolved spectra of one laser ablation line across the pyrite grain. 195

Figure 43. Element distribution maps of two euhedral pyrite grains surrounded by iss and mss from experiment P-13. 196

Index of appendices

Appendix 1. Approximate composition of PGM and metalloid minerals detected in K-series and KN-series experiments (semi-quantitative EDS analyses; in at.%). 201

Appendix 2. Semi-quantitative analyses of the metalloid phases[1]. 206

Chapter 1

Introduction

The highly siderophile elements (HSE: Ru, Rh, Pd, Re, Os, Ir, Pt and Au) are a group of elements that are economically relevant for industrial and commercial purposes. Among the HSE, Ru, Rh, Pd, Os, Ir and Pt form a sub-group known as platinum-group elements (PGE). The HSE preferentially partition into sulfide liquids, rather than into silicate liquids (e.g., Mungall and Brenan, 2014). Therefore, HSE are usually found as by-products in Cu-Ni magmatic sulfide deposits, such as those found in the Sudbury district, in Canada (Ames and Farrow, 2007), the Bushveld Complex in the Republic of South Africa (Armitage, 2002) and the Noril'sk-Talnakh intrusion in the Russian Federation (Barnes et al., 2006).

In magmatic sulfide deposits, the HSE are expected to exist dissolved in a sulfide melt and in high-temperature sulfides. For example, Ru, Os and Ir usually partition into mss (Ballhaus et al., 2001) and, at lower temperature, Pd has a preference for pentlandite (Barnes et al., 1997). Thus, understanding the behavior of the HSE in sulfide systems is essential to understand the behavior of the HSE in general. However, in most ore deposits the HSE are mostly found as discrete phases, usually called platinum-group minerals (PGM) or precious-metal minerals (PMM). The PGM can account for a big portion of the total HSE budget in a system (Keays et al., 1981) and be dominant repository of HSE in a deposit, such as Lac-des-Îles (Canada, Djon et al., 2012). The PGM can be sulfides (e.g., laurite, RuS_2), metallic alloys (e.g., isoferroplatinum, Pt_3Fe) or can be composed of one or more HSE and metalloids such as As, Bi, and Te (e.g., michenerite: (Pd,Pt)BiTe, merenskyite: (Pd,Pt)$(Te,Bi)_2$, sperrylite: $PtAs_2$, insizwaite: $PtBi_2$, irarsite: IrAsS, ruarsite: RuAsS, Cabri, 2002). Although 'metalloids' is a comprehensive term that indicates a group of elements that can display both metallic and non-metallic behavior (often including B, Si, Ge, As, Sb, and Te), the term is used through this dissertation to refer to a group of five elements (As, Se, Sb, Te, Bi). Although only Te, As and Sb are considered metalloids *sensu*

stricto (Westland, 1981), Se is often considered a metalloid and Bi (although usually classified as a metal) occurs in the minerals of interests substituting for Te; hence, as a metalloid. Frost et al. (2002) grouped those five elements, together with Ag, Hg, Sn and Tl, as low-melting-point chalcophile elements (LMCE) thus the term metalloid is preferred over LMCE to exclude Ag, Hg, Sn, Tl.

At early magmatic stages, metalloids are expected to partition into sulfide liquids. However, it has been suggested that metalloids may become immiscible during the last stages of crystallization of the sulfide melt and form a discrete liquid (Fleet et al., 1993). Helmy et al., (2007; 2010; 2013) suggested that the metalloid-rich liquids may sequester HSE and form PGM; however, those studies were limited to only a two HSE (Pt, Pd) and using only one metalloid at the time (Te in Helmy et al. 2007; As in Helmy et al. 2013). Thus, there is no documented experimental data on more complex systems containing all the HSE or combinations of metalloids.

Pyrite is a common accessory mineral in several deposits (Craig et al., 1998). Several studies on pyrite in natural occurrences have outlined that this sulfide can be significantly enriched in some HSE, particularly Ru, Os, Ir (e.g., Barkov et al., 1997; Lorand and Alard, 2010; Dare et al., 2011; Piña et al., 2011; Djon et al., 2012). Furthermore, Dare et al. (2010) also report significant HSE enrichment and alternate zonation in Co and Se in pyrite from McCreedy East deposit (Sudbury, Canada). Despite the relatively low abundance of pyrite in sulfide deposits, better constrains on the origin of Co-rich, HSE-bearing pyrite could be useful to understand the paragenesis of the sulfide assemblages in which it is found, specially because associated sulfides (pyrrhotite, chalcopyrite) typically loose any record of the HSE their precursor phases (mss, iss) may have contained (Craig and Soldberg, 1998). This is significant for the footwall mineralization in the

Sudbury district (as well as other localities elsewhere) where a clear origin of the mineralization (magmatic vs. hydrothermal) is not well understood. In the case of the Sudbury footwall ores, some models suggest that these systems either formed by the intrusion into the footwall or a differentiated magmatic sulfide liquid (Li et al., 1992, Morrison et al., 1994; Ebel and Naldrett, 1996), or by mobilization of some elements into the footwall due to the passage of hydrothermal fluids (Molnár et al., 2001; Péntek et al., 2008).

Structure of the thesis

To understand how metalloids affect a multi-component HSE-sulfide system, I undertook three distinct, but correlated, experimental studies. The results are presented in the following three chapters as manuscripts intended for publication in peer-reviewed journals. In the first study (chapter 2) I explored the role that metalloids may have in the differentiation and mobilization of HSE in both anhydrous and hydrous environments. Experiments contained sulfides, metalloids and highly siderophile elements and were carried out with piston-cylinder presses, at temperatures between 900 ℃ and 500 ℃, for periods ranging between 48 hours and 21 days. Pressure was kept at 0.5 GPa, which is the minimum operational pressure for the 19 mm (outer diameter of the assembly lodging) piston-cylinder used. Run products were brought to a scanning electron microscope (SEM), equipped with energy dispersive spectroscopy (EDS) at Geoscience Laboratories in Sudbury, where semi-quantitative analyses were performed. The experience gained with the first study strongly influenced and helped the planning and the execution of the second and third studies.

The second study (chapter 3) investigates the solubility of metalloids in sulfides, particularly mss and iss, to understand the metalloid content necessary to exsolve a metalloid phase. Experimental and analytical techniques were modified on the base of the results obtained previously. Two sets of experiments containing sulfides, metalloids and HSE were performed in evacuated silicate tubes loaded into a vertical furnace. One set was composed of three experiments doped with 3 wt.% of either As, Te or Bi and one experiment doped with 3 wt.% of As, Te and Bi, added as a mixture. The other set was composed of one experiment in which no metalloid was added and two experiments doped with a mixture of As, Se, Te, Sb and Bi, added at two different concentrations (2 wt.% and 0.0.5 wt.%) Starting materials were fused at 1200 ℃ and then temperature was slowly decreased to a run temperature of 1050 ℃, 900 ℃, 750 ℃ or 600 ℃, at which experiments dwelled before being quenched in cold water. This multi-temperature approach was chosen to investigate possible temperature dependence of metalloid solubility and temperature of crystallization of metalloid phases. Run products were examined with a reflected light optical microscope where photomicrographs were taken and then brought to the SEM for collecting back-scattered electron images (BSE). Quantitative analyses were performed with a microprobe using wavelength dispersive spectroscopy (WDS) for major elements. Trace elements were analyzed with laser ablation inductively coupled plasma mass spectrometry (LA-ICP-MS).

Finally, I designed the third study (chapter 4) as a continuation of the second, but thought to test the possibility of a magmatic origin for naturally occurring HSE-bearing pyrite that has been documented in several localities. For this study, the composition of the starting sulfides was richer in S, relative to the previous study, to obtain pyrite in the final sulfide assemblage. Experimental capsules were brought to 1200 ℃ to melt the starting materials. Subsequently,

temperature was lowered to 750 °C at a rate of 60 °C/h. Then, to promote crystallization of pyrite, the cooling rate was decreased and the capsules were cooled from 750 °C to 650 °C at a rate of 0.5 °C/h. When capsules reached 650 °C, they were quenched in water. As for experimental products of the previous study, also these products were mounted in epoxy, polished and analyzed. Photomicrographs of the products were taken with a digital camera mounted on an optical microscope and back-scattered electron images were obtained with a SEM. Microprobe (WDS) was used for quantitative analyses of major elements in the sulfides, whereas LA-ICP-MS was used for trace element analyses.

Chapter 2

An Experimental Study on the Role of Te, Bi and As in the Mobilization of Highly Siderophile Elements (HSE): Implications for the Formation of the Footwall Deposits of the Sudbury Igneous Complex (Ontario, Canada)

Abstract

The footwall of the Sudbury Igneous Complex (SIC), Ontario (Canada), hosts Cu-Ni-PGE deposits in veins, veinlets, stringers and disseminated sulfides mainly composed of Cu-rich sulfides. However, the origin of the footwall deposits is not completely understood. Hypotheses include simple magmatic fractionation of sulfide liquids from the contact into the footwall and late or post-magmatic remobilization of metals by the passage of hydrothermal fluids. Low-melting point chalcophile elements (LMCE) such as As, Te and Bi are important components of the deposits as they complex with platinum-group elements (PGE) to form platinum-group minerals (PGM). During the crystallization of a sulfide liquid, the presence of Te, As or Bi depresses the sulfide solidus and it has been suggested that they may form an immiscible LMCE-bearing melt that sequesters Pt, Pd and Au. We investigated if these three elements exert control on the fractionation and mobilization of highly siderophile elements (HSE) during the formation of footwall-type deposits. Sulfides and HSE were loaded, with either one or a combination of the three LMCE, in graphite capsules and sealed in Pt capsules. Anhydrous experiments were performed in piston-cylinder presses at temperatures between 900 °C and 500 °C and a pressure of 0.5 GPa. Experimental products were analyzed with SEM (EDS) and show that, at temperatures above 600 °C, Pd and Au fractionate from the other HSE and are mobilized out of the sample chamber, migrating through the low porosity walls of the graphite capsule, along with Te, As and Bi. At temperatures above 800 °C, Pt was also mobilized. This behavior was also observed in experiments in which LMCE were absent; therefore, LMCE do not seem responsible for fractionation and mobilization. Although the mechanism requires further investigation, the experimental results show that Au, Pd and

Pt can be mobilized and fractionated from the other HSE without requiring hydrothermal fluids. Thus, the thermal aureole during the cooling of the melt sheet that formed the SIC is likely a primary control in the mobilization of Pd, Pt and Au from contact-style sulfide ores to deeper part of the footwall.

2.1. Introduction

The footwall of the Sudbury Igneous Complex (SIC) hosts several Cu-Ni-PGE deposits. Copper and nickel are hosted in sulfides (e.g., chalcopyrite: $CuFeS_2$, pentlandite: $(Fe,Ni)_9S_8$, bornite: Cu_5FeS_4, millerite: NiS). Among the platinum-group elements (PGE: Ru, Rh, Pd, Os, Ir, Pt), Pd and Pt are the main elements of interest and are found mostly as platinum-group minerals (PGM) associated with elements such as As, Te and Bi (e.g., michenerite: (Pd,Pt)BiTe, merenskyite: $(Pd,Pt)(Te,Bi)_2$, sperrylite: $PtAs_2$, kotulskite: Pd(Te,Bi); Cabri and Laflamme, 1976, Ames and Farrow, 2007). These PGM are also important components of several other Ni-Cu-PGE deposits such as Lac-des-Iles (Canada), the Platreef in the Bushveld Complex (Republic of South Africa), Noril'sk and the Kola Peninsula (Russian Federation), Jinbaoshan (People's Republic of China), Kambalda (Australia) and the Niquelândia layered intrusion in Brazil (Djon and Barnes, 2012; Armitage et al., 2002; Barnes et al., 2006; Grokhovskaya et al., 2009; Wang et al., 2008; Hudson, 1986; Garuti et al., 2012). Gold is also a metal of interest in footwall ores and, together with Re and the PGE, constitutes the highly siderophile elements (HSE). Frost et al. (2002) grouped As, Te and Bi (together with Ag, Au, Hg, Sb, Se, Sn and Tl) as low-melting point chalcophile elements (LMCE); however, because As and Te are metalloids and Bi (a metal) typically substitutes for Te in all PGM of interest, these three elements will be described as 'metalloids' for simplicity.

The origin of the footwall mineralization in the Sudbury district is not completely understood and is still debated. In particular, the role of the metalloids has not been properly investigated. Helmy et al. (2007) proposed that Te and Bi are initially dissolved in sulfide liquids, but as sulfide crystallization proceeds, metalloids may form immiscible liquids that sequester Pt and Pd from the sulfides. Also, the presence of metalloids depresses the solidus of sulfides allowing

them to be mobilized at relatively low temperatures during metamorphism (Tomkins et al., 2007). In the case of the Sudbury district, the working hypothesis of this study is that metalloid-rich liquids may have been active in the mobilization and transport of PGE from the base of the SIC (current contact-type deposits) into the footwall during the late stages of crystallization of the SIC and the contact metamorphism of the footwall. However, some experimental studies documented that anhydrous S-bearing gas phases can efficiently transport base metals (Fe, Ni and Cu) and PGE. For example, Fleet and Wu (1993; 1995) suggest that metal transport by S-bearing vapor can occur when Cl is also present in the system. Baker et al. (2001) reported metal transport by a 'sulfurous fluid' in which the dominant component was H_2S formed by H_2 diffusion into the Pt capsule used in the experiments. Peregoedova et al. (2006) showed that Pt, Au and Pd can be transferred more efficiently than the other PGE by a S-dominated vapor. All these experiments were conducted at temperatures at and above 1000 °C.

Experiments were conducted to constrain the role of Te, As and Bi on the behavior of HSE and investigate the mobility of HSE in the presence of metalloids at temperatures appropriate for the thermal aureole of the SIC in the footwall (Pentek et al. 2008; Jørgensen et al. 2011). The results show that Pt, Pd, Au (and to a minor extent Rh) can be fractionated from the other HSE (Ru, Re, Os, Ir), and moved away from the main sulfide mass, at temperatures below the solidus of all major sulfide phases (down to ~600 °C) and under anhydrous conditions (i.e. in the absence of hydrothermal fluids). This behavior was observed in experiments containing metalloids but also in control experiments without added metalloids. Thus, the results are consistent with Pd, Pt and Au being transported by a S-bearing gas phase at temperatures down to 600 °C.

2.2. Regional Geology of the Sudbury District

Sudbury hosts a mining district composed of several world-class Ni-Cu-PGE deposits. These deposits formed as a consequence of a meteoritic impact (Dietz, 1964) 1850 ± 1 Ma (Krogh et al., 1984), at the boundary between Neoarchean granitoids of the Superior Province (North Range) and Paleoproterozoic metasediments and metavolcanics of the Southern Province (South Range; Ames and Farrow, 2007). The impact created a crater with a minimum initial diameter of the transient cavity of about 100 km and a final diameter between 175 km and 240 km (Grieve, 1994). The energy released by the impact instantly vaporized the meteorite and melted the crust, creating a magma pool that partially filled the crater (Zieg and Marsh, 2005). The magma pool was then overlain by the brecciated Onaping Formation that has been interpreted as fallback breccia (French, 1967). The cooling and differentiation of the melt sheet resulted in the Sudbury Igneous Complex (SIC), which is a hypoabyssal layered intermediate to felsic magmatic complex. The key units of the SIC are historically known as “norite” (Lower Unit), “quartz gabbro” (Middle Unit) and “granophyre” (Upper Unit; Therriault et al., 2002). Fractures and deformation zones around the crater were intruded by undifferentiated SIC melts and formed radial and concentric quartz-diorite offset dikes (Wood and Spray, 1998; Lightfoot et al., 2001). The area was subsequently deformed by several orogenic events (Rousell, 1984; Bailey et al., 1998, Raharimahefa et al., 2014) and then eroded, until it gained the current elongated shape.

The Cu-Ni-PGE deposits of the Sudbury District can be divided in three main types: marginal (contact) deposits, offset deposits and footwall deposits (Naldrett, 2004; Ames and Farrow, 2007). Contact deposits are hosted by depressions, embayments and radial troughs at the base of the SIC, within the sublayer norite and the footwall breccias. The sulfide and oxide assemblage of these deposits is composed of pyrrhotite, pentlandite, chalcopyrite, with minor pyrite and

magnetite (Ames and Farrow, 2007; Naldrett, 1984). The offset deposits are hosted by radial and concentric quartz-diorite dikes around the SIC. The mineralization occurs as semi-massive to disseminated sulfide veins within the dikes. The sulfide mineralogy is composed of dominant pyrrhotite, pentlandite and chalcopyrite (Farrow and Lightfoot, 2002). The footwall-type deposits are richer in Cu, Pd, Pt and Au, compared to the contact ores. They have been classified in two end members: “sharp-walled veins” and “disseminated, low-sulfide, high PGE” (Farrow and Jolette, 2004). The sharp-walled vein systems are characterized by veins of variable thickness, in cases still connected to contact-type deposits (e.g., McCreedy West 700; Farrow et al., 2005). Chalcopyrite is generally the dominant sulfide, with minor cubanite, pyrrhotite, pentlandite, millerite, bornite and magnetite. However, millerite-bornite dominated veins can also be observed (e.g., Morrison Deposit; Nelles, 2012). The low-sulfide, high PGE mineralization occurs in veinlets, stringers and disseminated sulfides and has a similar assemblage, but with a lower total sulfide content (< 5 % modal, Farrow et al, 2005). Farrow et al (2005) also describe a third type of footwall deposit, named “hybrid”, which displays features that are common to both end members. Both deposits are hosted by inclusion-bearing quartz-diorite (IQD) and metabreccia. In footwall-type deposits, Au is present as electrum and Pt and Pd are mainly found as PGM (moncheite, michenerite,, merenskyite, kotulskite and sperrylite), interstitial or hosted by sulfides and silicates, and located within veins or at their margin (Farrow et al., 2005).

The origin of footwall mineralization is not clear and there are multiple hypotheses for the processes that led to their formation (Péntek et al., 2008). For example, Li et al. (1992), Morrison et al. (1994) and Ebel and Naldrett (1996) attribute the formation of footwall ores to magmatic processes, suggesting that a highly fractionated sulfide liquid (derived from the melt sheet of the

SIC) intruded the Sudbury Breccia. In contrast, Molnár et al (2001) and Péntek et al. (2008), for example, suggest that the passage of hydrothermal fluids may have been the main agent, based on the presence of quartz and epidote-actinolite veins closely associated with the sulfides and the PGM. The two processes (magmatic and hydrothermal) are not necessarily exclusive and it has been suggested that hydrothermal fluids (e.g., highly saline and hydrocarbon-rich fluids; Hanley et al., 2005) may have remobilized metals from the massive sulfides of the contact ores into the footwall.

2.3. Sulfide melts, metalloids and HSE

When a mafic magma reaches sulfide saturation, an immiscible sulfide liquid may exsolve and follow its own independent evolution (Naldrett, 2004). The most common minerals in magmatic deposits are pyrrhotite (po), pentlandite (pn) and chalcopyrite (ccp). However, these are stable only at relatively low temperature. At high temperature, the first phase to crystallize from a sulfide melt (at ~1192 °C) is monosulfide solid solution (mss), which starts with a composition comparable to that of pyrrhotite, with only a small amount of Ni, and up to 10 wt.% Cu (if mss coexist with a Cu-rich melt). The Ni content in mss increases with decreasing temperature, eventually forming a complete solid solution between $Fe_{(1-x)}S$ and NiS at ~990 °C (Kullerud et al., 1969). If the system contains sufficient Cu, as expected for most natural systems, a Cu-rich sulfide melt will coexist with mss and crystallize intermediate solid solution (iss) at ~960 °C (in the system Cu-Ni-Fe-S; Kullerud et al., 1969). However, in experiments containing metalloids iss only crystallizes at ~ 880 °C (Liu and Brenan, 2015). In mss-bearing systems, iss has a composition roughly between chalcopyrite and cubanite (cbn) and those two phases are expected

to form from iss below 590 °C. When a sulfide liquid segregates from a silicate liquid, HSE strongly partition into the sulfide liquid (e.g., Mungall and Brenan, 2014), but after mss crystallization Ru, Os, Ir, and Rh will partition preferentially into mss, whereas Pt, Pd and Au behave incompatibly and remain in the residual Cu-rich liquid (Barnes et al., 1997; Ballhaus et al. 2001). Frost et al. (2002) introduced the term LMCE and highlighted some of the most important aspects of their geochemical behavior and Tomkins et al. (2007) summarized studies showing that the presence of metalloids can remarkably reduce the melting point of sulfides. Among the LMCE, Te, Bi and As are of particular interest because they are fundamental components of many PGM (Cabri and Laflamme, 1976) and those PGM often control a consistent portion of the Pt and Pd budget (e.g., Djon and Barnes, 2012). Cabri and Laflamme (1976) and Keays and Mitchell (1981) suggested that PGM exsolve from sulfides upon cooling. Prichard et al. (2004) and Barnes et al. (2006) proposed that the last droplets of residual sulfide liquid after crystallization of mss and iss would be enriched in metalloids and PGE, leading to crystallization of discrete PGM. The experimental study of Helmy et al. (2007) documented the presence of immiscible telluride melts coexisting with residual sulfides; they postulated that Pt and Pd would partition into telluride liquid, which could migrate away from the crystallized sulfides. Although Helmy et al. (2010) measured the partitioning coefficients of metalloids between mss and residual sulfide liquid, there is a paucity of studies investigating the role of metalloids in the behavior of HSE. To fill this gap, experiments were conducted to test the hypothesis that Te, Bi and As may transport HSE.

2.4. Experimental methods and analytical techniques

2.4.1 Starting materials

The starting materials were divided into three components: sulfides, HSE, and metalloids. Their chemical compositions are listed in Table 1, Table 2, and Table 3.

The sulfide mixture was designed and prepared to provide experimental products consisting of approximately 33% (by volume) pyrrhotite, 33% pentlandite and 33% chalcopyrite. This proportion was chosen to produce roughly equal amounts of these minerals (or roughly equal proportions of mss and iss), thus making them easier to find and analyze. However, the proportion is not representative of natural assemblages observed in Sudbury deposits, where the three minerals do not occur in an equal proportion, but vary depending on the type of deposit. For example, in contact deposits and offset dike deposits the dominant sulfide is pyrrhotite, followed by pentlandite and chalcopyrite, whereas in footwall type deposits chalcopyrite is dominant (Farrow and Lightfoot, 2002; Ames and Farrow, 2007). The sulfide mixture was made from synthetic sulfides (FeS, 99.9%, NiS, 99.9% and Cu_2S, 99.5% from Alfa Aesar) in the proportion of 66.4 wt.% FeS, 19.71 wt.% NiS and 13.85 wt.% Cu_2S, for an atomic total metal to S ratio (ΣM/S) of 1.1. The ΣM/S was chosen to be slightly higher than 1 to promote the formation of pentlandite (for simplicity, the Fe/Ni ratio of pentlandite was assumed equal to 1), for which ΣM/S = 1.125.

The PGE1 mixture was designed to obtain a 1:1 molar ratio of the Ru, Rh, Pd, Os, Ir, Pt and Au; PGE2 mixture contains a 1:1 molar ratio of the PGE alone, whereas HSE mixture contains a 1:1 molar ratio of all HSE (the PGE, Au and Re). The HSE used were added as native elements, with the exception of Pd (added as PdS) and Au (added as Au_2O_3), which sulfide and oxide forms

were considered more reactive. Each experiment contained one element among Te, Bi (added as native elements) and As (added as As_2S_3). Initial Te-bearing experiments did not contain the HSE mixture, but only PdS or the PGE2 mixture. The HSE mixture was subsequently prepared to monitor the fractionation of HSE. The presence of S in both PdS and As_2S_3 was taken into account for the calculations of the ΣM/S, even though the relatively low amount of S added in this manner did not significantly modify the ΣM/S.

Three hydrous experiments were performed to facilitate a comparison between hydrous and anhydrous environments. One experiment containing water was performed, but this approach was discarded because it is difficult to monitor water loss during welding of the precious metal capsules. Instead, the aqueous component was added as powdered $Mg(OH)_2$, which decomposes at 350 °C. $Mg(OH)_2$ was preferred over $Al(OH)_3$ because tests with the latter produced large (≥ 20 μm) Fe-Ni-bearing Al alloys as experimental products. In addition, some experiments contained small amounts of elemental Si powder as a sink for oxygen. However, the use of Si was abandoned because the system became too reduced and produced rounded alloys of Ni and Pd (± Rh).

2.4.2 Initial experimental protocol

The three starting components (sulfides, HSE and metalloids or hydroxide) were individually weighted and then mixed in the desired proportions in an agate mortar under acetone. Aliquots of the mixed material were loaded in graphite capsules. Each experiment contained between 50 mg and 55 mg of a mixture of starting materials. The ratio between the sulfide mixture and the HSE mixture was initially 10:1 (by mass) and then increased to 50:1 to reduce the amount of

unreacted HSE. The mass ratio between the HSE and the metalloids was initially 5:1 and was later modified to 1:1, 2:1 and 1:2 (Table 3). Graphite capsules were machined in-house with a lathe from graphite rods with a diameter of 4.5 mm. The capsules were carved with a wall thickness (walls and bottom) ranging between 0.75 mm and 1 mm. The chamber in which the starting materials were inserted had a diameter of 2.5 mm to 3 mm and a depth of approximately 4 mm. After insertion, the starting materials were lightly pressed with a clean metallic drill bit. Then, the capsules were closed with two graphite lids: the first with a diameter similar to the inner diameter of the container; the second, with the same diameter of the capsule. The overall height of the capsules was between 6.0 mm and 6.5 mm. The graphite assemblies were inserted in Pt or $Au_{80}Pd_{20}$ capsules and welded shut using a spot welder. The use of a spot welder considerably reduced the heating of the capsules (compared to other methods); thus, no additional precautions were taken to prevent loss of material during welding. The precious metal capsules were made from tubes (5 mm outside diameter and 0.127 mm wall thickness), closed by two lids made from foil of the same material (0.127 mm thick) and shaped in a capsule lid die ("ash can" technique, Sneeringer and Watson, 1985). After welding, the capsules were cold pressed at 8.3 MPa (1200 psi) and put into piston-cylinder assemblies (19 mm diameter) composed of an internal MgO sleeve, surrounded by a graphite furnace and two external sleeves, the first made of Pyrex and the second made of pyrophyllite (Figure 1). The complete assemblies were then inserted into the pressure plates of a non end-loaded piston-cylinder press (Boyd and England, 1960). The use of of a piston-cylinder press, providing confining pressure, was preferred to other experimental set ups to avoid explosive disruption of the capsule (e.g., Tomkins, 2010).

Temperature was measured with type-C (WRe_5 – WRe_{26}) thermocouples placed close to the bottom of the sample and separated from the capsule by a thin disk of Al_2O_3 (0.8 mm thick, 4.8 mm in diameter) to prevent the thermocouple piercing the capsule. The thermal gradients within the experimental assembly were not measured. However, Schilling and Wunder (2004) conducted detailed studies of temperature gradients in piston-cylinder assemblages under P-T conditions similar to those of the experiments documented here. The geometry of the pressure assemblies used in the experiments (central portion of an unstepped graphite furnace, Fig. 1) is similar to 'case 6' studied by Schilling and Wunder (2004). They estimated a temperature gradient of approximately 40 °C across gold capsules 10 mm long in experiments conducted at 1000 °C using straight graphite heaters. The experiments documented here are similar but used shorter precious metal capsules (~ 6 mm) lined with graphite capsules of roughly 1 mm wall thickness, meaning that the sample chamber was only about 3 mm to 4 mm in height; hence the temperature gradient was smaller (estimated at or below 25 °C).

All experiments were performed at a nominal pressure of 0.5 GPa. No pressure calibrations were done because pressure does not have a significant effect on the phase equilibria of sulfides (Arnold, 1962; Yund and Kullerud, 1966) and the experiments were designed to assess qualitatively metal transport as a function of temperature. Before heating, the experiments were over-pressurized 10% beyond the intended experimental pressure, to compensate for ductile adjustments of the assembly with increasing temperature. Oxygen and sulfur fugacities were not measured or monitored. However, the graphite capsules ensured the fO_2 of the experiments were at or below the C-CO-CO_2 buffer.

The initial protocol was to heat Te-bearing experiments to 1150 °C for 3 hours to melt the starting materials before equilibration at lower temperature. Those experiments consistently

failed during the ramp up segment of the protocol, roughly at ~1000 °C. Analyses on thermocouples from failed experiments revealed contamination of the thermocouple tip, which altered the difference of potential and therefore the temperature reading, causing failure. The cause of thermocouple contamination was found to be Te escaping from the capsules. Further SEM analyses on failed experiments showed the presence of Pt-tellurides within the walls of the graphite capsule and in the MgO sleeve surrounding the external Pt capsule (Figure 2). The Pt capsule was partially corroded and had a porous texture, meaning that Te escaped from the sample chamber, migrated through the graphite walls, reacted with the Pt capsule breaching it and deposited Pt-tellurides in the MgO sleeve and on the thermocouple tip. Because of this, the experimental protocol was modified to take advantage of metalloid and HSE migration through the graphite container.

2.4.3 Modified experimental protocol

Two significant modifications, involving temperature and time, were implemented. First, the overheating step was eliminated and subsequent experiments were heated directly to run temperature (up to 900 °C). Second, the duration of the experiments was set inversely proportional to run temperature because migration of metalloids through the graphite capsule wall was temperature dependent. Experiments at 900 °C were run for only 48 hours. This allowed the mobilization to develop, but be confined within the graphite capsule preventing capsule breach and experimental failure. Experiment duration was increased with decreasing temperature to 21 days for experiments at 500 °C and 550 °C. With these protocol modifications it was possible to limit the mobilization to within the capsule boundaries, quenching the

experiments before capsule contamination and failure, while preserving a record of element mobilization through the graphite capsule walls. The experimental conditions are summarized in Table 3. At the end of each run, experiments were quenched by terminating the power, recovered, sectioned longitudinally with a low-speed saw, mounted in epoxy and polished manually.

2.4.4 Analytical techniques

The experimental products were analyzed at the Central Analytical Facility at Laurentian University, with a JEOL 6400 SEM and at the Geoscience Laboratories (GeoLabs), with a Zeiss Evo 50 Scanning Electron Microscope (SEM). Images of the experimental products were taken with an accelerating voltage of 20 kV and a beam current of 750 pA. The contrast was strongly enhanced over brightness to highlight the presence of small particles (sulfides and PGM) within the graphite walls of the capsule. Pictures with normal brightness and contrast were also taken to highlight the compositional differences among the various sulfides and HSE-bearing minerals found in the experimental products. Subsequently, energy dispersive spectra (EDS) were acquired and processed with INCA software. Semi-quantitative spot analyses were performed on phases of interest with an acquisition time between 10 s and 20 s and using the same voltage and current conditions used for imaging. No attempts were made to fully characterize the phases present for several reasons. First, the main purpose of the analyses was to identify the elements being mobilized. Second, many of the phases of interest were very small and forming composite grains with other phases, meaning that accurate composition of each phase was difficult to obtain.

2.5. Results

Experimental products were observed not only in the sample chamber, where the starting materials had been placed (Figure 3A), but also in the interstices among the grains that form the graphite capsule (Figure 3B) forming a “halo” of dispersed material around the sample chamber.

Results are presented and described starting from the sample chamber of experiments at progressively lower temperature, from 900 °C to 500 °C, highlighting similarities and differences among experiments doped with different metalloids. Products observed in the halo will be described in section 5.2, following the same order. Table 4 contains a summary of the main distinguishing features observed in the experimental products.

2.5.1. The sample chamber

The average composition of the sulfide phases observed in all experiments at different temperatures is listed in Table 5. Large uncertainties in some of the analyses are due to the small size of the grains, especially for the Cu-Ni minerals. Moreover, some experiments, particularly those performed at lower temperatures, might not have attained complete equilibrium, although the phases analyzed had compositions different from the starting materials, indicating that reactions were taking place even at the lowest temperatures tested. Attainment of equilibrium is not a major concern in this study because the main focus is on the migration of elements through the capsule walls. In most cases, the size of the PGM was too small (< 5 μm) to obtain meaningful quantitative analyses because the activation volume of the SEM beam always

included the materials surrounding the grains of interest. Raman spectroscopy was tried to analyze PGM ranging in size between 2 µm and 5 µm, but this method was abandoned due to the lack of PGM reference spectra to compare with our experimental products.

In the sample chamber of experiments run at 900 °C, the products are composed of a mixture of sulfides and PGM. The sulfide products are divided in two domains. The upper portion of the chamber is occupied only by monosulfide solid solution (mss), whereas the lower portion is dominated by Ni-Cu sulfides and less abundant mss. The contact between the two domains is sharp, slightly concave and is clearly visible in most 900 °C experiments (Figure 4A); the only exception is the Bi-bearing experiment, in which the contact was accidentally obliterated during polishing of the sample. The mss domain (on average 50.44 at. % S, 40.31 Fe, 7.07 Ni and 2.17 Cu) is texturally homogeneous (Figure 4B). However, a few clusters of PGM were detected within it and are composed of all HSE, except Au and Pd. In contrast, the Ni-Cu-rich domain is not homogeneous and is composed of a fine intergrowth of Cu-rich and Ni-rich phases. The Cu-rich mineral is a bornite solid solution (42.09 at. % S, 15.16 Fe, 1.26 Ni and 41.49 Cu) surrounding rounded grains of mss (Figure 4C). The Ni-rich sulfide is pentlandite with Fe>Ni (46.85 at. % S, 28.15 Fe, 20.14 Ni, and 4.86 Cu). Pentlandite forms exsolution textures that follow the crystallographic directions of the mss matrix (Figure 4D). Analyses also showed the presence of intermediate solid solution (~ 42-46 at. % S, 23 to 27% Fe, 15 to 22% Cu and 9 to 12 % Ni). The lower domain of the 900 °C experiments is also richer in PGM, relative to the upper domain. Rhenium, Ru, Os and Ir have the tendency to cluster in grain aggregates (Figure 4C, to the left) composed mostly of Re-Ir-Os and Fe-Ir-Pt alloys. Rhenium, Ru and Os were also commonly found alone in small grains, less than 1 µm in size. Palladium and Au were always found together with or without a metalloid as small, anhedral grains (round to ellipsoidal) within

the sulfide intergrowths and at the grain boundaries among mss and the other sulfides. Platinum is often associated with Pd and Au, but also formed euhedral to subhedral alloys with Fe and Ir (e.g., in the Te-Bi-bearing experiment shown in Figure 4D). In the As-bearing experiment run at 900 °C, Pt formed euhedral crystals with As, Rh and Ir (Figure 5A). In the Te-bearing experiment, Pt formed euhedral alloys with Fe (Figure 5B) and elongated Pt-Te bearing minerals (Figure 5B).

In the experiments run at 800 °C, the vertical segregation between the mss domain and Cu-Ni-richer domain is still observable, but the boundary is not as sharp as in the 900 °C experiments. Figure 6A shows the irregular boundary of the domains in the sample chamber of a metalloid-free experiment performed at 800 °C. The image also shows how PGM are more evenly distributed, compared to experiments at 900 °C. The appearances and textures of the PGM in 800 °C experiments are similar to that of the 900 °C experiments.

In the products of the 700 °C experiments, the contact between the two domains is no longer visible and replaced by a gradational transition (Figure 6C). The texture of the mss is more granular and the size of the grains decreases, relative to the homogeneous ingot of the 900 °C experiments or the relatively large rounded grains observed in the 800 °C products. In the As-bearing experiment, net-textured Pt-Rh-Pd-bearing arsenides surround anhedral grains of mss. At the grain boundary of the arsenides, there are exsolutions richer in Pt (Figure 6D). Phases containing Au and Pd still have a rounded shape and can only be found associated with pentlandite and bornite, regardless of the metalloid added. Conversely, the clusters containing the alloys of the other HSE are more randomly distributed among the sulfides.

At 600 °C, there is no longer a clear distinction between the two domains, even though it is still possible to notice a slight increase of the proportion of Cu-Ni sulfides relative to mss towards the bottom of the capsule (Figure 6E). The PGM experimental products are the same as in the higher temperature experiments.

Finally, in experiments conducted at 550 °C and 500 °C the sulfides are evenly mixed and no vertical separation was noticed (Figure 6G). The sulfide products had granular textures and no exsolutions were observed. In some cases, the ratio of elements in the HSE alloys changes relative to the higher temperature products (e.g., 92.92 at. % Ir, 4.78 Fe and 2.31 Ni; Figure 6H).

2.5.2. Dispersion 'halo' through the graphite capsule

The haloes that formed around the sample chamber of the 900 °C experiments were relatively wide and, in a few cases (experiments at 36 to 48 hours) reached the metal capsule. In all experiments at 900 °C (and also in the Te-bearing 800 °C experiments), the products were also found in concentric fractures within the graphite capsule. The fractures depart from the corners of the sample chamber and join above or below it (Figure 7). In a tri-dimensional view, these fractures would likely have a conical shape and are interpreted to have formed by decompression during quenching. The products found in the haloes are sulfides and PGM. No compositional difference was noticed between the sulfides in the halo and those identified in the sample chamber. The shape of the sulfides is controlled by the interstitial spaces among the graphite grains and the size is generally below 10 µm (Figure 8). The only HSE detected in the haloes are Pt, Pd and Au, with or without metalloids. The only exception is the Te-bearing experiment, in which only Pt-bearing PGM were detected along with the sulfides. Rhodium was also detected

within the graphite capsule walls in some experiments, along with Pt, Pd and Au but not as commonly.

All the 800 °C experiments developed a halo. As with the 900 °C experiments, run times were long enough (72 to 96 hours) to allow the halo to extend far from the sample chamber (Figure 9A). Products are very similar to those in the 900 °C experiments, with small rounded PGM associated with interstitial sulfides. However, the presence of Pt is more limited relative to Au and Pd and to the 900 °C experiments, with the exception of As-bearing experiment in which Pd is less abundant than Pt. Moreover, in the As-bearing experiment and in the metalloid-free experiment, Rh is relatively more abundant (and associated with Pt) than in experiments with Te or Bi.

In the 700 °C experiments, the size of the halo is considerably smaller, compared to higher temperature experiments, despite the longer run durations (144 to 168 hours). The materials that formed the halo extended through the graphite capsule, but did not reach the precious metal external capsule. This is more evident in experiments containing As, Bi or OH (Figure 9B), whereas the Te-bearing experiment produced a slightly more extended halo. The assemblage of sulfides and the type of PGM observed is similar to those in the experiments at 800 °C and 900 °C, although the presence of Pt in all the 700 °C haloes is very rare.

At 600 °C, only the products of experiments containing Te or OH formed a detectable halo (Figure 9C). In the experiment containing As (Figure 9D) or Bi, only few grains of sulfides or PGM were observed within the graphite wall, but did not form a well-defined halo around the sample chamber, despite longer run times (288 and 336 hours) compared to the Te bearing experiment (240 hours). The composition of the minerals observed in the halo is not different

from those at higher temperature. In the Te-bearing experiments, only Pd-bearing PGM were detected, but in the OH-bearing experiment, the PGM contained Pd, Pt, Rh and Au was also present.

Only the metalloid-free experiment and experiments doped with Te or As were performed at 550 °C or 500 °C. These experiments were maintained at the desired temperature for 504 hours (21 days). Although the metalloid-free and the Te-bearing experiments did not produce any halo (Figure 9E), a small halo was observed in the As-bearing experiment (Figure 9F) and contained mainly Pd-, Au-, Pt- and Rh-bearing Ni-arsenides.

2.6. Discussion

2.6.1. Transport mechanisms

The most important result of these experiments is the fact that Au, Pd, Pt and Rh were fractionated from the other HSE (Re, Ru, Os, Ir) and mobilized through a container (graphite in these experiments) that kept most of the sulfides within the sample chamber. Such differentiation and mobilization are related to temperature, with more extensive transport at 900 °C than at 600 °C and no noticeable effect in experiments conducted at 550 °C and 500 °C. Also, with decreasing temperature, the experiments showed that transport of Pt becomes less efficient (relative to Au and Pd) and the presence of Pt in the halo decreases progressively between 700 °C and 600 °C.

The initial working hypothesis was that the metalloids (As, Bi, Te) caused the selective mobilization of Au, Pd and Pt. The presence of metalloids depresses the melting point of sulfides

(Tomkins et al., 2007) and it is likely that for experiments performed at 900 °C and 800 °C, at least partial melting of the sulfides was reached; thus, migration by capillarity of a sulfide melt may have contributed to the formation of the halo in the 900 °C experiments and possibly the 800 °C experiments. The studies of Hoffman and MacLean (1976) and Helmy et al. (2007) show that Te- and Bi-bearing minerals (e.g. moncheite, mereksyite) melt at relatively low temperatures (e.g. as low as 489 °C for Bi-rich michenerite); therefore, metalloid-bearing liquids may have migrated through pores by capillarity at all temperatures investigated. However, the dispersion halo containing Cu-Fe-Ni sulfides and Pt, Pd, and Au was also present in control experiments that were nominally metalloid-free (both anhydrous and OH-bearing), indicating that metalloids are not the main transporting agent.

An alternative explanation is that Au, Pd and Pt were transported by a S-bearing gas phase. Fleet and Wu (1993, 1995) observed that all PGE, Fe and Cu can be transported by S vapor when this is present together with Cl. Furthermore, Fleet and Wu (1993) argue that carbonyls (C, CO and CO_2) and metalloids (Te, Bi and As) are not efficient transport agents. However, Fleet and Wu (1993, 1995) added Cl to all the experiments; thus, the effect of S alone cannot be assessed. Baker et al. (2001) showed that Pt, Ni and Cu can be transported by a 'sulfurous fluid' at temperatures ranging from 1225 °C and 1450 °C (at 1.0 GPa). Peregoedova et al. (2006) showed that at or above 1000 °C S-vapor can transfer considerable amounts of Ni, Cu, Au, Pd and Pt, whereas the transport of Rh, Ru and Ir is negligible. The experiments documented here are consistent with S transport of Cu, Fe, Ni and some HSE (Pd, Pt, Au ± Rh) as shown by Peregoedova et al. (2006) and extends the temperature range of this phenomenon down to 600 °C. The experiments also highlight the fractionation of Pd, Pt and Au from Ru, Re, Os and Ir, which where not mobilized in the experiments and retained in the sample chamber.

Two other possible mechanisms cannot be discarded. First, all the experiments used graphite capsules and carbon has been suggested as a possible transporting agent. Although Fleet and Wu (1993) concluded that carbonyls do not transport metals and PGE, Hanley et al. (2005) and Kerr et al. (2015) analyzed fluid inclusions from footwall ores associated with the SIC and concluded that hydrocarbon-bearing volatile phases mobilized Cu, Pt, Au, Ag and Bi. Second, although the experiments were nominally anhydrous, the presence of trace amounts of H_2O cannot be completely discarded because Pt and AuPd capsules are slightly permeable to H_2 (Patiño Douce and Beard, 1994; Truckenbrodt and Johannes, 1999; Jakobsson, 2012). For example, Baker et al. (2001) performed nominally anhydrous experiments and suggested that Cu, Ni and Pt were transported via a sulfurous fluid that forms from S_2 present in the system and H_2 diffusing through the precious metal capsules. Future work is needed to further constrain the transport mechanisms, for example by conducting experiments without a carbon source.

2.6.2. Equilibrium

The preservation of the halo in the experiments was only possible with the modified experimental protocol. Shorter run times and elimination of the high temperature step (1150 °C – 1200 °C) meant that chemical equilibrium was likely not completed throughout the capsule. However, textural evidence, such as the vertical differentiation between mss and the Cu-Ni-rich quenched residue, as well as consistency in the composition of the synthesized sulfides (Table 5), indicate that chemical equilibrium was reached at least within the sample chamber. Reactions took place in subsolidus conditions because the composition of the synthesized sulfides is always different from the starting materials and fairly consistent among all experiments. Similar sulfides

assemblages are present throughout the experimental set: mss + pentlandite + bornite + iss, between 900 °C and 700 °C, and mss + bornite + pentlandite between 600 °C and 500 °C.

Concerning HSE, only Au, Pd and Pt found in phases with rounded drop-like shapes that suggest these components formed a molten phase. The other HSE (Ru, Rh, Re, Ir and Os) did not melt and only show signs of partial reaction. The euhedral alloys composed of Fe, Pt and Ir (Figure 4C), the clusters of IPGE alloys (Figure 4B; IPGE: Ir-like platinum-group elements; Barnes et al., 1985) and the euhedral Pt-Rh-bearing arsenides (Figure 5A) show that reactions took place, but the presence of submicron grains composed of elemental Re, Ru or Os indicate that not all of the starting materials reacted.

The presence of bornite solid solution among the products was unexpected. The sulfide mixture was designed to produce roughly equal volumes of pyrrhotite, chalcopyrite and pentlandite, or the equivalent high temperature phases (mss and iss). However, the ΣM/S of 1.1 is high enough to allow the formation not only of pentlandite, but also of bornite. If mss crystallizes from a mixture with the composition used in these experiments, the residue has a composition compatible with the coexistence of bornite, pentlandite and iss (Kullerud et al., 1969). In the experiments conducted at 900 °C, the Cu-Ni-rich residue sank to the bottom of the capsule. This is in contrast with the geometry of natural sulfide droplets observed by Prichard et al. (2004) and Barnes et al. (2006), who found pyrrhotite at the bottom and chalcopyrite originating from Cu-rich residual liquid on top with pentlandite in the middle. Initially, it was hypothesized that the residual liquid generated during the experiments that formed bornite among the final products, would probably be denser than the residual liquid that formed chalcopyrite-bearing natural sulfide blebs. Although we have no means to assess the density of the Cu-rich melt at run conditions, the density of bornite (4.9-5.1 g/cm^3) is higher than the density of both chalcopyrite

(4.1-4.3 g/cm^3) and pyrrhotite (4.5-4.6 g/cm^3), and comparable to the density of pentlandite (4.6-5.0 g/cm^3; Chesterman, 1979). Therefore, it seemed possible that, in the experiments, the denser Cu-Ni-rich residual liquid would have sunk towards the bottom of the capsule, leaving the mss ingot in the upper portion and that the surface tension of the Cu-Ni-rich residue trapped most of the HSE blebs that were found associated with it. An alternative explanation is that the thermal gradient across the capsule caused migration of the melt towards the hotter end of the capsule; however, as mentioned in section 2.4.2, the temperature gradient across the capsule was estimated to be ~ 25 °C, in experiments conducted at 900 °C and the capsule was centered in the pressure assembly; thus both ends of the capsule were likely at the same temperature.

2.6.3. Implications for sulfide and PGE mineralization within the footwall of the SIC

The results of these experiments show similarities with what can be observed in the footwall of the SIC, to both the sharp-walled and low-sulfide end-members of the footwall-type PGE mineralization. The sample chamber can be seen as an analogue of the massive sulfides in the contact-type deposits and the graphite capsule as footwall lithologies (e.g., the Sudbury breccia). It is important to underscore that the comparison between the graphite capsule and the Sudbury breccia is not from the point of view of chemical composition. The graphite capsules used for these experiments are composed of small graphite grains pressed together and a certain degree of porosity is present. Similarly, the Sudbury breccia is composed of fragments of various dimensions immersed in a finer matrix (Dressler, 1984) that may allow some porosity. In the experiments, the graphite capsule behaved as a low-porosity and low-permeability medium, through which some material could move. The materials were moving from the main sulfide

chamber through the graphite using pores and micro-fractures that constitute a preferential pathway for migration. Therefore, in both the experimental setup and the natural system, material moved from a source of massive sulfides (the sample chamber/contact ores) into a semi-permeable porous medium (the graphite capsule/Sudbury breccia) through pores and microfractures.

The experiments show a vertical differentiation with Cu-Ni-rich sulfides (in this case bornite-dominated) gathering at the bottom of the sample chamber. Similarly, in the natural environment, differentiated sulfide liquids, Cu, Ni, Au, Pd and Pt dominate the veins that intrude the footwall, but that are often still physically connected to the contact-type deposits (Farrow et al., 2005). The parallelism between experiments and natural occurrence supports the models suggesting that, during the cooling of the SIC, differentiated PGE-bearing Cu-rich sulfide liquids intruded the breccia from embayments and troughs in which the sulfide melts had collected, thus forming the stockwork of the sharp-walled veins (Morrison et al., 1994; Naldrett et al., 1994). Then, from the newly-formed veins and from the massive sulfides of the contact deposits S-bearing vapor phases would transport Au, Pd, Pt and other elements (including As, Te and Bi) through the porous matrix of the Sudbury Breccia and form the PGM found in the footwall.

As observed in experimental results, mobility is faster at higher temperature. In shorter run times, the halos of high-temperature experiments covered a greater distance through the capsule. As a consequence, the presence of Au-Pd-Pt-bearing PGM that fractionated from the SIC should be observable in the footwall at a distance proportional to the extension of the thermal aureole. In other words, Pt, Pd and Au can be efficiently mobilized up to where the 600 °C isotherm reached its maximum extension, with a decrease in Pt mobility between 800 °C and 600 °C, as the Pt mobilization in this temperature range is less effective. Figure 10 shows a proposed general

model for the expected mobility of Pt, Pd, Au and Rh due solely to S gas transport. IN this model, sharp-walled veins, originating from contact ores, intrude the Sudbury breccia. Platinum, Pd, Au and minor Rh, present in the contact ores and in the sharp-walled veins, are transported and form a dispersion halo that irradiates from the contact ores into the footwall breccia, up to where the 800 ℃ isotherm reached its maximum width. Palladium and Au move farther, approximately up to the maximum width of the 600 ℃ isotherm. Locally, especially around hotter "anomalies" in the footwall, such as the sharp walled veins, the isotherms bend, following the extension and orientation of the veins (as depicted in the close-up of Figure 10). Although the position and extension of the isotherms cannot be determined from the experimental results, Péntek et al. (2008) suggested, for the area around Broken Hammer, in the North Range, that the footwall reached temperatures of 600 °C up to 300 m from the contact. In the South Range, the thermal aureole was probably wider, as shown by the high temperature (~ 780 °C) two-pyroxene assemblage reported in hornfels up to 725 m from the contact (Jørgensen et al., 2011). Consequently, the possible extension of a dispersion halo of PGM-bearing disseminated sulfides might have potentially reached comparable distances.

The results of the experiments indicate that hydrothermal fluids are not required to mobilize these ore metals. The proposed model does not exclude the role that late or post-magmatic hydrothermal fluids had in the mineralization process, as the common presence of hydrous alteration minerals such as epidote indicate. However, our results suggest that hydrothermal fluids are not necessary to begin the differentiation and mobilization processes of Pt, Pd and Au metals and that fractionation and mobilization of the HSE were triggered and driven by the heat irradiating from the cooling SIC.

2.7. Conclusions

The results of this study add new information on the behavior of HSE and metalloids in sulfide systems under pressure and temperature appropriate to late magmatic and metamorphic conditions, helping to improve the knowledge of processes that lead to the formation of ore deposits.

In particular, it was determined that:

1. Gold, Pt, Pd and, to a minor extent, Rh can be fractionated from Ru, Re, Os and Ir at temperatures between 900 °C and 600 °C. This range of temperatures is lower than those used in most previous experimental studies and spans from late magmatic stage of sulfide liquids to subsolidus temperature of the sulfide system.
2. Metalloids (As, Te, Bi) were initially suspected to be the cause of fractionation and mobilization. Metalloids can sequester Pt and Pd (Helmy et al., 2007) and retain them in metalloid liquids that are stable at low temperatures (Hoffman and MacLean, 1976), but our results do not show evidence of PGE-bearing metalloid liquids percolation through the porous graphite. Furthermore, the formation of a dispersion halo in metalloid-free and OH-bearing experiments indicates that Au, Pt, Pd and Rh are mobilized but that metalloids are not the mobilizing agents.
3. The observed mobility in nominally anhydrous experiments indicate that hydrothermal fluids are not necessary to fractionate and mobilize Au, Pd, Pt and Rh.

4. The results are consistent with the findings of Peregoedova et al. (2006) documenting Au, Pd, and Pt transport by a 'sulfur-dominated vapor' at 1000 °C and extend the possible effect of S-dominated volatiles as transporting agents down to 600 °C.

The experimental results show similarities with the footwall-type deposits of the SIC. In both Au, Pd and Pt are dispersed from massive sulfides into the surrounding material, at temperatures consistent with those attained within the width of the SIC thermal aureole.

Acknowledgements

This manuscript is part of the Ph.D. thesis of the first author. Funded by NSERC, CEMI, Vale and Sudbury Integrated Nickel Operations (CRD grant). We would like to thank Sandra Clarke (GeoLabs) for her help with the SEM.

References

Ames, D.E. and Farrow, C.E.G., 2007, Metallogeny of the Sudbury mining camp, Ontario, *in* Goodfellow, W.D., ed., Mineral Deposits of Canada: A Synthesis of Major Deposit-Types, District Metallogeny, the Evolution of Geological Provinces, and Exploration Methods, Special Publication 5 ed., Geological Association of Canada, Mineral Deposits Division, p. 329.

Armitage, P.E.B., McDonald, I., Edwards, S.J. and Manby, G.M., 2002, Platinum-group element mineralization in the Platreef and calc-silicate footwall at Sandsloot, Potgietersrus District,

South Africa: Transactions of the Institution of Mining and Metallurgy. Section B-Applied Earth Science, v. 111, p. B36-B45.

Arnold, R.G., 1962, Equilibrium relations between pyrrhotite and pyrite from 325° to 743 °C.: Economic Geology, v. 57, p. 72-90.

Bailey J., Lafrance B., McDonald A.M., Fedorowich J.S., Kamo S. and Archibald D.A., 2004, Mazatzal-Labradorian-age (1.7-1.6 Ga) ductile deformation of the South Range Sudbury impact structure at the Thayer Lindsley mine, Ontario: Canadian Journal of Earth Sciences, v. 41, p. 1491-1505.

Baker, D.R., Barnes, S.J., Simon, G. and Bernier, F., 2001, Fluid Transport of sulfur and metals between sulfide melt and basaltic melt: Canadian Mineralogist, v. 39, p. 537-546.

Ballhaus, C., Tredoux, M. and Späth, A., 2001, Phase Relations in the Fe-Ni-Cu-PGE-S System at Magmatic Temperature and Application to Massive Sulphide ores of the Sudbury Igneous Complex: Journal of Petrology, v. 41, p. 1911-1926.

Barnes, S.J., Cox, R.A. and Zientek, M.L., 2006, Platinum-group element, Gold, Silver and Base Metal distribution in compositionally zoned sulfide droplets from the Medvezky Creek Mine, Noril'sk, Russia: Contributions to Mineralogy and Petrology, v. 152, p. 187-200.

Barnes, S.J., Makovicky, E., Makovicky, M., Rose-Hansen, J. and Karup-Moller, S., 1997, Partition coefficients for Ni, Cu, Pd, Pt, Rh and Ir between monosulfide solid solution and sulfide liquid and the formation of compositionally zoned Ni-Cu sulfide bodies by fractional crystallization of sulfide liquid: Canadian Journal of Earth Sciences, v. 34, p. 366-374.

Barnes, S.J., Naldrett, A.J. and Gorton, M.P., 1985, The origin of the fractionation of the platinum-group elements in terrestrial magmas: Chemical Geology, v. 53, p. 303-323.

Boyd, F.R. and England, J.L., 1960, Apparatus for Phase-Equilibrium Measurements at Pressures up to 50 kilobar and Temperatures up to 1750 °C. : Journal of Geophysical Research, v. 65, p. 741-748.

Cabri, L.J. and Laflamme, J.H.G., 1976, The Mineralogy of the platinum-Group Elements from Some Copper-Nickel Deposits of the Sudbury Area, Ontario: Economic Geology, v. 71, p. 1159-1195.

Chesterman, C.W., 1979, National Audubon Society Field Guide to North American Rocks and Minerals, Knopf Doubleday Publishing Group.

Dietz, R.S., 1964, Sudbury Structure as an Astrobleme: Journal of Geology, v. 72, p. 412-434.

Djon, M.L.N. and Barnes, S.J., 2012, Changes in sulfides and platinum-group minerals with the degree of alteration in the Roby, Twilight and High Grade Zones of the Lac-des-Iles Complex, Ontario, Canada: Mineralium Deposita, v. 47, p. 875-896.

Dressler, B.O., 1984, The Effects of the Sudbury Event and the Intrusion of the Sudbury Igneous Complex on the Footwall Rocks of the Sudbury Structure, *in* Pye, E.G., Naldrett, A.J. and Giblin, P.E., eds., The Geology and Ore Deposits of the Sudbury Structure, Special Volume 1 ed., Ontario Geological Survey, p. 97-132.

Ebel, D.S. and Naldrett, A.J., 1996, Fractional crystallization of sulfide ore liquids at high temperatures: Economic Geology, v. 91, p. 607-621.

Farrow, C.E.G. and Jolette, C., 2004, Sudbury Cu-PGE environments: Defining 'sharp-walled' and 'low-sulphide' systems: Abstract SS113-06, GAC-MAC Annual Meeting, May 12, 2004, St. Catherines, Ontario, Geological Association of Canada, St. Catherines, Proceedings, p. 248.

Farrow, C.E.G. and Lightfoot, P.C., 2002, Sudbury PGE revisited: Toward an Integrated model, *in* Cabri, L.J., ed., The Geology, Geochemistry, Mineralogy and Mineral Beneficiation of Platinum Group Element, Special Volume 54 ed., Canadian Institute of Mining, Metallurgy and Petroleum, p. 13.

Farrow, C.E.G., Everest, J.O., King, D.M. and Jolette, C., 2005, Sudbury Cu-(Ni)-PGE systems: Refining the classification using McCreedy West mine and Podolsky project case studies, *in* Mungall, J.E., ed., Exploration for Deposits of Platinum-Group Elements, Short Course Series 35 ed., Mineralogical Association of Canada, p. 163.

Fleet, M.E. and Wu, T.W., 1993, Volatile transport of platinum-group elements in sulfide-chloride assemblages at 1000 ℃: Geochimica et Cosmochimica Acta, v. 57, p. 3519-3531.

Fleet, M.E. and Wu, T.W., 1995, Volatile transport of precious metals at 1000 ℃: Speciation, fractionation, and effect of base-metal sulfide: Geochimica et Cosmochimica Acta, v. 59, p. 487-495.

French, B.M., 1967, Sudbury Structure, Ontario: Some Petrographic Evidence for Origin by Meteorite Impact: Science, v. 156, p. 1094-1098.

Frost, B.R., Mavrogenes, J.A. and Tomkins, A.G., 2002, Partial melting of sulfide ore deposits during medium- and high-grade metamorphism: Canadian Mineralogist, v. 40, p. 1-18.

Garuti, G., Zaccarini, F., Proenza, J.A., Thalhammer, O.A.R. and Angeli, N., 2012, Platinum-Group Minerals in Chromitites of the Niquelândia Layered Intrusion (Central Goias, Brazil): Their Magmatic Origin and Low-Temperature Reworking during Serpentinization and Lateritic Weathering: Minerals, v. 2, p. 365-384.

Grieve, R.A.F., 1994, An Impact Model of the Sudbury Structure, *in* Lightfoot, P.C. and Naldrett, A.J., eds., Proceedings of the Sudbury-Noril'sk Symposium, Special Volume 5, Ontario Geological Survey, p. 119-132.

Grokhovskaya, T.L., Lapina, M.I. and Mokhov, A.V., 2009, Assemblages and Genesis of Platinum-Group Minerals in Low-Sulfide Ores of the Monchetundra Deposit, Kila Peninsula, Russia: Geology of Ore Deposits, v. 51, p. 467-485.

Hanley, J.J., Mungall, J.E., Pettke, T., Spooner, E.T.C. and Bray, C.J., 2005, Ore metal redistribution by hydrocarbon-brine and hydrocarbon-halide melt phases, North Range footwall of the Sudbury Igneous Complex, Ontario, Canada: Mineralium Deposita, v. 40, p. 237-256.

Helmy, H.M., Ballhaus, C., Berndt, J., Bockrath, C. and Wohlgemuth-Ueberwasser, C., 2007, Formation of Pt, Pd and Ni tellurides: experiments on sulphide-telluride systems: Contributions to Mineralogy and Petrology, v. 153, p. 577-591.

Helmy, H.M., Ballhaus, C., Wohlgemut-Ueberwasser, C., Fonseca, R.O.C. and Laurenz, V., 2010, Partitioning of Se, As, Sb, Te and Bi between monosulfide solid solution and sulfide melt – Application to magmatic sulfide deposits: Geochimica et Cosmochimica Acta, v. 74, p. 6174-6179.

Hoffman, E. and MacLean, W.H., 1976, Phase Relations of Michenerite and Merenskyite in the Pt-Bi-Te System: Economic Geology, v. 71, p. 1461-1468.

Hudson, D.R., 1986, Platinum-Group Minerals from the Kambalda Nickel Deposits, Western Australia: Economic Geology, v. 81, p. 1218-1225.

Jakobsson, S., 2012,Oxygen fugacity control in piston-cylinder experiments: Contributions to Mineralogy and Petrology, v. 164, p. 397-406.

Jørgensen, T.R.C., Tinkham, D.K. and Lesher, C.M., 2011, Identification of Pyroxene Hornfels Facies Mafic Rocks Within the Metamorphic Aureole of the South Range of the Sudbury Igneous Complex, ON, Canada. Abstract S29-3, The Geological Society of America Annual Meeting, Oct. 9-12 2011, Minneapolis, MN, USA, Proceedings, p. 91.

Keays, R.R., Sewell, D.K.B. and Mitchell, R.H., 1981, Platinum and palladium minerals in upper mantle-derived lherzolites: Nature, v. 294, p. 646-648.

Kerr, M., Hanley, J., Morrison, G., Everest, J. and Bray, C., 2015, Preliminary Evaluation of Trace Hydrocarbon Speciation and Abundance as an Exploration Tool for Footwall-Style Sulfide Ores Associated with the Sudbury Igneous Complex, Ontario, Canada: Economic Geology, v. 110, p. 531-556.

Krogh, T.E., Davis, D.W. and Corfu, F., 1984, Precise U-Pb Zircon and Baddeleyite Ages for the Sudbury Area, *in* Pye, E.G., Naldrett, A.J. and Giblin, P.E., eds., The Geology and Ore Deposits of the Sudbury Structure, Special Volume 1 ed., Ontario Geological Survey, p. 431-447.

Kullerud, G., Yund, R.A. and Moh, G.H., 1969, Phase Relations in the Cu-Fe-S, Cu-Ni-S, and Fe-Ni-S Systems: Economic Geology Monograph 4, p. 323-343.

Li, C., Naldrett, A.J., Coates, C.J.A. and Johannssen, P., 1992, Platinum, palladium, gold and copper-rich stringers at the Strathcona mine, Sudbury: Their enrichment by fractionation of a sulfide liquid: Economic Geology, v. 87, p. 1584-1598.

Lightfoot, P.C., Keays, R.D. and Doherty, W., 2001, Chemical Evolution and Origin of Nickel Sulfide Mineralization in the Sudbury Igneous Complex, Ontario, Canada: Economic Geology, v. 96, p. 1855-1875.

Molnár, F., Watkinson, D.H. and Jones, P.C., 2001, Multiple Hydrothermal Processes in Footwall Units of the North Range, Sudbury Igneous Complex, Canada, and Implications for the Genesis of Vein-Type Cu-Ni-PGE Deposits: Economic Geology, v. 96, p. 1645-1670.

Morrison, G.G., Jago, B.C. and White, T.L., 1994, Footwall mineralization of the Sudbury Igneous Complex, *in* Lightfoot, P.C. and Naldrett, A.J., eds., Proceedings of the Sudbury-Noril'sk Symposium, Special Volume 5, Ontario Geological Survey, p. 57-64.

Mungall, J.E. and Brenan, J.M., 2014, Partitioning of platinum-group elements and Au between sulfide liquid and basalt and the origins of mantle-crust fractionation of the chalcophile elements: Geochimica et Cosmochimica Acta, v. 125, p. 265-289.

Naldrett, A.J., 1984, Mineralogy and composition of the Sudbury ores, *in* Pye, E.G., Naldrett, A.J. and Giblin, P.E., eds., The Geology and Ore Deposits of the Sudbury Structure , Special Volume 1 ed., Ontario Geological Survey, p. 309-326.

Naldrett, A.J., 2004, Magmatic Sulfide Deposits: Geology, Geochemistry and Exploration, Springer, 732 p.

Naldrett, A.J., Pessaran, R., Asif, M. and Li, C., 1994, Compositional variation in the Sudbury ores and prediction of the proximity of footwall copper-PGE ore bodies, *in* Anonymous , Special Volume 5 ed., Ontario Geological Survey, p. 133-146.

Nelles, E.W., 2012, Genesis of Cu-PGE-rich Footwall-Type Mineralization in the Morrison Deposit, Sudbury: Sudbury, M.Sc. Thesis, Laurentian University.

Patiño Douce, A.E. and Beard, J.S., H_2O loss from hydrous melts during fluid-absent piston-cylinder experiments: American Mineralogist, v. 79, p. 585-588.

Péntek, A., Molnár, F., Watkinson, D.H. and Jones, P.C., 2008, Footwall-type Cu-Ni-PGE Mineralization in the Broken Hammer Area, Wisner Township, North Range, Sudbury Structure: Economic Geology, v. 103, p. 1005-1028.

Peregoedova, A., Barnes, S.J. and Baker, D.R., 2006, An experimental study of mass transfer of platinum-group elements, gold, nickel and copper in sulfur-dominated vapor at magmatic temperatures: Chemical Geology, v. 235, p. 59-75.

Prichard, H.M., Hutchinson, D. and Fisher, P.C., 2004, Petrology and Crystallization History of Multiphase Sulfide Droplets in a Mafic Dike from Uruguay: Implications for the Origin of Cu-Ni-PGE Sulfide Deposits: Economic Geology, v. 99, p. 365-376.

Raharimahefa, T., Lafrance, B. and Tinkham, D,K,, 2014, New structural, metamorphic, and U-Pb geochronological constraints on the Blezardian Orogeny and Yavapai Orogeny in the Southern Province, Sudbury, Canada: Canadian Journal of Earth Sciences, v. 51, p. 750-774.

Rousell, D.H., 1984, Structural Geology of the Sudbury Basin, *in* Pye, E.G., Naldrett, A.J. and Giblin, P.E., eds., The Geology and Ore Deposits of the Sudbury Structure, Special Volume 1 ed., Ontario Geological Survey, p. 83-96.

Schilling, F. and Wunder, B., 2004, Temperature distribution in piston-cylinder assemblies: Numerical simulations and laboratory experiments: European Journal of Petrology, v. 16, p. 7-14.

Sneeringer, M.A. and Watson, E.B., 1985, Milk cartons and ash cans: two unconventional welding techniques: American Mineralogist, v. 70, p. 200-201.

Therriault, A.M., Fowler, A.D. and Grieve, R.A.F., 2002, The Sudbury Igneous Complex: A Differentiated Impact Melt Sheet: Economic Geology, v. 97, p. 1521-1540.

Tomkins, A.G., 2010, Wetting facilitates late-stage segregation of precious metal-enriched sulfosalt melt in magmatic sulfide systems: Geology, v. 38, p. 951-954.

Tomkins, A.G., Pattison, D.R. and Frost, B.R., 2007, On the Initiation of Metamorphic Sulfide Anatexis: Journal of Petrology, v. 48, p. 511-535.

Truckenbrodt, J. and Johannes, W., 1999, H_2O loss during piston-cylinder experiments: American Mineralogist, v. 84, p. 1333-1335.

Wang, C.Y., Prichard, H.M., Zhou, M.-. and Fisher, P.C., 2008, Platinum-group minerals from the Jinbaoshan Pd-Pt deposit, SW China: evidence for magmatic origin and hydrothermal alteration: Mineralium Deposita, v. 43, p. 791-803.

Wood, C.R. and Spray, J.G., 1998, Origin and Emplacement of Offset Dykes in the Sudbury impact Structure: Constraints form Hess: Meteoritics & Planetary Science, v. 33, p. 337-347.

Yund, R.A. and Kullerud, G., 1966, Thermal Stability of Assemblages in the Cu-Fe-S System, v. 7, p. 454-488.

Zieg, M.J. and Marsh, B.D., 2005, The Sudbury Igneous Complex: Viscous emulsion differentiation of a superheated impact melt sheet: Geological Society of America Bulletin, v. 117, p. 1427-1450.

Tables

Table 1. Composition of the sulfide mixture used as starting materials.

	Sulfide mixture	
	Wt. %	**At.%**
Fe	42.22	33.23
Ni	12.75	9.86
Cu	11.03	9.21
S	33.99	47.70
Total	100.00	100.00
ΣM/S		1.10

Table 2. Composition of the highly siderophile element mixtures.

(Wt. %)	PGE 1	PGE 2	HSE mix
Ru	8.90	10.99	7.62
Rh	9.00	11.19	7.75
PdS	12.10	15.05	10.44
Re			14.03
Os	16.68	20.67	14.33
Ir	16.81	20.89	14.48
Pt	17.11	21.21	14.70
Au_2O_3	19.41		16.65
Total	100.00	100.00	100.00

Table 3. Summary of the experimental conditions.

Run	Type of HSE mixture[1]	Metalloid or hydroxide	HSE to metalloid mix mass ratio	Sulfide mix to HSE mix mass ratio	Total weight loaded (mg)	T (°C)	Run time (hrs)[2]	Capsule material
FC-92	HSE	Te	1:1	50:1	50.9	900	48	Pt
FC-84	HSE	none	N/A	50:1	50.1	900	48	Pt
FC-81	HSE	Te and Bi	1:1	50:1	50.5	900	48	Pt
FC-79	HSE	As	1:1	50:1	56.8	900	48	Pt
FC-76	HSE	Te, As, Bi, OH	1:2	50:1		900	48	Pt
FC-74	HSE	OH	1:1	50:1	52.9	900	48	Pt
FC-62	HSE	Bi	2:1	50:1	52.9	900	36	AuPd
FC-83	HSE	none	N/A	50:1	48.5	800	96	Pt
FC-82	HSE	As	1:1	50:1	50.0	800	96	Pt
FC-64	HSE	Bi	2:1	50:1	53.3	800	72	AuPd
FC-57	PGE 2	Te	5:1	10:1	54.3	800	96	AuPd
FC-80	HSE	OH	1:1	50:1	52.9	700	144	Pt
FC-67	HSE	As	2:1	50:1	51.2	700	168	Pt
FC-66	HSE	Bi	2:1	50:1	50.8	700	168	Pt
FC-58	PGE 2	none	N/A	10:1	53.2	700	168	AuPd
FC-56	PGE 1	Te	5:1	10:1	54.4	700	144	AuPd
FC-77	HSE	OH	1:1	50:1	51.8	600	504	Pt
FC-69	HSE	As	2:1	50:1	52.6	600	336	Pt
FC-68	HSE	Bi	2:1	50:1	52.7	600	288	Pt
FC-54	PdS	Te	1:2	10:1	53.0	600	240	AuPd
FC-65	HSE	As	2:1	50:1	51.2	550	504	Pt
FC-70	PGE 2	Te	5:1	50:1	38.1	550	504	Pt
FC-60b	PGE 2	none	N/A	10:01	56.9	500	504	AuPd

[1]The sulfide mixture in all experiments was: 66.4 wt.% FeS, 19.7 % NiS, 13.8 % Cu2S. The compositions of PGE1, PGE2 and HSE mixtures are listed in table 2.

[2]Run time does not include ramp up. Assemblies were pre-pressurized to 0.55 GPa (run P + 10%) before heating, then P was adjusted to 0.5 GPa for the duration of the experiments.

Table 4. Summary of the main distinguishing features observed in experimental products.

T (ºC)	Metalloid or hydroxide	Sample chamber	Halo	
		Domain separation	Extension through the graphite	HSE present[1]
900	Te	Sharp	Complete	Pt
	Bi	Not recovered	Complete	Pt, Pd, Au, Rh
	As	Sharp	Complete	Pd, Pt, Au
	OH	Sharp	Complete	Pd, Pt, Au
	none	Sharp	Complete	Pt, Au, Pd
	Te and Bi	Sharp	Complete	Pd, Pt, Au
	Te, As, Bi, OH	Not visible	Complete	Pt, Au, Pd
800	Te	Gradational	Complete	Pd, Pt, Au
	Bi	Gradational	Partial	Pd, Au, Pt, Rh
	As	Gradational	Partial	Pt, Rh, Au
	none	Gradational	Partial	Au, Pd, Rh
700	Te	Not visible	Limited	Au, Pd, Rh
	Bi	Very gradational	Limited	Au, Pd, Pt, Rh
	As	Not visible	Very limited	Au
	OH	Very gradational	No halo observed	
	none	Not visible	Very limited	Pd, Rh
600	Te	Not visible	Limited	Pd
	Bi	Not visible	No halo observed	
	As	Not visible	No halo observed	
	OH	Not visible	Limited	Pd, Au, Pt, Rh
550-500	Te	Not visible	No halo observed	
	As	Not visible	No halo observed	
	none	Not visible	Limited	Pd, Au, Rh, Pt

[1]HSE are listed in order of relative abundance.

Table 5. Average composition of synthesized sulfides (semi-quantitative EDS, normalized to 100 at. %).

T (°C)	Phase[2]	n[3]	S		Fe		Ni		Cu		Total	ΣM/S
			at.%	2σ	at.%	2σ	at.%	2σ	at.%	2σ		
900	mss[1]	6	50.44	0.86	40.31	3.65	7.07	2.3	2.17	2.04	100	0.98
	bn_{ss}	4	42.09	1.74	15.16	4.84	1.26	2.23	41.49	8.51	100	1.38
	pn	5	46.85	1.91	28.15	4.53	20.14	5.21	4.86	8.03	100	1.13
	iss	4	47.24	4.94	27.16	3	9.18	10.76	16.42	6.24	100	1.12
800	mss	4	49.99	0.65	44.63	4.58	4.17	4.17	1.22	0.46	100	1
	bn_{ss}	4	39.78	0.43	14.63	2.81	4.36	2.62	41.22	3.53	100	1.51
	pn	3	46.24	0.79	29.89	7.7	19.27	2.03	4.59	7.45	100	1.16
	iss	2	43.37	0.56	23.98	2.92	9.79	3.37	22.86	6.84	100	1.31
700	mss	5	49.76	1.52	44.09	1.97	4.36	1.79	1.79	1.49	100	1.01
	bn_{ss}	4	39.76	5.53	14.72	8.14	4.09	3.83	41.43	16.55	100	1.52
	pn	4	45.92	1.21	29.96	5.04	18.19	3.29	5.93	2.35	100	1.18
	iss	1[4]	42.43	-	26.57	-	12.71	-	18.3	-	100	1.36
600	mss	4	49.63	1.03	42.38	5.87	5.7	3.38	2.28	3.57	100	1.01
	bn_{ss}	4	40.27	3.47	13.53	3.63	2.54	4.28	43.82	7.44	100	1.49
	pn	3	45.58	2.67	28.47	4.93	20.7	6.07	5.26	1.87	100	1.19
550-500	mss	2	50.08	0.05	39.72	5.28	8.44	7.15	1.76	1.82	100	1
	bn_{ss}	1	42.45	-	14.3	-	1.5	-	41.75	-	100	1.36
	pn	2	48.62	1.83	25	3.99	25.87	3.59	0.51	1.43	100	1.06

[1]Abbreviations: mss = monosulfide solid solution; bn_{ss} = bornite solid solution; pn = pentlandite; iss = intermediate solid solution.
[2]Averages and 2σ obtained on n analyses performed on sulfides products of experiments performed at the same temperature, regardless of the metalloid or hydroxide present in the starting materials.
[3]Phases recognized in one experiment only. All analyses from each phase are from one single experiment.
[4]Phase observed in one single analysis on one only product. 2σ could not be calculated on the base of one single datum.

Figures

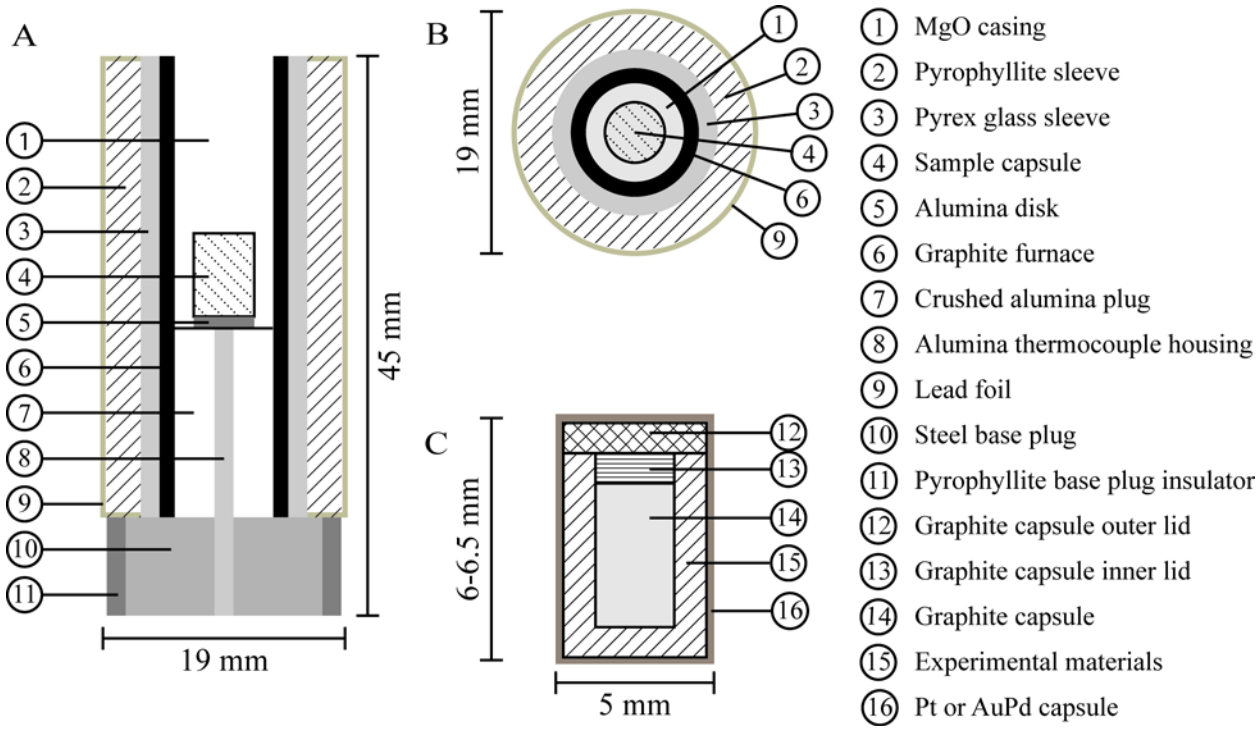

Figure 1. Schematic drawing of the experimental assembly used in the piston-cylinder experiments. A. Vertical section of the assembly. B. Horizontal section of the assembly. C. Vertical section of the sample capsule.

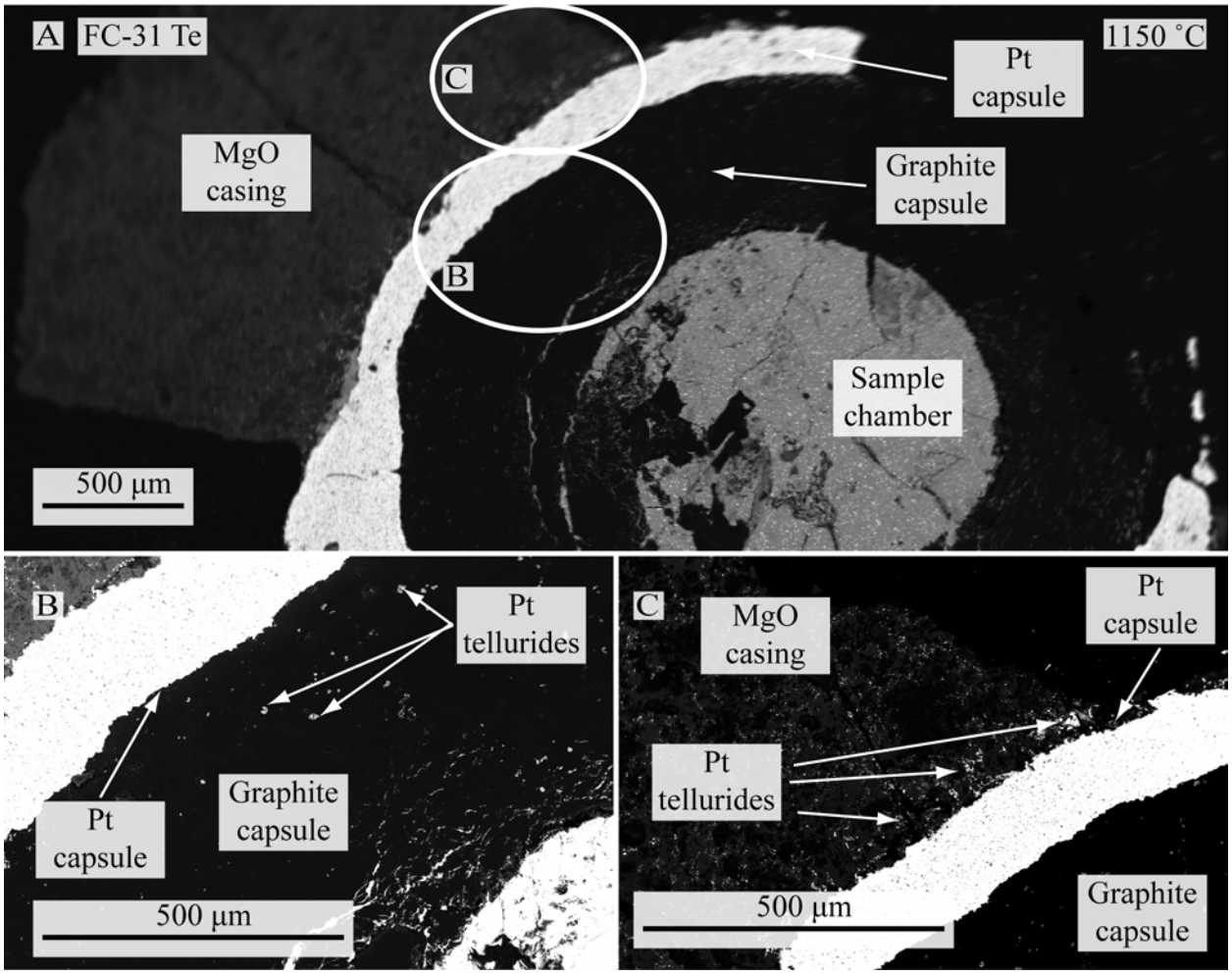

Figure 2. Back-scattered electron image (BSE) of the products of a failed experiment (FC-31), run at 1150 °C for 3 hours. A. Horizontal section of the experimental capsule. At the center, the sample chamber, surrounded respectively by the graphite capsule, the Pt capsule and the MgO casing. The areas highlighted in the ellipses are enlarged in B and C. B. Small Pt-tellurides within the graphite capsule, between the sample chamber and the Pt capsule. C. Dispersed Pt-tellurides outside the capsule. The porous texture of the Pt capsule, due to partial corrosion, can be observed.

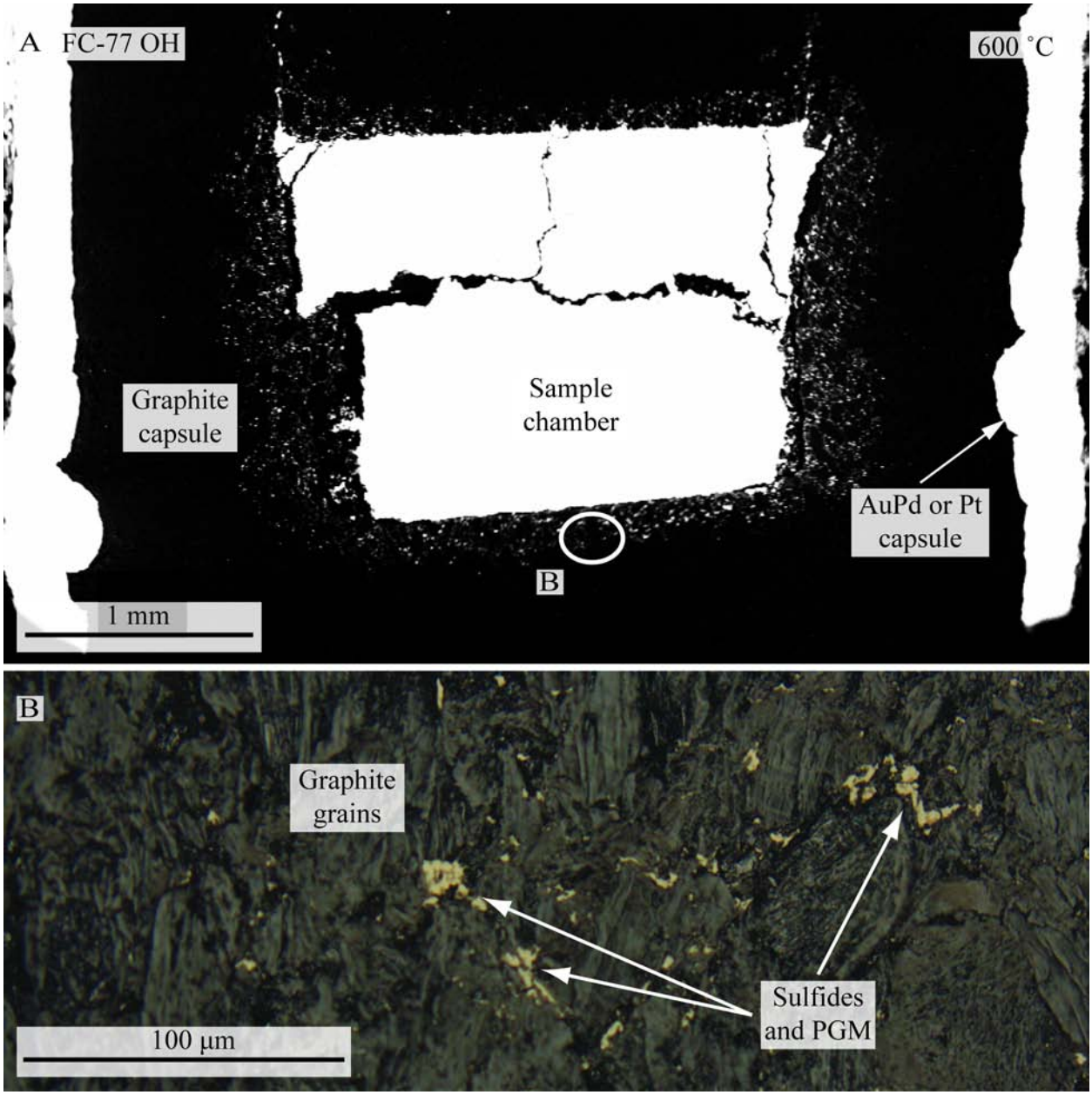

Figure 3. BSE image of the longitudinal section of a typical experimental product. A. OH-bearing experiment run at 600 °C for 504 hours. At the center of the capsule, the chamber with the product sulfides, surrounded by the graphite capsule in black, which is enclosed in the precious metal capsule (AuPd). A "dispersion halo" containing BMS and PGM formed around the main charge. The area encircled is enlarged in B. B. Reflected light optic image of a portion of the graphite. The dark grey and black areas are the compressed grains of graphite that form the graphite container. Sulfur, base metals and some PGE were transported through this low porosity material and precipitated forming the "halo" seen in A.

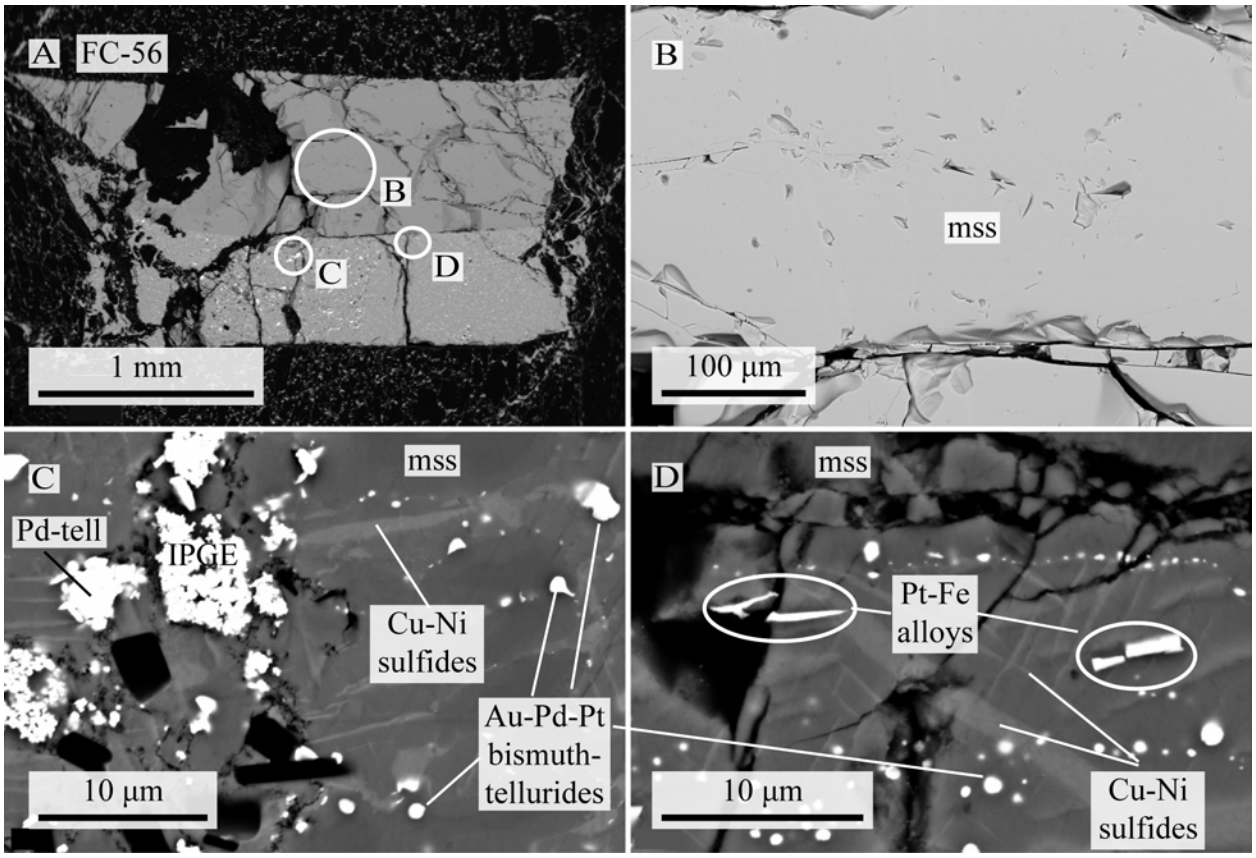

Figure 4. BSE images of the sample chamber of a Te-Bi-bearing experiment run at 900 °C for 48 hours (FC-81). A. General picture of the capsule sectioned longitudinally. The upper part of the photograph shows the superior portion of the capsule. It is possible to observe a sharp contact between the mss (upper portion) and the Cu-Ni-rich domain (lower portion). Three sulfide phases were observed in the lower portion: bornite solid solution, pentlandite and Ni-rich intermediate solid solution (bn_{ss}, pn and iss, respectively). B. Enlargement of the upper portion of the sample, with a texturally and compositionally homogeneous mss. C. Central portion of the sample. The dark gray is mss, whereas the light gray elongated exsolutions are Cu-Ni sulfides (bn and pn together) following crystallographic directions of mss. The large white minerals to the left are clusters of Pd-tellurides and mixtures of Ru, Re, Os and Ir. The small white rounded minerals to the right are Au-Pd (± Pt) bismuth-tellurides. The black subhedral crystals are silicates. D. At the very top of the figure, the mss, divided from the Cu-Ni sulfides by a fracture. The euhedral to subhedral PGM are Pt-Fe alloys, whereas the smaller rounded PGM are Au-Pd-Pt bismuth-tellurides.

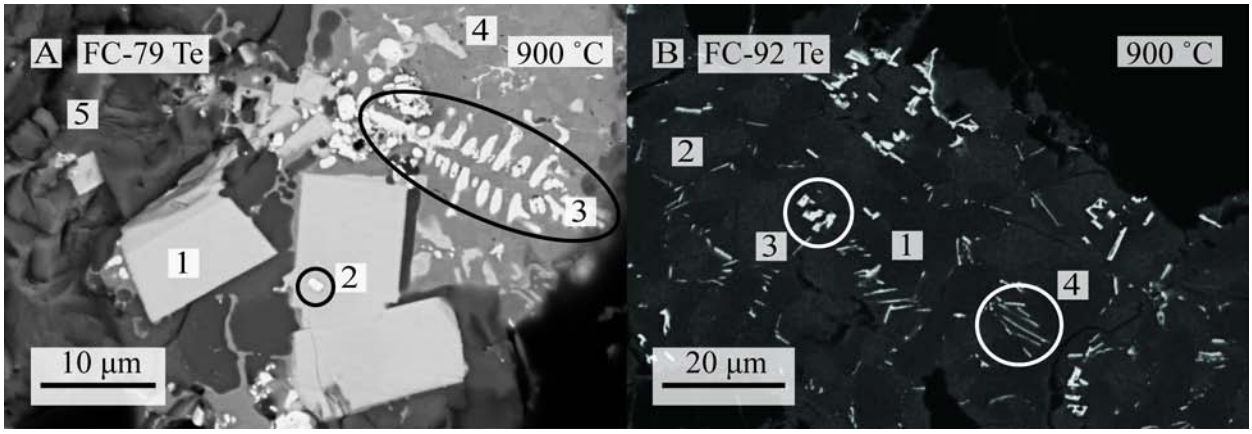

Figure 5. BSE images of Pt-bearing minerals in FC-79 and FC-92 (both at 900 °C). A. Arsenic bearing experiment (FC-79). The euhedral crystals (1) are Ir and Rh-bearing sperrylite. The inclusion highlighted in the circle on the central crystal (labeled with number 2) is a Re-Os-Ir alloy. The rounded symmetrical exsolutions with skeletal texture (in the oblique oval, labeled with number 3) contain Au, Cu, Ni, Pd, As and Fe. The area in (4) is composed of two Pd-Pt-bearing Ni-arsenides phases. The background (5) is mss (see table 4 for average composition). B. Te-bearing experiment (FC-92, 900 °C). The dark grey (1) is mss, the light grey (2) is bn_{ss}. The small cubic euhedral crystals (3) are Pt-Fe alloys, whereas the elongated smaller minerals (4) are tellurides. The high uncertainties are due to interference of the minerals surrounding the phase of interest that were too small to produce clear EDS spectra.

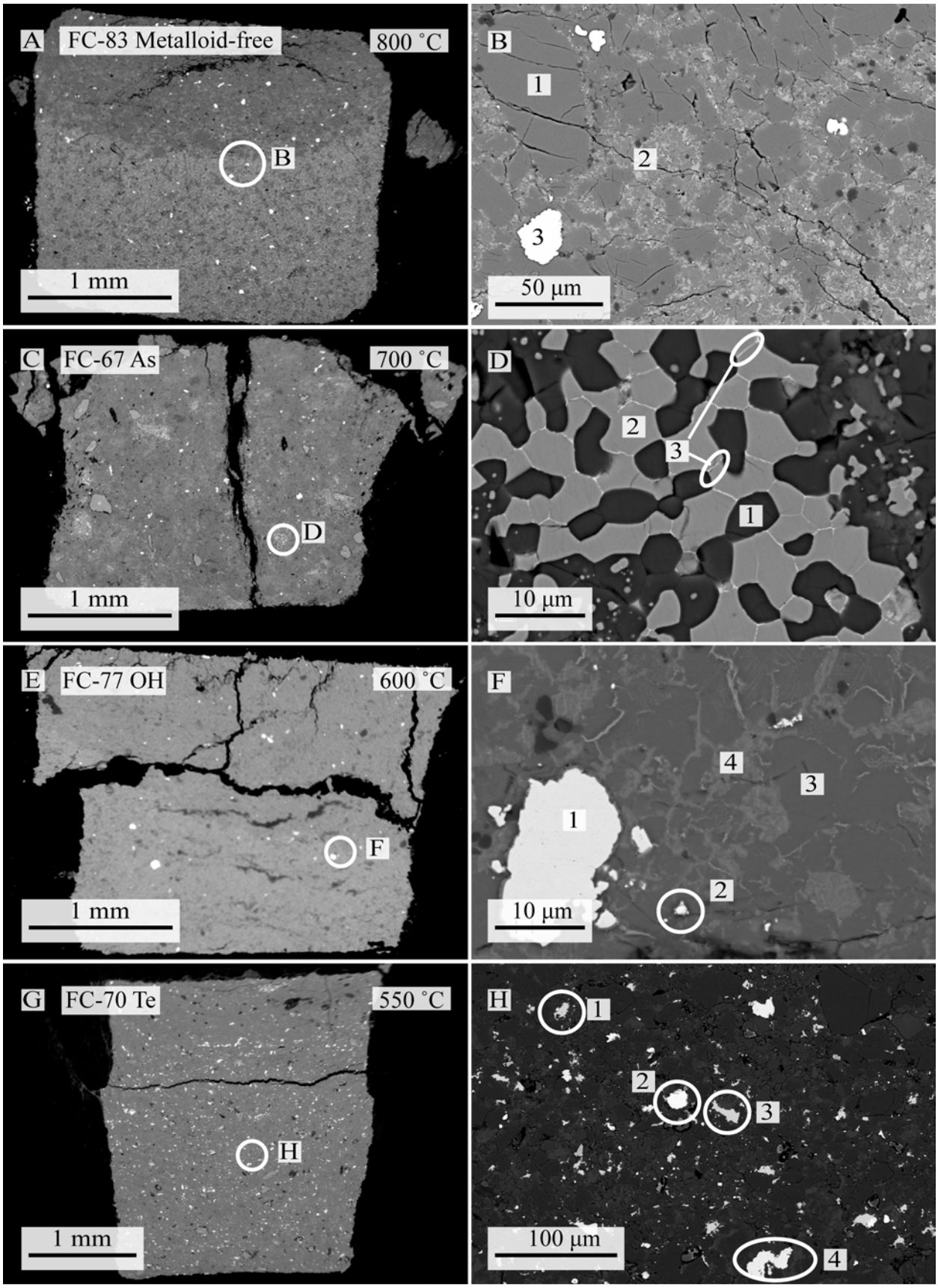
A
FC-83 Metalloid-free
800 °C
B
1 mm
B
1
2
3
50 μm
C
FC-67 As
700 °C
D
1 mm
D
2
3
1
10 μm
E
FC-77 OH
600 °C
F
1 mm
F
4
3
1
2
10 μm
G
FC-70 Te
550 °C
H
1 mm
H
1
2
3
100 μm
4

Figure 6. BSE images of four representative experiments showing variations of internal textures with decreasing temperature at 800 °C (96 hours, FC-83), 700 °C (168 hours, FC-67), 600 °C (504 hours, FC-77) and 550 °C (504 hours, FC-70). A. General BSE picture of the 800 °C metalloid-free experiment (FC-83). The division between mss and Cu-Ni-rich sulfide domain is present, but not as sharp as in the 900 °C experiments (Fig. 4). B. Enlargement of the circled area in A. Rounded mss crystals in dark gray are surrounded by interstitial Cu-Ni sulfides rich in Au, Pd and Pt exsolutions. The large white minerals (e.g., to the left of the picture) are Pt-Fe alloys. C. General BSE picture of the As-bearing experiment (700 °C, FC-67). The compositional division is no longer visible. D. Close-up of the circled area in C. The dark grey rounded grains (1) are mss, surrounded by Pd and Rh-bearing Ni arsenides (light gray, 2). The tiny exsolutions (3) at the grain boundaries of the arsenides are rich in Pt, but too small to analyze. E. General picture of the OH-bearing experiment (600 °C, FC-77). The circled area is enlarged in F. The large PGM (1) is an alloy containing Fe, Ir, Pt, Ni, Cu and Rh. The small ones (2) contain only Fe, Ni and Os. The sample is dominated by mss (dark gray, 3) associated with bornite (4). G. General picture of the Te-bearing experiment (550 °C, FC-70). No vertical segregation was observed. H. Enlargement of the area encircled in G. The sulfides show granular textures. No exsolution texture was observed in the experimental products at this temperature. The PGM in 1 contains mainly Ru, whereas (2) is an Ir-Fe alloy, (3) is a Rh-bearing telluride and (4) is a Pt-Fe alloy.

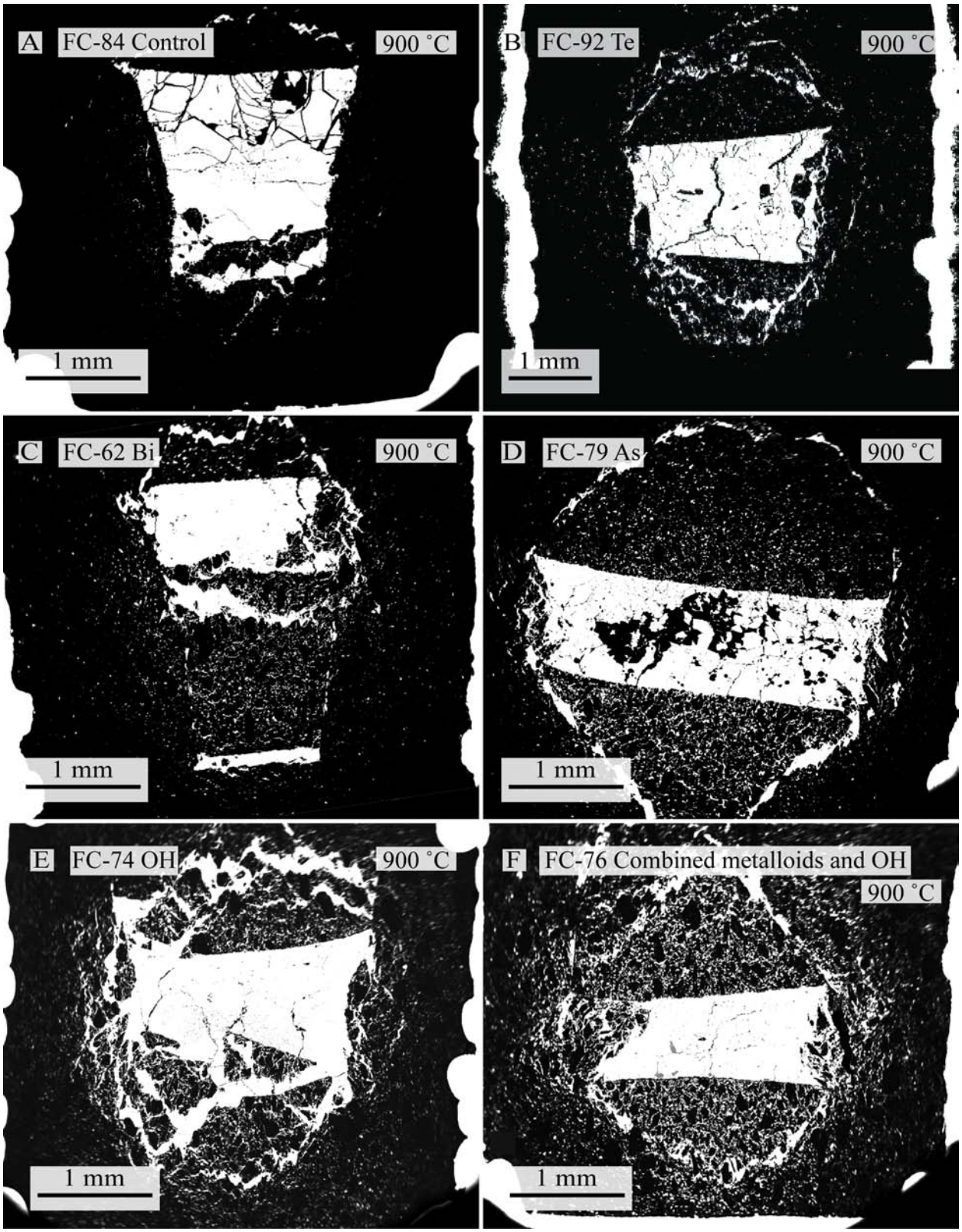

Figure 7. BSE images of the 900 °C experimental products (generally 48 hours, except FC-62, 36 hours). Brightness and contrast were enhanced to show the presence of the halo. A. FC-92, Te-bearing. B. FC-62, Bi-bearing. C. FC-79, As-bearing. D. FC-74, OH-bearing. E. FC-84, Metalloid-free (control experiment). F. FC-76, Te-Bi-As-OH-bearing. All the experiments performed at this temperature developed a halo that reached the AuPd or Pt capsule. The halo is composed

of sulfides and Au-Pd-Pt-(±Rh)-bearing PGM. The conjugate fractures on top and bottom of the sample are well visible in most of the experiments at this temperature.

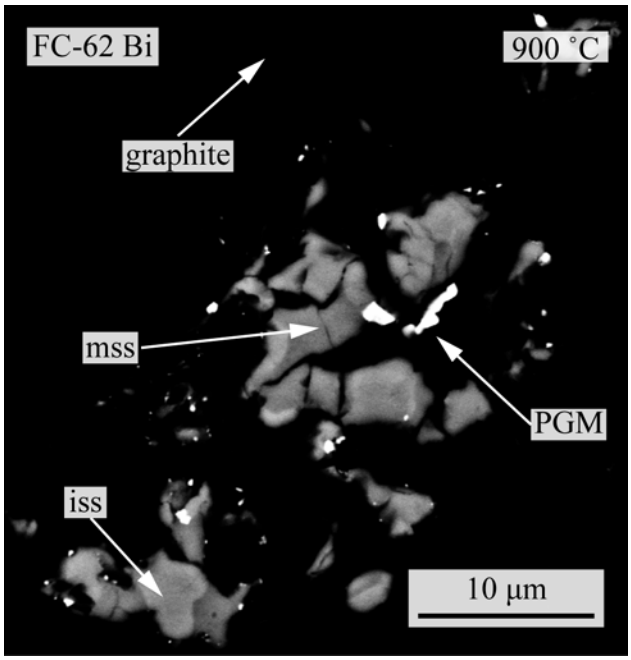

Figure 8. BSE detail of particles in the halo of the 900 °C Bi-bearing experiment (FC-62). The black background is the graphite capsule. The grey grains are sulfides: The dark grey is mss, whereas the slightly lighter gray is iss. The little white grains are PGM that contain Pd-Pt-Bi, Au-Pd-Pt-Bi and Pt-Fe-S. No composition of the PGM is documented because it was not possible to eliminate signal from the surrounding sulfides, due to their small size.

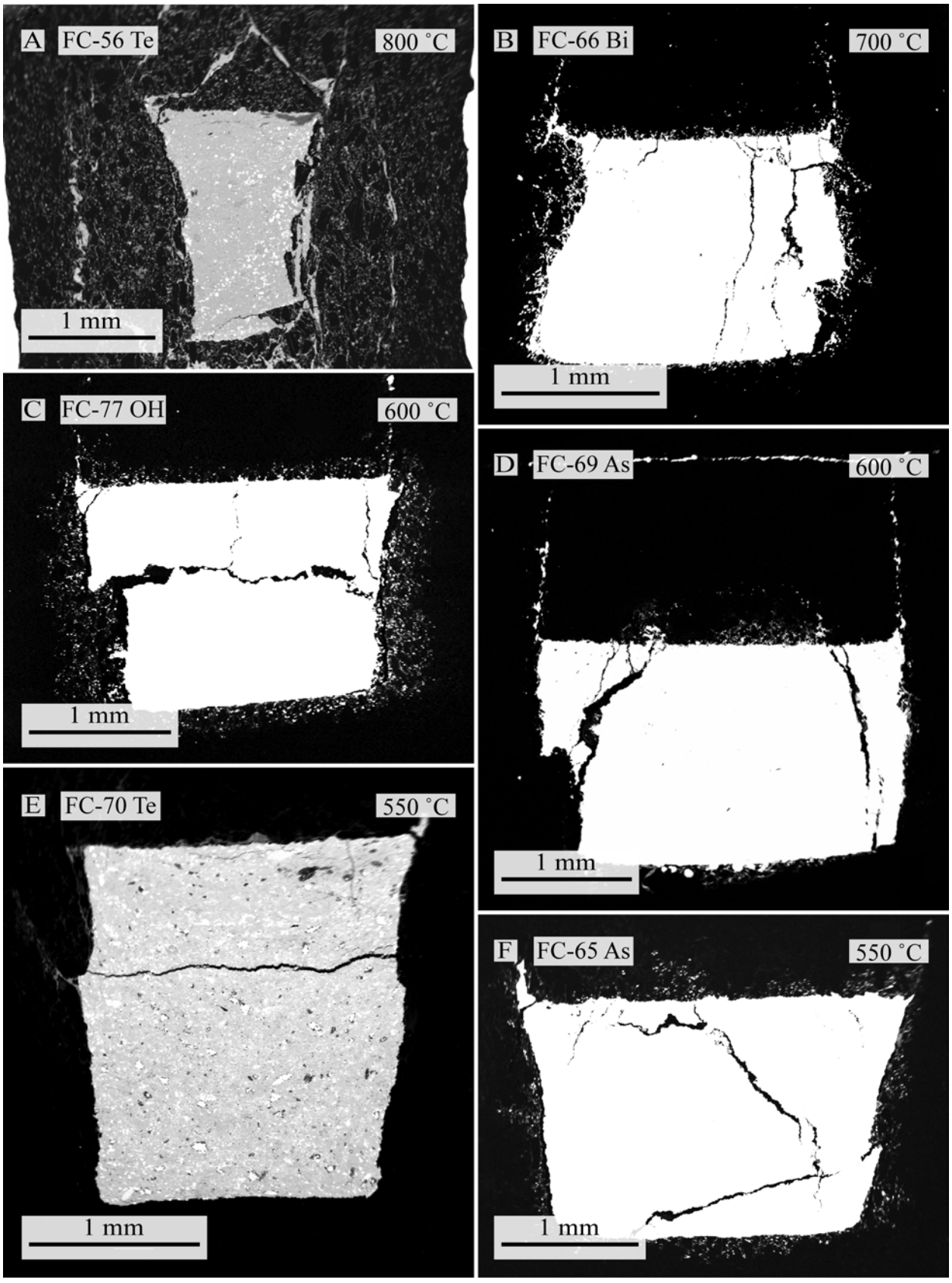
A
FC-56 Te
800 ˚C
1 mm
B
FC-66 Bi
700 ˚C
1 mm
C
FC-77 OH
600 ˚C
1 mm
D
FC-69 As
600 ˚C
1 mm
E
FC-70 Te
550 ˚C
1 mm
F
FC-65 As
550 ˚C
1 mm

Figure 9. Comparison of experimental products at decreasing temperature: the halo is progressively less wide from 800 °C (FC-57, Te-bearing in A) to 700 °C (FC-66, Bi-bearing, in B) and 600 °C (FC-77, OH-bearing, in C and FC-69, As-bearing in D) until it is completely absent in the Te-bearing experiment at 550 °C (FC-70, E), but weakly developed in the As-bearing experiment (FC-65, F).

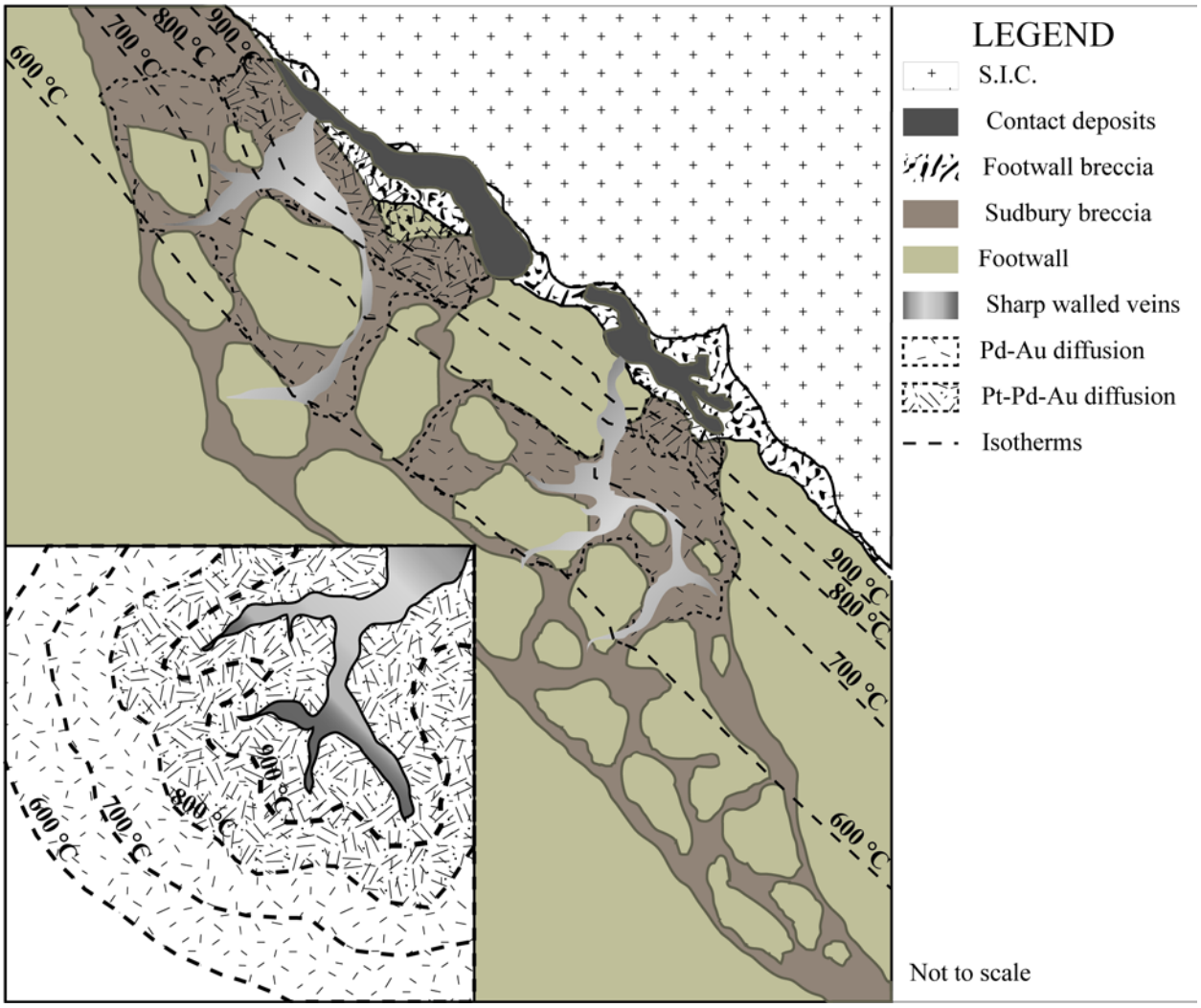

Figure 10. Proposed model for the influence of a thermal aureole on the mobility of Pd, Pt, and Au and the origin of the footwall deposits. Cu-Ni-PGE-rich differentiated sulfide liquids intrude the footwall forming sharp-walled veins that are progressively richer in denser bornite with increasing distance from the contact. The heat released from the cooling SIC allows Pt, Pd, Au and some base metals to migrate into the footwall (e.g., through Sudbury breccia). Platinum is transported only down to ~800 °C, whereas Pd and Au can be mobilized down to 600 °C, thus further away than Pt from the contact of the SIC. The enlargement depicts isotherms being influenced by veins intruding the footwall. The model is not to scale and the isotherms are only schematic (the base of the drawing was modified from Ames and Farrow, 2007).

Chapter 3

Exsolution of Immiscible Metalloid-bearing Liquids from Sulfides and the Role of Metalloids in the Behavior of Highly Siderophile Elements: Constraints from Experiments Synthesized Between 1050 °C and 600 °C

Abstract

Platinum-group minerals (PGM) such as sperrylite, michenerite, moncheite, platarsite and irarsite can account for a significant portion of the precious metal budget in magmatic ore deposits. These minerals are generally composed of highly siderophile elements (HSE: Ru, Rh, Pd, Re, Os, Ir, Pt and Au) and elements broadly known as metalloids (As, Se, Sb, Te and Bi). Consequently, understanding the behavior of metalloids in sulfide systems is relevant to understand the behavior of HSE during ore forming processes. When a sulfide melt forms, the metalloids and HSE partition into it. It has been hypothesized that during cooling of such sulfide melts, metalloids may exsolve and form an immiscible metalloid-rich liquid that sequesters HSE from which PGM would later crystallize. A critical aspect that needs to be addressed is establishing the critical metalloid content at which such immiscible metalloid phases may form. To fill this gap, experiments were conducted to determine the solubility of metalloids in sulfides, as well as the effect of temperature on metalloid solubility and how immiscible metalloid-rich liquids can influence the distribution of HSE. Approximately 50 ppm of each HSE were diluted in a mixture of natural sulfides (pyrrhotite, pentlandite and chalcopyrite) to which Co and metalloids were added either individually (3 wt.% of Te, Bi or As) or as a mixture of As, Se, Sb, Te and Bi (2 wt.% or 0.05 wt.% total). Starting materials were sealed in evacuated silica tubes, heated to 1200 °C, slowly cooled to 1050 °C, 900 °C, 750 °C, 650 °C or 600 °C, then quenched. Results show that exsolution of immiscible metalloid-bearing liquids may only occur when the metalloid content in high temperature sulfides (monosulfide solid solution, mss and intermediate solid solution, iss) reaches several hundreds ppm. The results also show that metalloids form two distinct groupings: one dominated by As and crystallizing gersdorffite-

cobaltite and sperrylite at (and above) 1050 °C; one containing the remaining metalloids and remaining as an immiscible melt to lower temperatures (a least to 650 °C). In addition, the results show that Ru, Rh, Re, Os and Ir are not affected by metalloids and partition preferentially in mss. In contrast, Pt, Pd and Au are strongly affected by metalloids. Particularly, Pt partitions into the As-bearing phase, whereas Pd and Au partition into immiscible liquids containing Bi and Te. Comparison with metalloid content in pyrrhotite and pentlandite from various localities indicates that exsolution of immiscible metalloid-bearing phases is, at best, an unlikely and rare phenomenon requiring unusual initial amount of metalloids or addition of metalloids from other sources.

3.1. Introduction

The highly siderophile elements (HSE), which include the platinum-group elements (PGE: Ru, Rh, Pd, Os, Ir and Pt) as well as Au and Re, are defined as those with strong preference for Fe-bearing alloys (such as those comprising the Earth's core). In addition to their relevance to understand planetary formation (e.g., core-mantle separation), the HSE are of economic interest due to the value of those metals for industrial use (e.g., catalytic converters, electronics), jewelry or as investment vehicles. The HSE are extracted economically from magmatic sulfide deposits, such as those associated with the Sudbury Igneous Complex (Canada), Noril'sk (Russia) and the Bushveld Complex (Republic of South Africa). It is well documented that HSE are collected by immiscible sulfide liquids (e.g., Mungall and Brenan, 2014), but follow different paths during cooling of the sulfide melt. Some of them (Ru, Re, Os and Ir) partition mostly into pyrrhotite, whereas Pd (± Rh) partition into pentlandite and Pt and Au prefer to form discrete minerals (Barnes et al., 1997; Ballhaus et al., 2001; Crocket, 2002). However, in most ore deposits the PGE are typically present as discrete platinum-group minerals (PGM), many of which contain low-melting-point chalcophile elements (LMCE, Frost et al., 2002) as essential constituents. Among the LMCE, As, Te and Bi are the elements most commonly associated with PGM, followed by Sb and Se (Cabri and Laflamme, 1976; Cabri, 1981, 2002). Some of the most common PGM are arsenides and bismuth-tellurides such as sperrylite ($PtAs_2$), merenskyite [$(Pd,Pt)(TeBi)_2$], michenerite [(Pd,Pt)BiTe] and moncheite ($PtTe_2$) although sulfosalts such as irarsite (IrAsS), platarsite (PtAsS), and hollingworthite (RhAsS) and others PGM may also be present (Cabri and Laflamme, 1976; Cabri, 1981, 2002; Dare et al., 2010a, 2014; Djon et al., 2012; Godel and Barnes, 2008; Hanley, 2007; Krivolutskaya et al., 2011; Prichard et al., 2013; Spiridonov, 2010; Tomkins, 2010). Although Bi is usually not classified as a metalloid, it tends

to substitute for Te; thus, the term ‘metalloid’ will be used henceforth to distinguish those five elements (As, Se, Sb, Te, Bi) from other LMCE (e.g., Ag, Hg, Sn, Tl).

Despite the close link between metalloids and HSE, the mechanisms of formation of metalloid-bearing PGM are not clear. One hypothesis is that during cooling of a sulfide melt an immiscible metalloid liquid exsolves from the last droplets of sulfide liquid and sequesters most of the Pt and Pd from the sulfides (Fleet et al., 1993; Prichard et al., 2004; Helmy et al., 2007; Holwell and McDonald, 2010). Such metalloid-rich melts would form PGM at a late stage of cooling. Conversely, Leblanc et al. (1990), Gervilla et al. (1996), Hanley (2007) and Dare et al. (2010a) suggested that metalloid liquids, As-rich liquid in particular, may exsolve at higher temperature (T > 1200 °C) and may sequester not only Pd ant Pt, but also IPGE (IPGE: Ir-like platinum-group elements, Ru, Os and Ir; Barnes et al., 1985). The exsolved As-rich liquid crystallizes at relatively high temperature forming minerals such as sperrylite, which is often associated with minerals of the gersdorffite-cobaltite group and other PGE-bearing sulfarsenides, such as irarsite-platarsite-hollingworthite solid solutions (Prichard et al., 2013).

A critical aspect to assess whether immiscible metalloid-phases could form during cooling of a sulfide melt is to establish the solubility of metalloids in sulfides. However, available data are few and incomplete. Makovicky et al. (1990) indicated that pyrrhotite can dissolve up to 0.4 at. % As at 850 °C and Fleet et al. (1993) estimated that 0.1 wt.% is the As content in sulfide at arsenide saturation (sperrylite). Helmy et al. (2007) document experiments, equilibrated between 900 °C and 320 °C, in a system containing Pt, Pd and an immiscible Te-bearing liquid (or tellurides) coexisting with in monosulfide solid solution (mss) and intermediate solid solution (iss). The Te content in mss in those experiments ranged from 0.29 wt.% to 0.39 wt.%, whereas the Te content in iss ranged from 0.07 wt.% to 0.17 wt.%. Helmy et al. (2010) calculated the

partition coefficients of Se, As, Sb, Te and Bi between mss and Cu-rich sulfide melts, but the concentration of metalloids in the sulfides was not documented. Helmy et al. (2013) document experiments similar to those summarized in Helmy et al. (2007) but using As instead of Te and equilibrated at temperatures ranging from 1230 °C to 700 °C. Their results show that, in systems saturated with arsenide melts, a sulfide melt can contain up to 3.8 wt.% As (at 1150 °C) and the As content in mss ranges between 2300 ppm (at 1000 °C) and 1300 ppm (at 770 °C). They concluded that natural, mantle-derived and uncontaminated sulfide melts are not likely to reach arsenide saturation, but that arsenide saturation may be achieved if As is 'distilled' from surrounding rocks. More significantly, Helmy et al. (2013) suggested that other PGE may also show affinity for arsenide minerals, although they acknowledged that such behavior has to be tested.

In summary, despite the close relationship between metalloids and HSE in natural systems there are significant gaps in experimental data to constrain how metalloids affect the behavior of the HSE during the evolution of a sulfide melt. To fill some of those gaps and better constrain how metalloids affect the behavior of the HSE, we performed experiments containing the three most relevant metalloids (As, Te, Bi) as well as a complete suite of HSE. The main goals of the study were to determine the metalloid content required to produce metalloid-rich phases and assess how the presence of metalloids affect the behavior of HSE.

3.2. Experimental methods

All experiments were run in silica tubes (6 mm, outside diameter and 1.5 mm wall thickness). The material was evacuated to approximately 50 mtorr (ca. 6.7 Pa), using a E2M two stage

rotary vane pump. The desired vacuum was obtained within few minutes. Vacuum was constantly controlled with an electronic gauge connected to the line. The capsules were repeatedly flushed with Ar before final evacuation and sealing with a hydrogen-oxygen torch. The capsules were placed in a vertical furnace equipped with a programmable temperature controller and the temperature was monitored with two type R thermocouples. Prior to running the experiments, the profile of the temperature gradient was measured throughout the vertical tube by inserting a third thermocouple at different heights. It was observed that the hot spot is located approximately at the center of the tube and that the temperature is constant over a span of approximately 7 cm. Particular care was taken to place the lower portion of the capsules (where the starting material are) as close as possible to the center of the hot spot. Experiments belonging to the same subset were run simultaneously, hanging from a custom-made alumina sample holder, in Pt wire baskets (Figure 11).

Two sets of experiments were conducted because the volume of iss produced in the first set of experiments (K-series) was too small for adequate characterization. A complementary set of experiments (KN-series), with higher Cu and Ni content, was designed to obtain better data on HSE and metalloid content in iss. Each set is described below.

3.2.1. First set of experiments (K-series)

The starting materials for the experiments were divided in three groups: sulfides, HSE, and metalloids. A mixture of natural sulfides was created using pyrrhotite (po) from North Bend (USA), chalcopyrite (ccp) from Messina (South Africa) and pentlandite (pn) from the Podolsky Mine, Sudbury (Canada). The three sulfides were mixed in the weight proportion of 70 %

pyrrhotite, 15 % chalcopyrite and 15 % pentlandite (atomic ΣMetal/S = 0.93). This proportion of sulfides translates into a bulk composition that has 37.76 wt.% S, 50.89 % Fe, 6.14 % Ni and 5.21 % Cu, which is roughly the estimate of Kullerud et al. (1969) for the average bulk composition of the contact ores in Sudbury (hence, the experiments with this sulfide composition were labeled “K-series”).

The HSE were added following roughly the dilution protocols documented in Sylvester et al. (2005) and Wohlgemuth-Ueberwasser et al. (2007) to make pyrrhotite spiked with ~30 ppm of HSE for use as standards for LA-ICP-MS analyses. To make a sulfide assemblage containing a nominal bulk concentration of 50 ppm per HSE, two dilution steps were used. For the first step, 1 mg of each of the eight HSE (for a total of 8 mg) was mixed with 492 mg of pyrrhotite (from Strathcona Mine, Sudbury, Canada). The mixture was fused in evacuated silicate tubes at 1200 °C for 5 hours to allow equilibration and dissolution of HSE in the sulfide liquid, then quenched in water. Thus, we obtained a ‘pyrrhotite’ with a nominal content of 0.2 wt.% for each HSE (but in reality consisting of a quenched mss that was HSE-saturated plus excess, un-reacted HSE alloys). The synthesized material, labeled “0.2po”, was recovered and ground in an agate mortar. For the second step, 75 mg of ground 0.2po were mixed with 2025 mg pyrrhotite, 450 mg pentlandite, and 450 mg chalcopyrite, fused at 1200 °C for 5 hours and quenched. This product, consisting of a sulfide mixture nominally spiked with 50 ppm of each HSE, was recovered, stored in a desiccator and used as sulfide starting material for all runs belonging to the K-series.

To study the effect of metalloids, the HSE-spiked sulfides mixture was split into 4 batches. One batch was enriched with 3 wt.% of elemental Te, one with 3 wt.% of elemental Bi and one with 3 wt.% of As. The fourth batch was enriched with 3 wt.% of a mixture of the three metalloids, added in a 1:1:1 molar proportion. These concentrations are considerably higher than the

metalloid content in mss at metalloid saturation (Makovicky et al., 1990; Fleet et al., 1993; Helmy et al., 2007, 2010, 2013) and were chosen to ensure that metalloid phases were present in the experimental products. Concentrations much higher than 3 wt.% were avoided to prevent explosive failure of the silica capsules as discussed in Tomkins (2010). Each batch was then split into four aliquots for a total of 16 experiments. Four identical sets were then created, having one capsule of each composition (only Te, only As, only Bi and one with the mixture of metalloids) and each set was run simultaneously.

All experiments were heated from room temperature to 1200 °C at a slow temperature rate (60 °C/h) and kept at 1200 °C for 4 hours to achieve complete melting and homogenization of the starting materials. Subsequently, the temperature for each set of experiments was decreased at a constant rate (2 °C/h) to the target temperature (1050 °C, 900 °C, 750 °C, 600 °C) and maintained at the target temperature for durations shown previously to be sufficient for equilibrium to be established (e.g., Misra and Fleet, 1973; Peregoedova and Ohnenstetter, 2002; Helmy et al. 2007). Thus, after reaching the target temperature, experiments at 1050 °C, 900 °C, 750 °C, and 600 °C were maintained at constant temperature for 3.5 days, 7 days, 14 days, and 28 days, respectively.

3.2.2. Second set of experiments (KN-series)

Experiments of the second set of experiments followed the same protocol as the first set, but with three significant changes. First, the proportion of sulfides used was changed to 50 % pyrrhotite, 25 % pentlandite and 25 % chalcopyrite (compared to 70:15:15 in the K-series) to increase the amount of iss produced in the experiments. Second, a small amount of Co was added to the

system as CoS (99.5 % from Alfa Aesar) because Co is an important component in sulfarsenide systems (Dare et al., 2010a; 2010b). The resulting bulk composition of the sulfide mix was nominally 50.94 wt.% S, 35.32 wt.% Fe, 6.94 wt.% Ni, 6.06 wt.% Cu, and 0.73 Co. Third, a mixture of five metalloids (As, Se, Sb, Te, Bi) was added to the starting materials (no Se or Sb were added to the K-series). The metalloids were added in a molar proportion of 1:1 among each other. This new set of experiments was labeled 'KN-series' (Kullerud-New) to differentiate it from the first set.

Three experiments were conducted using the composition designed for the KN-series: (1) a control experiment with no metalloid added, only containing the concentration that was already present in the natural sulfides, (2) an experiment containing approximately 2 wt.% of the mixture of metalloids to have metalloid-rich phases in the experimental products and (3) an experiment containing approximately 0.05 wt.% of the mixture of metalloids to test whether metalloids would be completely dissolved in the sulfides without segregating discrete metalloid phases, as predicted from the metalloid concentrations in sulfides documented in Helmy et al., 2007; 2013. The three experiments were conducted simultaneously in evacuated silica tubes loaded into a vertical-tube furnace following a protocol similar to that described for the K-series. Temperature was increased from room temperature to 1200 °C at a rate of 60 °C/h and kept at this temperature for 4 hours, then the temperature was decreased to 750 °C at a rate of 60 °C/h and from 750 °C to 650 °C at a rate of 0.5 °C/h. The experiments were terminated by quenching the capsules in water when temperature reached 650 °C. These experiments were not kept at 650 °C because the cooling rate used to reach the final temperature was considered slow enough to allow equilibration.

3.3. Analytical techniques

After completion of the experiments, the silica tubes were carefully sectioned longitudinally to extract the experimental products as a single ingot and preserve the vertical orientation, textures and any possible density differentiation within the sulfide assemblage. Samples were mounted in epoxy and polished manually using silicon carbide powder (progressively finer: 400-600-1000 grit) and then finished with alumina powder (0.25 μm grain size).

Photomicrographs of the run products were taken under reflected light optical microscope. A Zeiss Evo 50 Scanning Electron Microscope (SEM) equipped with Energy Dispersive Spectroscopy (EDS, Texas Instruments), at the Ontario Geoscience Laboratories (Ontario GeoLabs), was used for the acquisition of back-scattered electron images (BSE) and for semi-quantitative EDS analyses of metalloid phases. The accelerating voltage of the SEM was 20 kV and the current 750 pA. The dwell time for semi-quantitative analyses was 10 s.

Major elements in the sulfides were analyzed with a Cameca SX100 electron microprobe at the Ontario GeoLabs. The accelerating voltage was 20 kV. For experiments of the K-series, S, Fe, Ni and Cu were analyzed for 15 s at 20 nA, whereas Mn, Zn, As, Te, Pb and Bi were analyzed for 20 s at 200 nA. Iron, Mn and Zn were analyzed using a LiF crystal; Cu, Ni (Kα2) and As with a LLiF crystal; Te (Lα) with a PET crystal; Bi and Pb with a LPET crystal. For experiments of the KN-series, Co, Se and Sb were added to the analytical routine. These elements were analyzed for 20 s at 200 nA. Cobalt was analyzed using a LiF crystal, Se with a LLiF crystal and Sb with a LPET crystal.

Trace elements were analyzed with laser ablation inductively coupled plasma mass spectrometry (LA-ICP-MS) at Laurentian University, using a Resonetics RESOlution M50 laser probe and a

Thermo-Fisher XSeriesII ICP-MS. For the K-series, the masses analyzed correspond to ^{33}S, ^{55}Mn, ^{59}Co, ^{60}Ni, ^{61}Ni, ^{63}Cu, ^{65}Cu, ^{66}Zn, ^{68}Zn, ^{75}As, ^{77}Se, ^{99}Ru, ^{101}Ru, ^{103}Rh, ^{105}Pd, ^{108}Pd, ^{111}Cd, ^{118}Sn, ^{121}Sb, ^{125}Te, ^{185}Re, ^{189}Os, ^{193}Ir, ^{195}Pt, ^{197}Au, ^{208}Pb and ^{209}Bi. Spot analyses were performed on mss with a laser beam size of 26 μm, frequency of 5 Hz, fluence of 7 J/cm^2 and ablation time of 40 s. For iss, both spot analyses and line scans were performed, but the beam diameter had to be reduced to 10 μm because of the small size of the iss and the complex intergrowth with other phases present. The speed of the laser for the line scans was 5 μm/s and the average length of the lines was 166 μm (approximately 30 s acquisition time per line). Using lines instead of spots reduces the penetration depth of the laser, thus decreasing the chance of drilling into another phase underneath the iss. However, several lines crossed different phases, therefore only part of the signal could be used for integration and in some cases it was not possible to isolate the signal produced solely by iss. For the KN-series, the masses analyzed are the same as those listed for experiments of the K-series. Only line scans were performed on the samples from the KN-series of experiments using a laser beam diameter of 26 μm, ablating the sample at a speed 10 μm/s. The laser energy was 90 mJ, the fluence 5 J/cm^2, and the repetition rate 5 Hz. Approximately 40 s of acquisition time (for an average length of 430 μm) and less interference with other phases were possible because the size of the phases (particularly iss) was considerably bigger than in the sulfide produced in the experiments of the K-series. For all LA-ICP-MS analyses, the dwell time was 5 ms for major elements and 15 ms for trace elements (except for ^{57}Fe which was used as the internal standard and analyzed for 10 ms). The reference materials used were Po725 sulfide for ^{99}Ru, ^{101}Ru, ^{103}Rh, ^{189}Os, ^{193}Ir, ^{195}Pt and NIST610 glass for all other elements. The concentration of elements overlapping in both standard materials were confronted and returned very similar results. Data were processed and integrated using Iolite 2.5 for Igor Pro 6.34A. All the time

resolved spectra were inspected to identify the presence of metalloid-bearing nuggets. The detection limits are shown in the footnotes of all tables. Nuggets would appear as sudden spikes of high intensity in the time resolved spectra and removed from the integration interval. Figure 12 shows time resolved spectra from run products of both K and KN-series experiments, with examples of signal attributed to metalloid inclusions (nuggets) and the portions of signal that were integrated.

An additional step was used to correct for the interference of ^{40}Ar complexed with ^{59}Co, ^{61}Ni, ^{63}Cu and ^{68}Zn on the masses corresponding to the light HSE (^{99}Ru, ^{101}Ru, ^{103}Rh and ^{108}Pd, respectively). At the beginning and at the end of each analytical session, samples of natural cobaltite, millerite, chalcopyrite and sphalerite, which all had HSE below detection limits, were also analyzed. Using the protocol described in Guillong et al. (2011), the argide production was estimated (Table 6) and used to subtract argide interference from ^{59}Co, ^{61}Ni, ^{63}Cu and ^{68}Zn on the signal corresponding to the masses for ^{99}Ru, ^{101}Ru, ^{103}Rh and ^{108}Pd. The analyses of the experimental run products were proportionally corrected using the following equation:

$$[\mathrm{HSE}]_{real} = [\mathrm{HSE}]_{measured} \times [\mathrm{M}]_{interfering} \times \mathrm{C}$$

were $[\mathrm{HSE}]_{measured}$ is the concentration of ^{99}Ru, ^{101}Ru, ^{103}Rh or ^{108}Pd affected by the argide interference; $[\mathrm{M}]_{interfering}$ is the concentration of the metal causing interference (^{59}Co, ^{61}Ni, ^{63}Cu or ^{68}Zn) and C is the correction factor. To estimate Ru content, ^{101}Ru was preferred over ^{99}Ru because ^{61}Ni argide production is smaller than ^{59}Co argide production (only 1.31 ppm in 100 % ^{61}Ni, as opposed to 88.45 ppm in 100 % ^{59}Co.). To estimate Pd content, ^{108}Pd was preferred because Zn is present in much lower concentrations than Cu. However, ^{103}Rh is the only naturally-occurring isotope for Rh and the argide interference caused by ^{63}Cu is often much

larger than the signal from ^{103}Rh (especially in Cu-rich phases). Therefore, Rh content in iss could not be assessed.

3.4. Results

3.4.1. First set of experiments (K-series)

Results of the first set of experiments are summarized and described below by comparing phases present and textural relations, major element content and trace element content from experiments equilibrated at 1050 °C to experiments equilibrated at progressively lower temperatures. Experimental conditions and phases present at the end of the experiments are summarized in Table 7.

Phases present and textural relationships

Three of the four experiments equilibrated at 1050 °C show a vertical segregation into two domains that are separated by a sharp and convex contact (Figure 13A and Figure 13B). The lower domain is completely occupied by a texturally homogeneous mss whereas the upper domain is heterogeneous and composed of a mixture of three of four different phases. The dominant phase of the heterogeneous upper domain is also mss (labeled 'mss-b' henceforth), but forming rounded homogeneous grains (10 μm to 30 μm across). The mss-b grains are separated from each other by an interstitial Cu-rich phase interpreted to be quenched residual sulfide liquid (Figure 13C and Figure 13D). Metalloid-rich phases are located within the Cu-rich phase and were not found in contact with mss. In the experiments containing a mixture of metalloids, two

distinct metalloid phases were present (Figure 13D): one, As-rich, with sharp edges and interpreted to be a crystalline phase during the experiments; the other, a Bi-Te-rich with rounded edges and interpreted to be a quenched Bi-Te-rich melt which surrounded the As-rich phase. For the fourth experiment conducted at 1050 °C (Te-rich) only the fraction matching the texturally homogenous mss could be recovered and analyzed. The main significant change in the results from experiments between 900 °C and 600 °C is the disappearance of the heterogeneous, mixed domain (containing mss-b) that was observed in the experiment conducted at 1050 °C. Instead, a homogeneous mss was the dominant phase in all experiments and only very small amounts of Cu-rich sulfides (iss) and metalloid-rich phases were present, usually together and forming a thin rim along the contact with the silica tube (Figure 14,), similarly to what observed by Ebel and Naldrett (1996). Because iss and metalloid-rich phases were located along the contact with the silica tube, part of that material was often lost when recovering the experiments and in some experiments no iss could be found. In the assemblages equilibrated at 750 °C metalloid-rich phases were also present in nuggets and fractures within the mss (Figure 15A). In mss from experiments equilibrated at 600 °C small ($\leq$ 1 μm), metalloid-rich inclusions were randomly distributed; this type of inclusions were not observed in experiments conducted at higher temperature.

Sulfide composition

The major element composition of the sulfides is listed in Table 8. In experiments at 1050 °C, the presence of mss-b in the upper domain is not clear, but it is interpreted to be a quench product (cf. Ballhaus et al., 2001). Mss-b has a higher Ni content than the homogeneous mss in

the lower domain (9.7 wt.% Ni vs. 4.9 wt.%, respectively) and a lower Fe content (48.9 wt.% Fe vs. 53.6 wt.%, respectively). The composition of mss in all the experiments between 900 °C and 600 °C is very homogeneous and comparable with the composition of homogeneous mss synthesized at 1050 °C, although the Ni content is slightly higher (between 5.3 wt.% and 5.7 wt.%). Regarding the composition of the Cu-rich phase, the composition is very similar in all experiments (Table 8) and, if Ni and Cu are accounted together, roughly approaches the composition of cubanite (ideal composition: 35.4 S, 41.2 Fe, 23.4 Cu, all in wt.%). The only systematic variations found were a slight decrease in Ni content (from 3.4 wt.% at 1050 °C to 1.7 3.4 wt.% at 600 °C) and a slight increase in Cu content (from 19.6 wt.% and 19.7 wt.% Cu at 1050 °C and 900 °C to 23.0 and 21.4 wt.% Cu at 750 °C and 600 °C).

Metalloid phases present

The metalloid phases present were consistent with the metalloid added. Crystals (as inferred form the texture showing sharp edges) of the cobaltite-gersdorffite group (Figure 17) were found in experiments enriched only with As. In experiments enriched only with Bi, an unidentified Pb-bearing bismuthide with elongated habit was found immersed in anhedral Bi-rich phases, also interpreted to be quenched Bi-rich liquids. Although Pb was not added to the experiments, it was likely present in trace amounts in naturals sulfides used as the starting materials and preferentially sequestered into the Bi-rich liquid (Figure 15B). In experiments enriched only with Te the composition of the telluride approached the stoichiometry of melonite and in experiments at 600 °C, relatively large melonite crystals were present (Figure 16). Other metalloid phases were also identified but they were typically too small for proper characterization (semi-

quantitative EDS analyses of those phases are listed in Appendix 1). In experiments containing the mixture of metalloids, two distinct phases were found; one consisting mostly of As, with the composition of gersdorffite-cobaltite surrounded by a Te-Bi-rich phase (Figure 13). In experiments containing the mixture of metalloids, a few crystals of sperrylite were also observed.

Trace element content in mss

The trace element content of mss is summarized in Table 9 and illustrated in Figure 18 for metalloids and Figure 19 for HSE. In experiments at 1050 °C and containing a single-metalloid the concentration of the added metalloids in mss was relatively high: Te exceeds 4000 ppm, As reaches nearly 2000 ppm, and Bi exceeds 200 ppm. Similar results were found in experiments conducted from 900 °C to 600 °C (Figure 18A). With the exception of As content in mss, which shows a slight decrease with decreasing temperature, the metalloid content in mss remains significantly high at all the temperatures investigated. However, in experiments containing a mixture of metalloids, the metalloid contents in mss were significantly lower (Figure 18B). Mss from the experiment at 1050 °C was the most anomalous, containing only 5 ppm Te and 1 ppm Bi; whereas mss in experiments having the same bulk composition but equilibrated at lower temperature the Te content in mss ranged from 620 ppm to 1030 ppm and the Bi content ranged from 69 pm to 310 ppm. The main difference at 1050 °C is the existence of a Cu-rich melt; thus, the very low Bi and Te content could indicate that those two elements partition strongly in a Cu-rich melt and less strongly into iss; the As content in mss, in contrast, showed less variation than Bi and Te.

Result for the HSE content in mss are summarized in Table 9 and shown in Figure 19. The most significant result is that Re, Os, Ir, Ru, and Rh are largely unaffected by the presence of As, Bi, or Te and are present in similar amounts. In contrast, Pt, was strongly affected by the presence of As, especially in experiments at 750 °C and 600 °C.

Trace element content in Cu-rich domains

The LA-ICP-MS analyses performed on the upper domain gave mixed results and high uncertainties because the ablation almost invariably included Cu-rich liquid, mss-b and metalloid phases together. Therefore, the results summarized in Table 10 do not represent content in a single phase but a rough representation of the bulk content of the region analyzed. The data, although qualitative, are still valuable to indicate whether a particular element had a strong preference for the Cu-rich domain (quenched Cu-rich melt or iss mixed with metalloid-rich phases) relative to mss. Figure 20 shows the compared time resolved spectra of metalloids and HSE in the upper domain of the 1050 °C metalloid mixture-bearing experiment. Particularly, the spectra show that there is a correspondence only between the spikes of metalloids and those of Au, Pd and Pt, indicating that these three elements alone, among the HSE, concentrated in metalloid phases.

3.4.2. Second set of experiments (KN-series)

To complement the data, the experiments of the KN-series (designed to produce larger amounts of iss) were conducted. The three experiments of this series were cooled from 750 °C to 650 °C

and quenched. The results are intended to provide data regarding the behavior of metalloids and HSE in iss, which could not be obtained in the experiments of the K-series. As intended, the sulfide assemblages synthesized in this set had a higher abundance of iss compared to the run products of the first set of experiments (K-series). In all three runs, mss is still volumetrically dominant, but iss is no longer limited to a thin veneer on the external portion of the sample. Mss formed rounded grains that are separated by interstitial iss (Figure 21A) whereas iss formed a continuous network around mss grains. Discrete metalloid phases were found within iss or at the boundary between mss and iss. Unlike the K-series experiments, accessory magnetite occurs in KN-series run products (Figure 21B). The major element composition of the sulfides is homogeneous throughout the three runs (Table 11). On average, the composition of mss in the KN-series is 37.6 S, 48.2 Fe, 9.4 Ni, 3.0 Cu, 1.2 Co (all in wt.%) and the average composition of iss is 34.5 S, 38.0 Fe, 23.1 Cu, 2.8 Ni, 0.58 Co (all in wt.%). Despite the higher volume of iss produced in this set of experiments, some analyses were affected by the presence of nuggets within iss. Care was taken to avoid visible nuggets (Figure 22B) during ablation and to remove the signal caused by nuggets during integration of the ablation spectra for estimates of element content. Metalloids concentrated mainly in separate domains within the iss or at the boundary between iss and mss. Two distinct groups of metalloid-bearing phases were recognized (Figure 22). The first group is composed of arsenides (mainly euhedral to subhedral gersdorffite-cobaltite) that in reflected light look pale grey to white, had a smooth polish (Figure 22A) and are light gray in BSE images (Figure 22B). Small sperrylite crystals were also present (Figure 23) and were completely hosted within gersdorffite-cobaltite. The second group has a granular texture and is composed of multiple phases, is As poor but contains all the other metalloids, generally surrounds the arsenides, and seems to occupy interstices in iss (Figure 22 and Figure

24A). In BSE images, it is possible to distinguish at least six different phases (Figure 24B) with complex intergrowth that likely were formed from quenching of a metalloid-bearing liquid.

The trace element content in mss and iss is summarized in Table 12. Calculated Nernst partitioning coefficients between mss and iss are summarized in Table 13 and plotted in Figure 25. Several results are significant. First, the results are consistent with the experiments of the K-series and show that Ru, Rh, Re, Os and Ir partition preferentially into mss and are not affected by the presence of metalloids. Second, Pd, Pt and Au were affected by the presence of metalloids. In the absence of metalloid-bearing phases, Au partitions preferentially into iss. However, the Au content in iss decreased significantly in experiments with high metalloid content, implying that Au goes into the metalloid phases (from 171 ppm in experiments with no added metalloids to only 7 ppm in experiments containing 2 wt.% of a metalloid mixture). The partition coefficient for Pd between mss and iss was estimated between 3 and 4 but Pd was lost from both mss and iss when metalloid-bearing phases were present. The results for Pt are similar to those of Pd, showing preferential partitioning of Pt into mss (relative to iss). The high uncertainties in Pt content in mss for experiments with 2 wt.% of a metalloid mixture indicate that some of those analyses may be biased by the presence of Pt-rich inclusions. Third, the metalloid content in mss is consistent with experiments of the K-series having a mixture of As, Bi, and Te. Partitioning coefficients of metalloids and HSE between mss and iss were compared with analogues from Liu and Brenan (2015) for the same suite of elements and from Jugo et al. (1999) for Au (Figure 26). The coefficients of Re, the IPGE and Au are in good agreement with those of Liu and Brenan (2015) and Jugo (1999) within error. However, the coefficients for Pt, Pd are considerably higher (~20 to 50 times higher) than those from both Liu and Brenan (2015).

Concerning metalloids, the coefficients for As and Se are in very good agreement with Liu and Brenan, but the coefficients for Sb, Te and Bi are higher.

The addition of metalloids at different initial concentrations allowed to evaluate whether metalloids followed a Henrian behavior (Prowatke and Klemme, 2006). Partitioning coefficients of metalloids between mss and iss were plotted against the metalloid concentrations in mss (Figure 27). Arsenic and Sb show that their partitioning coefficients are independent on their initial concentrations, therefore they follow Henry's law. However, Se, Te and Bi show that their partitioning coefficients are higher when added at higher concentration. Hence, these three metalloids do not respect Henry's law.

Sulfur fugacity of the run products was calculated using a modified version of the equation from Toulmin and Barton (1964). In the original equation, the factor N is calculated from the moles of Fe and S in pyrrhotite (mss). Mengason et al. (2010) modified the calculation to obtain N to account for other metals in pyrrhotite, such as Co, Zn, Mn, Ni, Cu, Ag and Au. The fS_2 averaged among the K-series run products decreases with decreasing temperature from -0.1 Log units at 1050°C (~ 2 Log units above the fayalite-quartz-magnetite-pyrrhotite buffer, FQMPo; Shi 1992) to -4.5 Log units at 600 °C (also ~2 Log units above the FQMPo buffer). For the three runs of the KN-series, the average fS_2 is -4.4 Log units at 650 °C (Figure 28). The sulfur fugacity estimated from the composition of mss was compared with that from the experiments documented in Liu and Brenan (2015) who did similar experiments (at temperatures ranging from 860 °C to 926 °C). The results show that fS_2 in the experiments documented here are roughly 1 Log unit higher than those in Liu and Brenan (2015). Sulfur fugacity estimated by Wallace and Carmichael (1992) for sulfide saturated natural basaltic magmas range between -1.74 Log units (at 1184 °C, TK-14, Kane Fracture zone) and 0.83 (at 1115 °C, sample 997-3, Galapagos Spreading Center).

This corresponds to a range of fS_2 between the FQMPo buffer and 3 Log units above it, meaning that the fS_2 in the experiments is within the natural range

3.5. Discussion

There are three aspects of interest for which the experimental results documented here provide significant insight:

- The nature of the metalloid phase(s) that may form
- The metalloid content at saturation, defined as the concentration of metalloids in sulfides required to saturate the system in metalloid-bearing phases.
- The effect of metalloids and metalloid-bearing phases on the behavior of HSE.

3.5.1. Nature of metalloid phases

The most significant aspect from the results of our experiments is that metalloids form two distinct groups, one dominated by arsenide phases, which were crystalline even at the highest temperature investigated (sperrylite, gersdorffite-cobaltite) and the other one dominated by Bi and Te, which remained as a liquid and typically surrounded (wetted) the arsenide crystals. This is consistent with the associations and intergrowths of PGM or minerals containing different metalloids in natural occurrences (e.g., Spiridonov, 2010; Dare et al., 2014). Provided that sufficient metalloids are available to produce saturation of metalloid phases, the textural relationships observed in our experiments support the model of the immiscibility of metalloid

liquids in sulfides (Fleet et al., 1993; Gervilla et al., 1996; Hanley, 2007; Helmy et al., 2007; Piña et al., 2014). Above the liquidus temperature of a sulfide assemblage (≥ 1200 °C), metalloids are dissolved in the sulfide melt. As soon as mss begins to crystallize (~1190 °C, Kullerud et al., 1969), part of the metalloids enter into the mss structure, but the bulk portion of the metalloid budget remains within the residual Cu-rich liquid and may form another immiscible metalloid-rich liquid. From this metalloid liquid, arsenides (sperrylite followed by gersdorffite-cobaltite) crystallize, with the other metalloids retained in a residual metalloid-rich liquid that wets the arsenides. As temperature decreases, the Cu-rich liquid crystallizes into iss, slightly above 900 °C. The Bi-Te-rich metalloid phase is still liquid and will wet the sulfides, likely migrating along fractures within the sulfides. Between 650 °C and 600 °C, the residual Bi-Te-rich melt starts to forms metalloid minerals (e.g., melonite). In the experiments documented in Helmy et al. (2007) the tellurides include moncheite, merenskyite and kotulskite; however, the starting material in those experiments contained a considerably higher amount of Pt and Pd. It is possible that our experiments were equilibrated at temperatures too high to allow the presence of michenerite, stable up to 489 °C or Bi-rich merenskyite (525 °C), but not for the presence of stoichiometric merenskyite (740 °C), kotulskite (720 °C, Hoffman and MacLean, 1976) or moncheite (observed up to 920 °C, Helmy et al., 2007).

3.5.2. Metalloid content required to produce metalloid-bearing phases

Previous experiments (e.g., Fleet et al., 1993; Makovicky et al., 1990; Helmy et al. 2007, 2013) focused on simpler systems designed to constrain the effect of a single metalloid (e.g., Te or As). For Te, Helmy et al. (2007) estimated that the Te content in mss and iss coexisting with

moncheite is approximately 0.2 wt.% and established that there was no temperature dependency. The results of our experiments yield higher values, with the Te content in mss at telluride saturation consistently at approximately 0.4 wt.% in all experiments in which only Te was added. However, in experiments with mixtures of metalloids, the Te content in mss at metalloid saturation is much lower ranging from only 5 ppm in an experiment at 1050 °C to up to 1030 ppm in an experiment at 900 °C. For As, Helmy et al. (2013) estimated the As content in a sulfide melt coexisting with an arsenide melt to be between 0.5 wt.% and 1.5 wt.%, although data for experiments at 950 °C and 1000 °C show that the As content in mss was 600 ppm and 840 ppm respectively. In contrast, the As content in mss in the experiments documented here was consistently higher (approximately 2000 ppm) in experiments in which only As was added, the only exception was the experiment conducted at 600 °C for which the As content in mss only reached 800 ppm. To our knowledge there is no available data regarding the Bi content in sulfides saturated with bismuthide liquids, thus the experiments documented here provide some of the first data to evaluate the effect of Bi. In experiments in which only Bi was added, the Bi content in mss at bismuthide liquid saturation was relatively low and approximately 200 ppm.

Data from experiments containing mixtures of metalloids showed significantly different results. In all experiments, the As and Te content in mss at saturation with metalloid-bearing phases was lower than in experiments saturated only with arsenides or tellurides. The effect was strongest for Te, for which the content in mss dropped from approximately 4000 ppm (in all Te-only experiments) to as low as 5 ppm (in an experiment at 1050 °C), but ranging from circa 400 ppm to 1000 ppm. The effect on As was also significant: in the experiment at 1050 °C, the As content in mss was roughly five times lower in experiments with a mixture of metalloids that in a similar experiment containing only As. Two significant aspects may provide indications regarding the

causes of the documented behavior. First, only the experiments at 1050 °C contained a Cu-rich melt; thus, the contrast in metalloid behavior compared to experiments at lower temperature likely reflected a change in metalloid behavior when the Cu-rich phase changes from a sulfide melt to crystalline iss. If this is the case, then the results indicate that As, Bi, and Te partition into a Cu-rich sulfide melt more strongly than into iss. Second, the Bi content in mss at metalloid saturation (~ 200 ppm) is much lower than that of Te (~ 4000 ppm) or As (~ 2000 ppm). One possible explanation is that a small amount of Bi is needed to saturate a metalloid phase, but once such metalloid phase forms, the other metalloids partition into it as well. The significance of these results is that proper assessment of the role of metalloid in natural sulfide systems requires investigation in complex systems and that data from experiments isolating the effect of a single metalloid likely over estimate the amount of metalloids required for metalloid saturation to occur.

3.5.3. Effects of metalloids on HSE

It is well established that HSE fractionate between sulfide phases. Experimental work shows that Re, the IPGE (Os, Ir, Ru) and Rh generally partition into mss, whereas Au, Pd and Pt have stronger preference for the Cu-rich residual liquid (e.g., Fleet et al., 1993; Li et al., 1996; Ballhaus et al., 2001; Brenan, 2002; Mungall et al., 2005; Barnes et al., 2006; Peregoedova et al., 2004; Sinyakova et al., 2001; Holwell and McDonald, 2010). Helmy et al. (2007; 2013) showed that Te- or As-bearing phases sequester Pt and Pd from coexisting sulfides but there is no available data to evaluate the effect on the other HSE. The results of our experiments confirm that Re, Os, Ir, Ru and Rh are hosted mostly in mss. In addition the results show that this

behavior is largely unaffected by the presence of metalloid-bearing phases. In contrast, Pt, Pd, and Au were affected by the presence of metalloids, confirming the results of Helmy et al. (2007, 2013). However, in the presence of several metalloids, Pt was sequestered into the arsenide component and Au and Pd into the Bi-Te component.

3.5.3. Behavior of other trace elements

Although not the primary focus on this study, the data collected in this study (KN-series, equilibrated at 650 °C; Table 12) allows for some insight into the behavior of other trace elements (Mn, Co, Zn, Se, Cd, Sn, Sb, Pb). Both mss and iss contained significant amounts of Mn, with iss contain roughly twice the amount of Mn relative to mss; Zn partitions strongly into iss (roughly 60 times more than in mss); Cd, Sn and Sb also partition preferentially into iss; Pb has affinity for the Bi-Te-rich metalloid phases but otherwise partitions preferentially into iss (with iss containing roughly twice the Pb than mss); Co was present in the arsenides but mss and iss retained significant amounts of Co (mss roughly twice as much as iss); Se also has a slight preference for iss (roughly twice the amount of Se in iss than in mss).

3.6. Conclusions

The experiments documented here successfully reproduced a system containing mss, Cu-rich melt (or iss) and metalloid bearing phases (both liquid and solid). The results indicate that:

- A high amount of metalloids can be dissolved in mss (and iss) meaning that it is unlikely that immiscible metalloid phases may exsolve during cooling of immiscible sulfide melts.

- When metalloid-bearing phases exsolve, they form two distinct domains: one that is As-dominant, more refractory and with a higher affinity for Pt versus a Bi-Te-dominant, which incorporates Sb, Pb, as well as Pd and Au and which persist as immiscible melt to temperatures well below the solidus of a typical Cu-Fe-Ni-S system (i.e., 650 °C and lower).

- The As-rich domain may result in early crystallization (> 1050 °C) of sperrylite and gersdorffite-cobaltite.

- The Te-Bi-rich phase may form PGM and other minerals (e.g., melonite) at relatively low temperatures.

- The presence of metalloid phases did not affect the partitioning of Re, Rh, Ir, Os and Ru, all of which preferentially partitioned into mss. In contrast, Pt, Pd and Au are largely affected by presence of metalloid phases. Platinum, in particular, is extremely sensitive to presence of As and would be efficiently scavenged by an arsenide phase to form sperrylite.

- Additional experimental work is needed to assess changes in solubility of metalloids and the partitioning of HSE at lower temperature, in particular at temperatures relevant to the appearance of pentlandite or the breakdown of iss into chalcopyrite and cubanite.

Acknowledgments

This manuscript is part of a Ph.D. project followed by the first author, funded by NSERC, CEMI, Vale, and Sudbury Integrated Nickel Operations. The authors would like to thank Sandra Clarke and Dave Crabtree (Ontario Geoscience Laboratories) for their help with SEM and EMPA and Joseph Petrus (Laurentian University) for the help with LA-ICP-MS.

References

Ballhaus, C., Tredoux, M. and Späth, A., 2001, Phase Relations in the Fe-Ni-Cu-PGE-S System at Magmatic Temperature and Application to Massive Sulphide ores of the Sudbury Igneous Complex: Journal of Petrology, v. 42(10), p. 1911-1926.

Barnes, S.-J., Cox, R.A. and Zientek, M.L., 2006, Platinum-group element, Gold, Silver and Base Metal distribution in compositionally zoned sulfide droplets from the Medvezky Creek Mine, Norl'sk, Russia: Contributions to Mineralogy and Petrology, v. 152, p. 187-200.

Barnes, S.J., Makovicky, E., Makovicky M., Rose-Hansen J. and Karup-Moeller, S., 1997, Partition coefficients for Ni, Cu, Pd, Pt, Rh and Ir between monosulfide solid solution and sulfide liquid and the formation of compositionally zoned Ni-Cu sulfide bodies by fractional crystallization of sulfide liquid: Canadian Journal of Earth Sciences, v. 34, p. 366-374.

Barnes, S.J., Naldrett, A.J. and Gorton, M.P., 1985, The origin of the fractionation of the platinum-group elements in terrestrial magmas: Chemical Geology, v. 53, p. 303-323.

Brenan, J.M., 2002, Re-Os fractionation in magmatic sulfide melt by monosulfide solid solution: Earth and Planetary Science Letters, v. 199, p. 257-268.

Cabri L.J., 1981, Introduction, in Cabri L.J., ed., Platinum-Group Elements: Mineralogy, Geology, Recovery: Canadian Institute of Mining and Metallurgy, Special Volume 23, p. 3-4.

Cabri L.J., 2002, The Platinum-Group Minerals, in Cabri L.J. Ed., The Geology, Geochemistry Mineralogy and Mineral Beneficiation of Platinum-Group Elements: Canadian Institute of Mining, Metallurgy and Petroleum, Special Volume 54, p. 13-129.

Cabri, L.J. and Laflamme, J.H.G., 1976, The Mineralogy of the platinum-Group Elements from Some Copper-Nickel Deposits of the Sudbury Area, Ontario: Economic Geology, v. 71, p. 1159-1195.

Crocket, J.H., 2002, Platinum-group Element Geochemistry of Mafic and Ultramafic Rocks, in Cabri, L.J., ed., The Geology, Geochemistry Mineralogy and Mineral Beneficiation of Platinum-Group Elements: Canadian Institute of Mining, Metallurgy and Petroleum, Special Volume 54, p. 177-210.

Dare, S.A.S., Barnes, S.-J. and Prichard, H.M, 2010a, The distribution of platinum-group elements (PGE) and other chalcophile elements among sulfides from the Creighton Ni-Cu-PGE sulfide deposit, Sudbury, Canada, and the origin of palladium in pentlandite: Mineralium Deposita, doi: 10.1007/s00126-010-0295-6.

Dare, S.A.S., Barnes, S.-J., Prichard, H.M. and Fisher, P.C. 2010b, The Timing and Formation of Platinum-Group Minerals from the Creighton Ni-Cu-Platinum-Group Element Sulfide

Deposit, Sudbury, Canada: Early Crystallization of PGE-Rich Sulfarsenides: Economic Geology, v. 105, p. 1071-1096.

Dare, S.A.S., Barnes, S.-J., Prichard, H.M. and Fisher, P.C., 2014, Mineralogy and Geochemistry of Cu-Rich Ores from the McCreedy East Ni-Cu-PGE Deposit (Sudbury, Canada): Implications for the Behavior of Platinum Group and Chalcophile Elements at the End of Crystallization of a Sulfide Liquid: Economic Geology, v. 109, p. 343-366.

Djon, M.L.N. and Barnes, S.-J., 2012, Changes in sulfides and platinum-group minerals with the degree of alteration in the Roby, Twilight and High Grade Zones of the Lac-des-Iles Complex, Ontario, Canada: Mineralium Deposita, v. 47 (8), p. 875-896.

Ebel, D.S. and Naldrett, A.J., Crystallization of sulfide liquids and the interpretation of ore composition: Canadian Journal of Earth Sciences, v. 34, p. 352-365.

Fleet, M.E., Chryssoulis, S.L., Stone, W.E. and Weisener, C.G., 1993, Partitioning of platinum-group elements and Au in the Fe-Ni-Cu-S system: experiments on the fractional crystallization of sulfide melt: Contributions to Mineralogy and Petrology, v. 115, p. 36-44.

Frost, B.R., Mavrogenes, J.A. and Tomkins, A.G., 2002, Partial melting of sulfide ore deposits during medium- and high-grade metamorphism: Canadian Mineralogist, v. 40, p. 1-18.

Gervilla, F., Leblanc, M., Torrez-Ruiz, J. and Hach-Alí, P.F., 1996, Immiscibility between arsenide and sulfide melts: a mechanism for the concentration of noble metals: The Canadian Mineralogist, v. 34, p. 485-502.

Godel, B. and Barnes, S.-J., 2008, Image Analysis and Composition of Platinum-group Minerals in the J-M Reef, Stillwater Complex: Economic Geology, v. 103, p. 637-651.

Guillong, M., Danyushevsky, L., Walle, M. and Raveggi, M., 2011, The effect of quadrupole ICPMS interface and ion lens design on argide formation. Implications for LA-ICPMS analysis of PGE's in geological samples: Journal of Analytical Atomic Spectrometry, v. 26, p. 1401-1407.

Hanley, J.J., 2007, The Role of Arsenic-rich Melts and Mineral Phases in the Development of High-grade Pt-Pd Mineralization within Komatiite-associated Magmatic Ni-Cu Sulfide Horizons at Dundonald Beach South, Abitibi Subprovince, Ontario, Canada: Economic Geology, v. 102, p. 305-317.

Helmy, H.M., Ballhaus, C., Berndt, J., Bockrath, C. and Wohlgemuth-Ueberwasser, C., 2007, Formation of Pt, Pd and Ni tellurides: experiments in sulfide-telluride systems: Contributions to Mineralogy and Petrology, v. 153, p. 577-591.

Helmy, H.M., Ballhaus, C., Wohlgemuth-Ueberwasser, C., Fonseca, R.O.C. and Laurenz, V., 2010, Partitioning of Se, As, Sb, Te and Bi between monosulfide solid solution and sulfide melt – Application to magmatic sulfide deposits: Geochimica et Cosmochimica. Acta, v. 74, p. 6174-6179.

Helmy, H.M., Ballhaus, C., Fonseca, R.O.C. and Nagel, T.J., 2013, Fractionation of platinum, palladium, nickel and copper in sulfide-arsenide systems at magmatic temperature: Contributions to Mineralogy and Petrology, DOI: 10.1007/s00410-013-0951-9.

Hoffman, E. and MacLean, W.H., 1976, Phase Relations of Michenerite and Merenskyite in the Pt-Bi-Te System: Economic Geology, v. 71, p. 1461-1468.

Holwell, D.A. and McDonald, I., 2010, A Review of the Behaviour of Platinum Group elements within Natural Magmatic Sulfide Ore Systems: Platinum Metals Reviews, v. 54(1), p. 26-36, DOI: 10.1595/147106709x480913.

Jugo, P.J., Candela, P.A. and Piccoli, P.M., 1999, Magmatic sulfides and Au:Cu ratios in porphyry deposits: an experimental study of copper and gold partitioning at 850 °C. 100 MPa in a haplogranitic melt-pyrrhotite-intermediate solid solution-gold metal assemblage, at gas saturation: Lithos, v. 46, p. 573-589.

Kullerud, G., Yund, R.A. and Moh, G.H., 1969, Phase Relations in the Cu-Fe-S, Cu-Ni-S, and Fe-Ni-S Systems: Economic Geology Monograph 4, p. 323-343.

Krivolutskaya , N.A., Gongalskiy, B.I., Yushin, A.A., Shlychkova, T.B., Kononkova, N.N., Petrus, J.A. and Tushentsova, I.N., 2011, Mineralogical and Geochemical Characteristics of PGE-Cu-Ni Ores of the Maslovsky Deposit in the Noril'sk Area, Russia: The Canadian Mineralogist, v. 49, p. 1479-1504, DOI: 10.3749/canmin.49.6.1479.

Leblanc, M., Gervilla, F. and Jedwab, J., 1990, Noble Metals Segregation and Fractionation in Magmatic Ores from Ronda and Beni Bousera Lherzolite Massifs (Spain, Morocco): Mineralogy and Petrology, v. 42, p. 233-248.

Li, C., Barnes, S.-J., Makovicky, E., Rose-Hansen, J. and Makovicky, M., 1996, Partitioning of nickel, copper, iridium, rhenium, platinum, and palladium between monosulfide solid solution

and sulfide liquid: Effects of composition and temperature: Geochimica et Cosmochimica Acta, v. 60(7), p. 1231-1238.

Liu, Y. and Brenan, J.M., 2015 (in press), Partitioning of platinum-group elements (PGE) and chalcogens (Se, Te, As, Sb, Bi) between monosulfide solid solution (MSS), intermediate solid solution (ISS) and sulfide liquid at controlled fO_2-fS_2 conditions: Geochimica et Cosmochimica Acta, http://dx.doi.org/10.1016-j.gca.2015.03.021.

Makovicky, M., Makovicky, E. and Rose-Hansen, J., 1990, Experimental studies on the phase system Fe-Ni-Pd-S and Fe-Pt-Pd-As-S applied to PGE deposits: Mineralogy and Petrology, v. 42, p. 307-319.

Mengason, M.J., Piccoli, P.M. and Candela, P., 2010, An evaluation of the effect of copper on the estimation of sulfur fugacity (fS2) from pyrrhotite composition: Economic Geology, v. 105, p. 1163-1169.

Misra, K.C. and Fleet, M.E., 1973, The Chemical Compositions of Synthetic and Natural Pentlandite Assemblages: Economic Geology, v. 68, p. 518-539.

Mungall, J.E. and Brenan, J.M., 2014, Partitioning of platinum-group elements and Au between sulfide liquid and basalt and the origins of mantle-crust fractionation of the chalcophile elements: Geochimica et Cosmochimica Acta, v. 125, p. 265-289.

Mungall, J.E., Andrews, D.R.A., Cabri, L.J., Sylvester, P.J. and Turbett, M., 2005, Partitioning of Cu, Ni, Au and platinum-group elements between monosulfide solid solution and sulfide melt under controlled oxygen and sulfur fugacities: Geochimica et Cosmochimica Acta, v. 69(17), p. 4349-4360, DOI: 10.1016/j.gca.2004.11.025.

Peregoedova, A., Barnes, S.-J. and Baker, D.R., 2004, The formation of Pt-Ir alloys and Cu-Pd-rich sulfide melts by partial desulfurization of Fe-Ni-Cu sulfides: results of experiments and implications for natural systems: Chemical Geology, v. 208, p. 247-264.

Peregoedova, A. and Ohnenstetter, M., 2002, Collectors of Pt, Pd and Rh in a S-poor Fe-Ni-Cu sulfide system at 760 ºC: experimental data and application to ore deposits: Canadian Mineralogist, v. 40, p. 527-561.

Piña, R., Gervilla, F., Barnes, S.-J., Ortega, L. and Lunar, R. 2014, Liquid immiscibility between arsenides and sulfide melts: evidence from a LA-ICP-MS study in magmatic deposits at Serranía de Ronda (Spain): Mineralium Deposita, DOI: 10.1007/s00126-014-0534-3.

Prichard, H.M., Hutchinson, D. and Fisher, P.C., 2004, Petrology and Crystallization History of Multiphase Sulfide Droplets in a Mafic Dike from Uruguay: Implications for the Origin of Cu-Ni-PGE Sulfide Deposits: Economic Geology, v. 99, p. 365-375.

Prichard, H.M., Fisher, P.C., McDonald, I., Knight, R.D., Sharp, D.R. and Williams, J.P., 2013, The Distribution of PGE and the Role of Arsenic as a Collector of PGE in the Spotted Quoll Nickel Ore Deposit in the Forrestania Greenstone Belt, Western Australia: Economic Geology, v. 108, p. 1903-1921.

Prowatke, S. and Klemme, S., Rare earth element partitioning between titanite and silicate melts: Henry's law revised: Geochimica et Cosmochimica Acta, v. 70, p. 4997-5012.

Shi, P., 1992, Fluid fugacities and phase equilibria in the Fe-Si-O-H-S system: American Mineralogist, v. 77, p. 1050-1066.

Sinyakova, E.F., Kosyakov, V.I. and Kolonin, G.R., 2001, Behavior of PGE on the cross-section of melts in the system Fe-Ni-S (FexNi0.49-xS0.51): Russian Geology and Geophysics, v. 42, p. 1287-1304.

Spiridonov, E.M., 2010, Ore-magmatic systems of the Noril'sk ore fields: Russian Geology and Geophysics, v. 51(9), p. 1059-1077.

Sylvester P.C., Cabri L.J., Turbett M.N., McMahon G., Laflamme J.G.H. and Peregoedova A. (2005) Synthesis and evaluation of a fused pyrrhotite standard reference material for platinum-group element and gold analyses by laser ablation-ICPMS. Geological Survey of Finland, Espoo, Finland, 16-20, 10th International Platinum Symposium; Platinum-group elements; from genesis to beneficiation and environmental impact; extended abstracts.

Tomkins, A.G., 2010, Wetting facilitates late-stage segregation of precious metal-enriched sulfosalts melt in magmatic sulfide systems: Geology, v. 38(10), p. 951-954.

Toulmin, P. and Barton, P.B., 1964, A thermodynamic study of pyrite and pyrrhotite: Geochimica et Cosmochimica Acta, v. 28, p. 641-671.

Wohlgemuth-Ueberwasser, C.C., Ballhaus, C., Berndt, J., Stotter Paliulionyte, V. and Meisel, T., 2007, Synthesis of PGE sulfide standards for laser ablation inductively coupled plasma mass spectrometry (LA-ICP-MS): Contributions to Mineralogy and Petrology, v. 154, p. 607-617.

Tables

Table 6. Correction factors for argide interferences.

$^{59}Co^{40}Ar \rightarrow {}^{99}Ru$	$^{61}Ni^{40}Ar \rightarrow {}^{101}Ru$	$^{63}Cu^{40}Ar \rightarrow {}^{103}Rh$	$^{68}Zn^{40}Ar \rightarrow {}^{108}Pd$
88 ppm	1.3 ppm	72 ppm	75 ppm
in 100 % Co	in 100 % Ni	in 100 % Cu	in 100 % Zn
n = 18	n = 18	n = 20	n = 20
Cobaltite	Millerite	Chalcopyrite	Sphalerite

Table 7. Summary of experimental conditions and results.

Run#	Metalloid	(wt.%)	T (°C)	time[1] (days)	Log fS_2	phases present
K-series						
K-Tg-3-1050	Te, Bi, As	3 (Σmet.)	1050	3.5	-0.331	mss, mss-b, Cu-rich liquid, As-bearing phase, Bi-Te-bearing liquid
K-Te-3-1050	Te	3	1050	3.5	0.158	mss, Te-bearing quenched liquid
K-Bi-3-1050	Bi	3	1050	3.5	-0.239	mss, mss-b, Cu-rich quenched liquid, Bi-bearing quenched liquid
K-As-3-1050	As	3	1050	3.5	0.192	mss, mss-b, Cu-rich quenched liquid, As-bearing phase
K-Tg-3-900	Te, Bi, As	3 (Σmet.)	900	7	-1.113	mss, iss, Bi-Te-bearing quenched liquid, As-bearing phase
K-Te-3-900	Te	3	900	7	-1.186	mss, iss, Te-bearing quenched liquid
K-Bi-3-900	Bi	3	900	7	-1.327	mss, iss, Bi-rich quenched liquid
K-As-3-900	As	3	900	7	-0.489	mss, iss, As-bearing phase (sperrylite)
K-Tg-3-750	Te, Bi, As	3 (Σmet.)	750	14	-2.193	mss, iss
K-Te-3-750	Te	3	750	14	-2.409	mss, iss, sperrylite, Te-bearing quenched liquid
K-Bi-3-750	Bi	3	750	14	-2.810	mss, iss, Bi-rich quenched liquid
K-As-3-750	As	3	750	14	-1.534	mss, As-bearing phase
K-Tg-3-600	Te, Bi, As	3 (Σmet.)	600	28	-4.550	mss, iss, gersdorffite, Bi-Te-bearing quenched liquid
K-Te-3-600	Te	3	600	28	-4.935	mss, iss, melonite
K-Bi-3-600	Bi	3	600	28	-5.476	mss, Bi-bearing quenched liquid
K-As-3-600	As	3	600	28	-3.119	mss, iss, gersdorffite
KN-series						
KN-01	not added	N/A	650		-4.340	mss, iss, gersdorffite
KN-02	Te, Bi, As, Sb, Se	2 (Σmet.)	650		-4.655	mss, iss, gersdorffite-cobaltite, sperrylite, metalloid-bearing quenched liquid
KN-03	Te, Bi, As, Sb, Se	0.05 (Σmet.)	650		-4.325	mss, iss, gersdorffite-cobaltite, sperrylite, metalloid-bearing quenched liquid

[1]Intended as equilibration time at a fixed temperature after cooling from 1200 °C. Experiments belonging to the KN-series were not kept at 650 °C for equilibration, but quenched as soon as they reached 650 °C.

Table 8. Major element composition of sulfides synthesized in experiments of the K-series.

Run T (°C)	Metalloid added	n	S[1]		Fe		Ni		Cu		Total
			wt.%	2σ	wt.%	2σ	wt.%	2σ	wt.%	2σ	
Monosulfide solid solution											
1050	Mix	5	38.12	0.42	53.38	3.00	5.10	0.67	3.21	4.21[2]	99.81
(mms1)	Te	10	38.43	0.31	53.75	1.02	4.53	0.46	2.78	0.95	99.49
	Bi	5	38.23	0.22	54.10	1.21	4.72	0.58	2.65	0.62	99.70
	As	5	38.35	0.64	53.01	1.09	5.03	0.75	3.09	0.68	99.48
	Average		38.28	0.27	53.56	0.94	4.85	0.54	2.93	0.53	
1050	Mix	5	37.48	0.63	47.05	1.74	13.31	1.54	1.75	0.40	99.60
(mss-b)	Te	Not recovered									
	Bi	5	37.93	0.43	49.48	0.60	8.54	1.00	3.52	0.60	99.46
	As	4	38.61	0.32	50.21	0.93	7.27	0.70	3.42	0.75	99.51
	Average		38.01	1.14	48.91	3.30	9.71	6.37	2.90	1.98	
900	Mix	5	38.06	0.12	52.09	0.41	5.31	0.15	4.19	0.55	99.64
	Te	10	37.98	0.36	52.04	0.97	5.28	0.32	4.25	1.63	99.55
	Bi	5	37.96	0.22	52.29	0.33	5.37	0.09	4.09	0.11	99.71
	As	5	38.50	0.18	51.88	0.25	5.30	0.07	3.77	0.16	99.45
	Average		38.12	0.51	52.07	0.34	5.31	0.08	4.08	0.43	
750	Mix	5	38.21	0.14	51.70	0.28	5.54	0.09	4.16	0.15	99.62
	Te	5	38.02	0.21	51.82	0.24	5.42	0.04	4.21	0.15	99.47
	Bi	5	37.83	0.19	52.20	0.20	5.38	0.04	4.14	0.13	99.54
	As	5	38.45	0.16	51.04	0.67	5.41	0.08	4.32	0.43	99.22
	Average		38.12	0.53	51.69	0.96	5.44	0.15	4.21	0.16	
600	Mix	8	38.32	0.30	53.22	0.18	5.76	0.21	2.47	0.22	99.78
	Te	8	38.23	0.35	53.53	0.35	5.74	0.13	2.54	0.28	100.04
	Bi	6	37.98	0.34	53.57	0.37	5.99	0.20	2.49	0.06	100.02
	As	5	39.28	0.23	53.37	0.34	5.29	0.11	2.29	0.05	100.23
	Average		38.45	1.14	53.42	0.32	5.70	0.58	2.45	0.21	
Cu-rich residual liquid and intermediate solid solution											
1050	Mix	5	34.69	0.38	39.22	0.93	2.88	0.20	21.87	0.35	98.64
	Te	Not recovered									
	Bi	5	34.68	1.05	38.47	1.45	3.29	0.22	21.19	1.46	97.63
	As	4	36.15	2.37	42.95	11.90	4.03	4.09	15.65	17.67	98.79
	Average		35.17	1.70	40.21	4.80	3.40	1.17	19.57	6.82	
900	Mix	6	34.42	0.65	36.28	3.76	1.30	0.91	25.38	4.28	97.38
	Te	2	38.33	3.76	47.16	12.48	3.80	4.38	10.71	19.71	100.00
	Bi	5	35.46	1.39	39.95	8.65	3.13	4.44	19.75	13.51	98.29
	As	5	35.52	0.74	37.94	3.35	2.07	0.38	22.85	2.86	98.38
	Average		35.93	3.36	40.33	9.58	2.58	2.21	19.67	12.80	
750	Mix	5	35.09	0.94	38.36	1.77	1.81	0.11	22.44	2.04	97.70
	Te	5	34.41	0.33	37.89	0.46	1.68	0.11	21.92	0.62	95.90
	Bi	5	34.75	0.62	34.16	5.30	3.28	1.97	25.64	2.86	97.84
	As	3	33.63	1.60	37.60	0.22	1.19	0.08	22.13	0.20	94.56
	Average		34.47	0.62	37.00	1.92	1.99	0.90	23.03	1.75	

Table 8. (*cont.*) Major element composition of sulfides synthesized in experiments of the K-series.

Run T (°C)	Metalloid added	n	S[1]		Fe		Ni		Cu		Total
			wt.%	2σ	wt.%	2σ	wt.%	2σ	wt.%	2σ	
600	Mix	5	35.13	0.50	40.06	0.35	1.52	0.06	21.63	0.32	98.35
	Te	5	35.05	0.38	40.19	0.25	1.60	0.05	21.63	0.20	98.47
	Bi	6	34.97	0.41	40.59	0.58	1.78	0.04	21.12	0.16	98.47
	As	9	34.96	0.37	40.52	0.63	1.77	0.05	21.21	0.47	98.47
	Average		35.03	0.15	40.34	0.51	1.67	0.25	21.40	0.54	

[1]By EPMA (WDS). Limits of detection: S = 0.018; Fe = 0.026; Ni = 0.022; Cu = 0.028 (in wt.%).
[2]High uncertainties (2σ > mean) are due to small Cu-rich phases (quench melt or iss) interstitial to mss.

Table 9. Trace element content in monosulfide solid solution synthesized in experiments of the K-series (in ppm).

Run	n	Mn[1]	Co	Zn	As	Se	Ru[2]	Rh[2]	Pd[2]	Cd	Sn	Te	Re	Os	Ir	Pt	Au	Pb	Bi
	isotope	*55*	*59*	*68*	*75*	*77*	*101*	*103*	*108*	*111*	*118*	*125*	*185*	*189*	*193*	*195*	*197*	*208*	*209*
1050 °C																			
Mix	8	4830	374	970	356	51	29	34	4.26	1.20	1.00	5	46	46	51	21	3.0	9.6	1.02
	2σ	550	50	120	75	18	7	5	0.39	1.30	0.48	5	9	13	9	4	1.0	1.6	0.25
Te	7	3910	365	1490	136	46	37	33	2.14	1.99	0.98	4040	54	69	58	10	1.3	4.0	0.15
	2σ	400	33	270	28	15	22	7	0.48	0.83	0.37	630	25	55	30	2	0.4	0.6	0.05
Bi	12	3700	363	1470	104	48	37	34	2.08	2.00	2.25	57	46	59	59	10	1.6	4.0	201
	2σ	460	60	470	35	12	12	9	0.39	1.50	0.65	15	13	19	18	3	0.5	1.0	51
As	6	3560	332	1250	1960	71	34	30	1.80	2.40	1.30	18	44	48	49	7	0.9	3.8	0.41
	2σ	760	57	610	200	19	7	5	1.10	6.20	2.60	6	6	9	7	3	0.6	6.7	0.25
900 °C																			
Mix	5	3750	324	1820	1199	48	29	24	3.34	4.40	3.86	1030	39	47	21	1.3	1.33	7.75	108
	2σ	220	9	110	72	13	10	1	0.37	1.30	0.45	170	7	17	10	0.3	0.30	0.42	5
Te	5	4000	348	2070	258	42	30	24	1.10	7.40	3.52	4790	45	53	45	4.0	0.37	11.4	0.14
	2σ	280	12	190	18	4	12	3	0.18	1.50	0.60	630	12	23	15	0.5	0.06	1.0	0.05
Bi	5	3800	356	1530	231	47	30	26	5.30	4.50	4.60	55	42	47	45	27.2	2.38	10.7	263
	2σ	190	29	140	15	11	8	2	0.50	1.70	0.42	28	9	17	10	1.4	0.29	0.3	16
As	5	3750	352	1670	2480	84	25	23	4.51	2.31	2.23	27	39	35	23	2.0	1.62	5.5	0.38
	2σ	190	18	100	120	11	5	1	0.22	0.27	0.17	7	7	10	11	0.4	0.19	1.3	0.04
750 °C																			
Mix	8	3760	339	610	700	68	19	19	6.90	2.40	5.10	620	29	20	26	0.004	1.70	55	69
	2σ	720	71	130	350	21	5	12	4.90	1.50	1.30	300	4	7	9	0.016	1.90	56	35
Te	7	3630	330	590	650	41	24	24	0.62	2.70	2.90	3840	34	34	37	3.7	1.40	16	0.39
	2σ	660	68	80	240	23	5	4	0.50	1.70	0.80	960	7	8	7	4.9	2.40	18	0.57
Bi	8	3500	340	650	610	44	33	32	2.90	5.30	5.50	55	48	52	49	9.3	0.44	9	207
	2σ	1400	130	400	210	37	14	13	1.10	3.10	2.60	30	18	22	18	3.6	0.31	6	78

Table 9. (*cont.*) Trace element content in monosulfide solid solution synthesized in experiments of the K-series (in ppm).

Run	n	Mn	Co	Zn	As	Se	Ru^2	Rh^2	Pd^2	Cd	Sn	Te	Re	Os	Ir	Pt	Au	Pb	Bi
	isotope	***55***	***59***	***68***	***75***	***77***	***101***	***103***	***108***	***111***	***118***	***125***	***185***	***189***	***193***	***195***	***197***	***208***	***209***
As	5	3790	329	820	1780	78	34	18	8.60	3.05	6.20	34	46	50	35	*b.d.l.*[3]	2.7	14	1.0
	2σ	570	53	110	140	27	4	4	0.75	0.81	2.30	18	7	8	15		0.3	2	0.1
600 °C																			
Mix	7	3430	329	89	690	59	25	15	1.12	0.10	0.94	820	36	34	37	*b.d.l.*	2.5	22	310
	2σ	380	25	18	390	27	17	16	0.44	0.21	0.36	380	18	35	27		2.7	18	410
Te	11	3510	370	94	280	60	32	27	0.75	0.09	0.63	4200	40	46	46	17	2.7	50	2.2
	2σ	690	83	51	97	29	13	18	0.43	0.14	0.31	1700	13	17	16	13	3.4	46	4.3
Bi	9	3500	358	86	239	43	30	31	0.84	0.12	1.21	38	44	49	48	1.99	0.3	13	140
	2σ	360	59	57	64	18	8	5	0.25	0.32	0.68	15	10	14	12	0.83	0.4	9	80
As	6	3250	244	94	790	78	28	20	0.29	0.14	0.93	20	42	46	43	*b.d.l.*	1.3	12	1.35
	2σ	270	24	12	150	14	10	12	0.08	0.18	0.15	15	12	22	17		0.2	11	0.15

[1]Llimits of detection (in ppm): Mn=3; Co=1; Zn=13; As=8; Se=3; Ru=0.02 Rh=0.01; Pd=0.003; Cd=0.09; Sn=0.15; Te=0.24; Re=0.003; Os=0.002; Ir=0.001; Pt=0.01; Au=0.002; Pb=0.03; Bi=0.03.
[2]The Ru, Rh, and Pd content were determined after subtraction of the argide interference of ^{61}Ni on ^{101}Ru, ^{63}Cu on ^{103}Rh and ^{68}Zn on ^{108}Pd.
[3]b.d.l.= below detection limits.

Table 10. Trace element content in the multiphase upper domain and in the intermediate solid solution synthesized in experiments of the K-series (in ppm).

Run	n	Mn	Co	Zn	As	Se	Ru[2]	Rh[2]	Pd[2]	Cd	Sn	Te	Re	Os	Ir	Pt	Au	Pb	Bi
isotope		*55*	*59*	*68*	*75*	*77*	*101*	*103*	*108*	*111*	*118*	*125*	*185*	*189*	*193*	*195*	*197*	*208*	*209*
1050 °C (multiphase upper domain)																			
Mix	2	4190	214	5500	13700	164	*b.d.l.*	84	30	21.8	66	190	7.50	3.8	7.00	59	533	7800	690
		780	23	1000	6600	72		51	44	2.3	34	140	0.01	0.3	0.57	51	190	6800	450
Te		not recovered																	
Bi	2	3700	223	6730	147	170	1.60	62.3	33	58	215	2300	10.1	6.15	9.30	150	290	2600	78000
		1000	37	200	410	170	0.45	9.4	43	37	82	2700	2.3	0.14	0.85	180	200	2600	79000
As	4	3530	236	120000	182000	1000	1.5	*b.d.l.*[3]	16	19	78	1500	7.0	5.1	16.6	1100	66	2400	350
		450	41	410000	82000	1100	4.1		45	13	30	1100	1.7	3.3	3.9	1100	33	780	200
900 ° C (multiphase upper domain)																			
Mix	5	4130	182	11000	190000	620	7	100	240	220	1300	330000	12	8	4.4	42	1500	39000	380000
		820	82	8800	320000	1300	16	230	630	180	1500	510000	19	16	9.3	160	2900	60000	600000
Te		not recovered																	
Bi		not recovered																	
As	3	6000	228	13000	298000	350	9.8	134	269	210	380	2500	19.7	13.6	8.0	89	880	15200	740
		2600	21	8900	80000	150	5.2	45	59	170	210	650	5.1	6.4	1.8	72	520	9100	270
750 °C (intermediate solid solution)																			
Mix	1	2290	202	307	244	*b.d.l.*	13.5	16.3	4.57	*b.d.l.*	2.73	353	19.0	12.6	11.10	b.d.l	0.99	41.5	35.4
		160	14	30	17		1.8	1.2	0.43		0.51	34	1.4	1.4	0.79		0.29	3.3	1.9
Te	4	2600	160	24000	160	100	9	13	*b.d.l.*	140	75	12000	13	12.7	18	8	7	80	*b.d.l.*
		1500	29	48000	120	23	10	22		300	160	10000	12	8.0	17	21	10	91	
Bi		not recovered																	
As	1	4040	120	44800	5940	76	18.4	181	3.0	178	223	97	0.78	21	23	4.7	142.8	62	*b.d.l.*
		240	7	2300	880	13	8.4	93	1.7	15	14	12	0.69	11	13	2.3	9.1	8	

Table 10. (*cont.*) Trace element content in the multiphase upper domain and in the intermediate solid solution of the K-series run products[1].

Run	n	Mn[1]	Co	Zn	As	Se	Ru[2]	Rh[2]	Pd[2]	Cd	Sn	Te	Re	Os	Ir	Pt	Au	Pb	Bi
isotope		***55***	***59***	***68***	***75***	***77***	***101***	***103***	***108***	***111***	***118***	***125***	***185***	***189***	***193***	***195***	***197***	***208***	***209***
600 °C (intermediate solid solution)																			
Mix	10	6100	152	10000	500	120	15	1	0.5	59	148	560	26	19	5	0.9	8.7	95	400
		1500	22	2100	1000	100	39	28	3.4	18	64	1600	67	55	13	5.6	6.5	130	660
Te	1	4270	156	9870	68.4	*b.d.l.*	*b.d.l.*	*b.d.l.*	*b.d.l.*	61.8	89.4	2050	*b.d.l*	*b.d.l*	0.02	*b.d.l*	15.4	349	28
		310	13	770	9.8					8.9	5.9	240			0.03		2.7	65	6
Bi	10	3610	142	9500	56.5	*b.d.l.*	*b.d.l.*	*b.d.l.*	*b.d.l.*	58	165	*b.d.l.*	32	7	1.3	0.9	3.4	73	195
		680	28	1000	9.2					14	19		50	12	5.4	5.0	1.6	11	61
As	7	4200	84	9400	2900	89	5	4	0.1	55	84	*b.d.l.*	8	8	1.8	0.05	194	36	*b.d.l.*
		540	28	1400	2500	55	15	34	2.4	11	13		27	25	6.4	0.22	22	20	

[1]Limits of detection: Mn=30; Co=1.7, Zn=67; As=39; Se=54; Ru=1.05; Rh=0.25; Pd=0.03; Cd=0.55; Sn=2.36; Te=30.20; Re=0.002; Os=0.01; Ir=0.01; Pt=0.01; Au=0.36; Pb=2.3; Bi=28.
[2]The concentration of Ru, Rh and Pd was determined after subtraction of the argide interference of ^{61}Ni on ^{101}Ru, ^{63}Cu on ^{103}Rh and ^{68}Zn on ^{108}Pd.
[3]b.d.l.= below detection limits.

Table 11. Major element composition of the sulfides synthesized in experiments of the KN-series.

Run T (°C)	n	S[1]		Fe		Co		Ni		Cu		Total
Phase		wt.%	2σ[2]	wt.%	2σ	wt.%	2σ	wt.%	2σ	wt.%	2σ	
No metalloid added												
mss	5	37.67	0.09	47.90	0.93	1.40	0.49	9.50	0.65	3.05	0.12	99.51
iss	5	34.53	0.13	37.87	0.40	0.66	0.21	2.80	0.15	23.21	0.14	99.06
2 wt.% metalloid mixture												
mss	10	37.59	0.25	48.20	0.43	1.09	0.02	9.28	0.31	3.01	0.52	99.17
iss	10	34.51	0.25	38.04	0.30	0.54	0.02	2.65	0.12	22.85	0.44	98.59
0.05 wt.% metalloid mixture												
mss	5	37.57	0.20	48.49	0.35	1.07	0.01	9.42	0.22	2.97	0.10	99.52
iss	5	34.44	0.26	38.04	0.36	0.54	0.01	2.85	0.08	23.28	0.39	99.16
Averages												
mss		37.61	0.10	48.20	0.60	1.19	0.37	9.40	0.22	3.01	0.08	
iss		34.49	0.09	37.98	0.20	0.58	0.14	2.77	0.21	23.11	0.46	

[1]By EPMA (WDS). Limits of detection: S=0.016; Fe=0.023; Co=0.010; Ni=0.023; Cu=0.028.

Table 12. Trace element content in sulfides synthesized in experiments of the KN-series (in ppm).

Phase	n	Mn[1]	Zn	As	Se	Ru[2]	Rh[2]	Pd[2]	Cd	Sn	Sb	Te	Re	Os	Ir	Pt	Au	Pb	Bi
isotope		*55*	*68*	*75*	*77*	*101*	*103*	*108*	*111*	*118*	*121*	*130*	*185*	*189*	*193*	*195*	*197*	*208*	*209*
No metalloid added																			
mss	6	1700	24	748	21.4	32.9	27.8	7.5	*b.d.l.*[3]	*b.d.l.*	0.95	2.4	42.3	50.5	51	14.1	1.76	92	8.9
2σ		400	15	79	7.5	5.1	4.2	1.2			0.29	2.2	5.7	6.4	8	6.5	0.42	11	1.5
iss	6	3260	1460	920	48.3	1.1	*b.d.l.*	2.36	7.55	5.36	5.02	29	1.3	1.4	1.4	1.7	171	285	21.2
2σ		830	130	150	9.1	2.3		0.49	0.86	0.50	0.44	9	4.1	4.7	4.4	1.1	25	17	1.4
2 wt.% metalloid mixture																			
mss	8	2440	20	678	890	25.5	10	1.00	*b.d.l.*	0.28	83	393	39.9	37.3	28	6.8	1.60	8.5	122
2σ		190	17	92	150	4.5	15	0.24		0.09	31	83	5.6	9.6	17	9.9	0.95	4.3	62
iss	13	4760	1690	760	1210	0.27	*b.d.l.*	*b.d.l.*	9.3	22.3	350	527	0.15	0.09	0.03	*b.d.l.*	6.9	15.9	116
2σ		5320	180	200	100	0.45			1.3	2.3	28	77	0.63	0.36	0.17		1.1	2.4	24
0.05 wt.% metalloid mixture																			
mss	7	2260	27	603	54.5	28.7	24.3	6.91	*b.d.l.*	0.15	11.30	29	39.9	41.8	43.4	*b.d.l.*	1.38	51.4	43.6
2σ		290	21	94	8.5	4.7	1.4	0.31		0.11	0.77	18	6.0	8.7	8.0		0.22	5.5	4.3
iss	16	4360	1390	770	104	2	*b.d.l.*	1.6	7.4	4.6	66	316	2.8	3	2.5	0.4	112	182	101
2σ		830	350	310	26	7		2.2	3.3	1.4	22	88	10	10	8.5	3.0	40	65	31

[1]Limits of detection: Mn=4; Co=1.5; Zn=14; As=11; Se=5; Ru=0.11; Rh=0.03; Pd=0.02; Cd=0.28; Sn=0.13; Sb=0.11; Te=1.1; Re=0.01; Os=0.01; Ir=0.03; Pt=0.01; Au=0.1; Pb=0.8; Bi=0.07.

[2]The concentration of Ru, Rh and Pd was determined after subtraction of the argide interference of ^{61}Ni on ^{101}Ru, ^{63}Cu on ^{103}Rh and ^{68}Zn on ^{108}Pd.

[3]b.d.l.= below detection limits.

Table 13. Partitioning coefficients between mss and iss for KN-series experiments.

Mn	Co	Zn	As	Se	Ru	Rh	Pd	Cd	Sn	Sb	Te	Re	Os	Ir	Pt	Au	Pb	Bi
σ[1]	σ	σ	σ	σ	σ	σ	σ	σ	σ	σ	σ	σ	σ	σ	σ	σ	σ	σ
No metalloids added																		
0.515	2.13	0.0167	0.813	0.442	30	*n.a.*[2]	3.19	*n.a.*	*n.a.*	0.189	0.081	33	35	36	8.2	0.0103	0.324	0.421
0.089	0.50	0.0050	0.079	0.088	30		0.42			0.030	0.041	54	57	56	3.3	0.0014	0.022	0.038
2 wt.% metalloid mixture																		
0.513	2.024	0.0121	0.89	0.739	94	*n.a.*	*n.a.*	*n.a.*	0.0125	0.237	0.75	260	410	940	*n.a.*	0.231	0.53	1.06
0.035	0.045	0.0051	0.13	0.068	79				0.0022	0.045	0.10	530	830	2700		0.071	0.14	0.29
0.05 wt.% metalloid mixture																		
0.519	1.993	0.0194	0.78	0.527	14	*n.a.*	4.4	*n.a.*	0.033	0.172	0.090	14	14	17	*n.a.*	0.0123	0.282	0.434
0.059	0.017	0.0079	0.17	0.078	23		3.1		0.013	0.029	0.031	26	26	30		0.0024	0.053	0.069

[1]Uncertainties (1σ) from propagation of uncertainties.
[2]n.a.=not applicable (content in one of the phases involved was below detection limit)

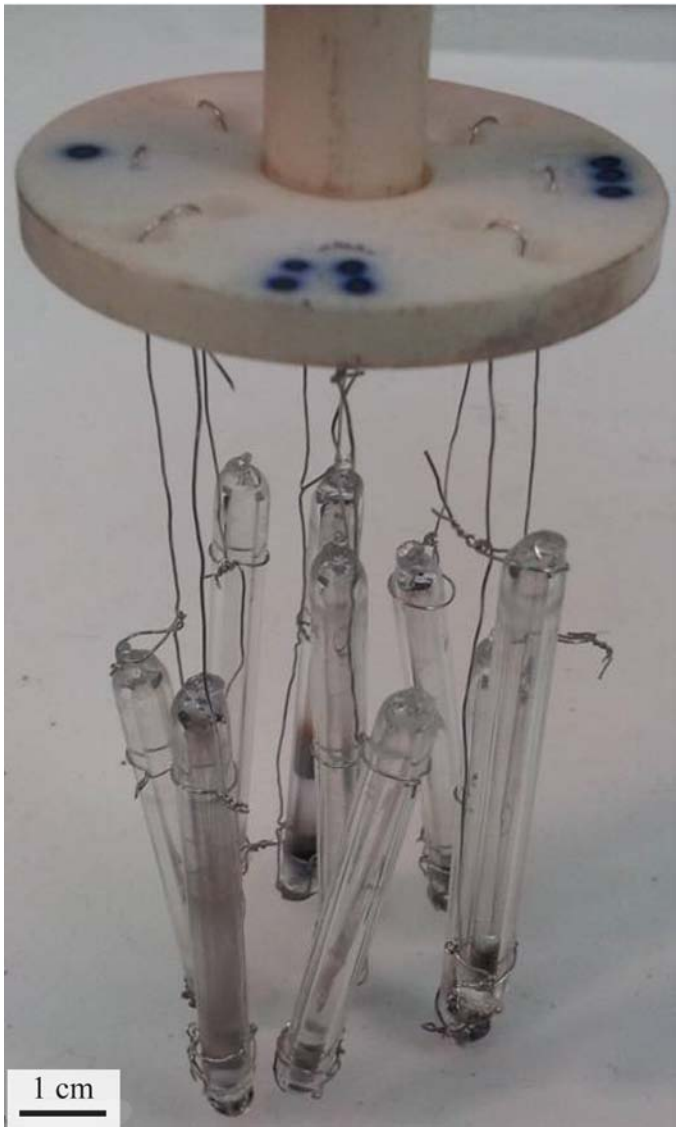

Figure 11. Sample holder used to run several experiments simultaneously. The capsules hang from a custom-made alumina disk using Pt wire and baskets. The diameter of the disk fits loosely within the alumina tube of the furnace (63 mm). The disk was held such that the charges were positioned in the hot spot of the furnace.

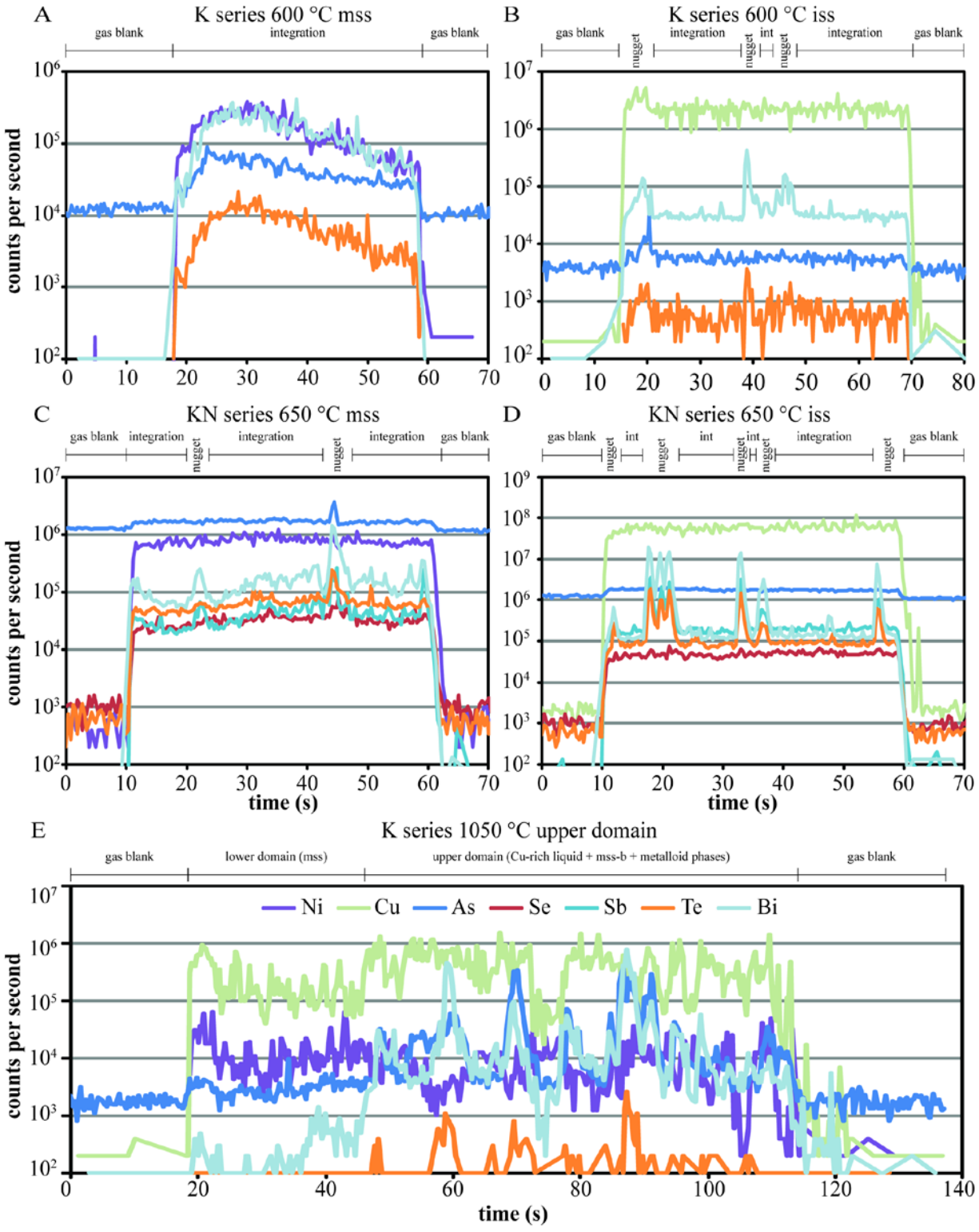

Figure 12. Examples of time-resolved spectra of metalloids signal intensity (from LA-ICP-MS analyses) used to detect the presence of metalloid-bearing nuggets. A. Spectra from mss of a K-series experiment (containing As, Bi, and Te) equilibrated at 600 °C showing absence of inclusions. B. Spectra from the iss-rich domain of the same experiment showing signal that was excluded due to the presence two different types of nuggets (Bi-rich vs. As-rich). C. Example of

metalloid spectra from mss of an experiment of the KN-series. Two portions were eliminated, one with an As-rich nugget and one with a nugget containing all metalloids. D. Spectra from the iss of the same KN-series experiment. A wider portion of the signal was not integrated, for the presence of several nuggets. E. Time resolved spectra of the upper domain of a As-Te-Bi-bearing experiment of the K-series equilibrated at 1050 °C. Discriminating the Cu-rich residual liquid from the mss-b and from the metalloid phases was not possible, therefore, the integration was done over the upper domain signal as a whole. Nickel or Cu signals are shown for comparison, as representatives of homogeneous elements in mss and iss, respectively (both are shown in figure E.).

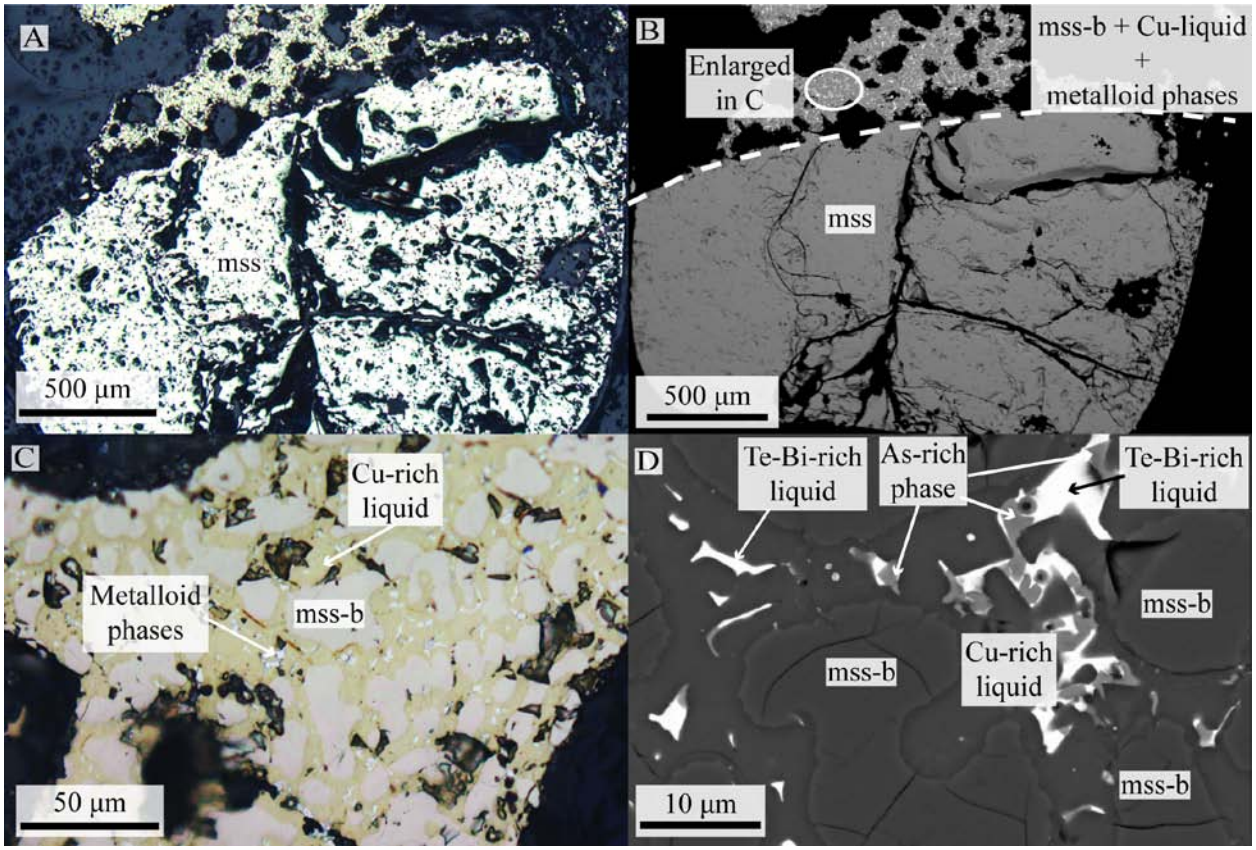

Figure 13. Images showing the run products of an experiment of the K series containing a mixture of As, Bi, Te and equilibrated at 1050 °C. A. Reflected light image. B. BSE image. The lower portion is completely occupied by a homogeneous and fractured mss. A convex contact separates the mss domain from the upper domain, which is composed of a different mss (mss-b), interstitial Cu-rich phase (interpreted to be a quenched residual liquid) and metalloid phases. The dark-grey background is the silica capsule. C. Reflected light image of the area circled in B. The pinkish grains are mss-b, the yellow interstitial phase is quenched Cu-rich residual liquid and the white specs are metalloid phases. D. BSE image of part of the Cu-rich domain showing two distinct metalloid-bearing phases. The first (light gray) is an As-rich phase with sharp corners (indicating that it is a crystalline phase) and composition consistent with gersdorffite-cobaltite, whereas the second phase (in white) is interstitial, anhedral (with rounded corners) and interpreted to be a quenched Te-Bi-rich liquid. The Cu-rich melts wets the mss and keeps the metalloid-bearing phases away from mss.

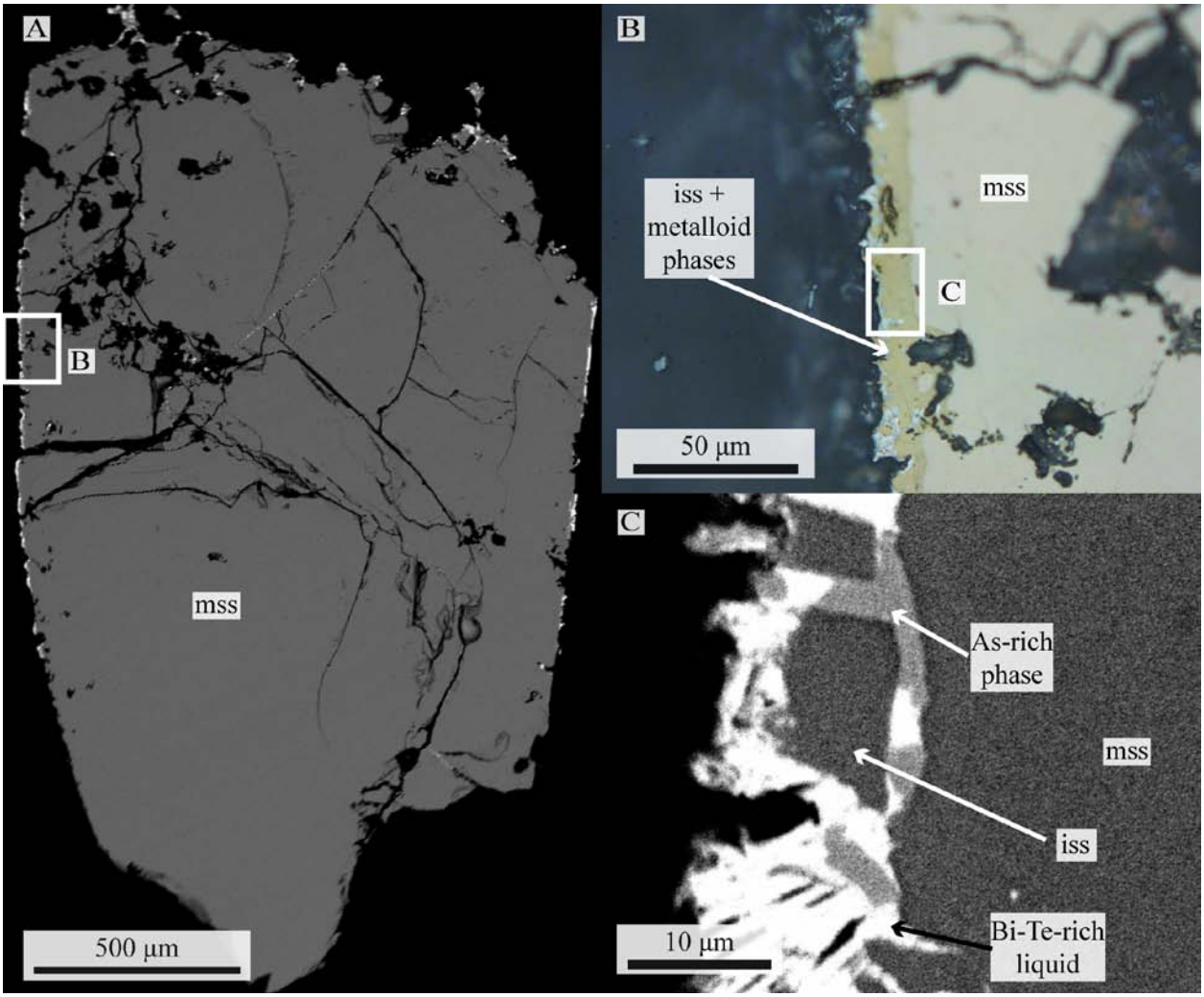

Figure 14. Images showing the results of an experiment containing As, Bi, and Te (K-series) and equilibrated at 900 °C. A. BSE image showing that the sample is dominated by mss; Iss is almost absent and concentrated in a thin veneer at the interface between the run product and the silica capsule. B. Reflected light image showing the iss-rich veneer (yellow) in more detail as well as some metalloid-bearing phases (silver-grey) which are concentrated with iss at the margin of the sample. C. BSE image showing the relationship between iss (dark grey), As-bearing phase (medium gray) and Bi-Te-rich phase (white).

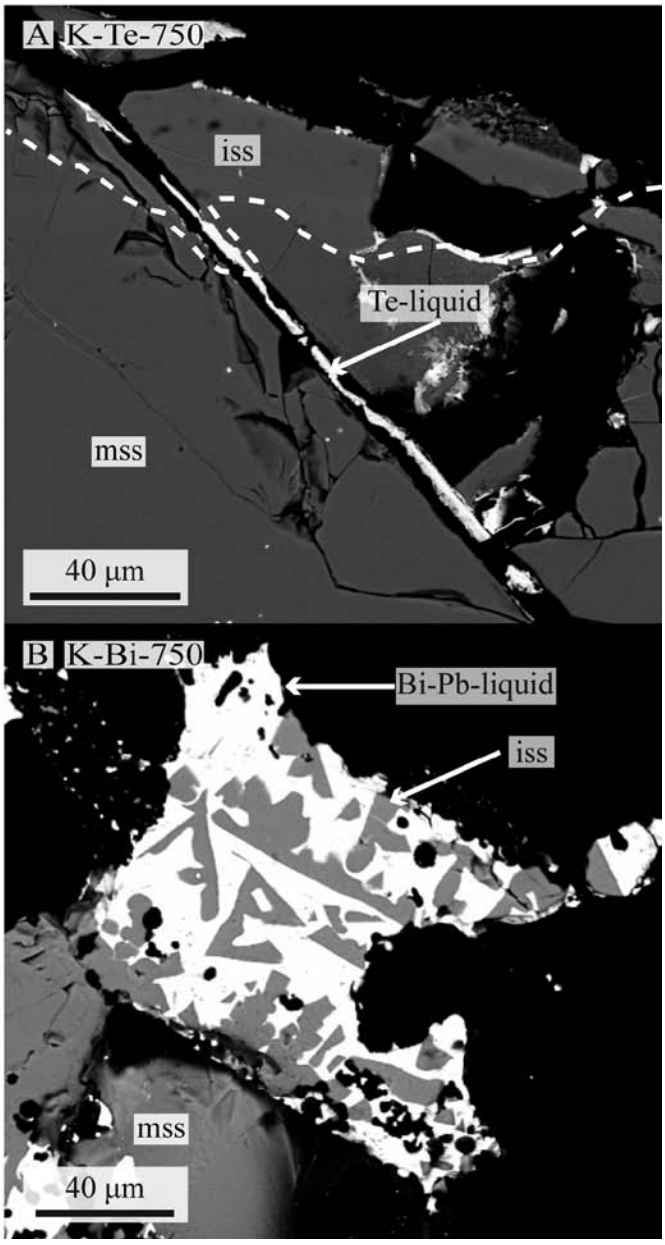

Figure 15. BSE images of experimental products equilibrated at 750 °C. A. Te-rich run (K-Te-750). Metalloid liquid is mainly associated with iss at the interface between the sample and the capsule or filling fractures within mss. B. Bi-rich run (K-Bi-750). Bi-Pb-bearing phases (white) and iss (gray).

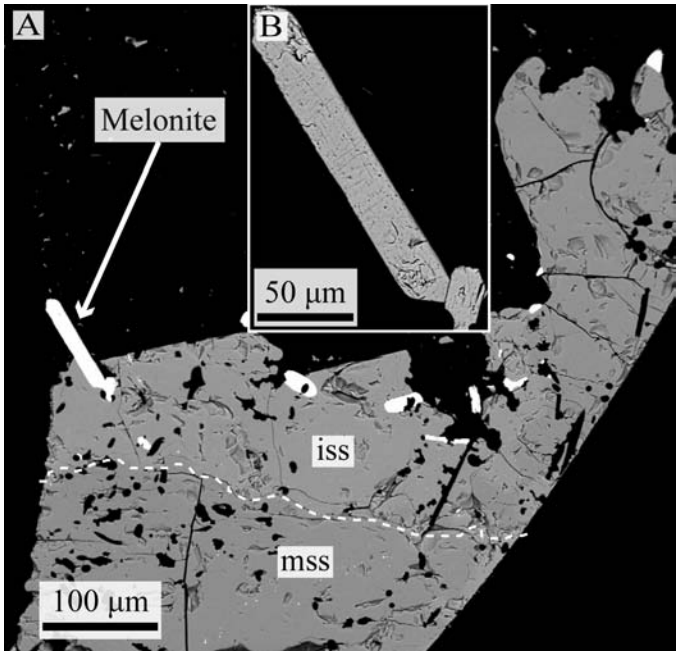

Figure 16. Example of Te-bearing run, equilibrated at 600 °C. A. BSE image showing melonite crystals hosted by iss, overlaying mss. B. (Insert) Detail of the largest euhedral melonite crystal observed.

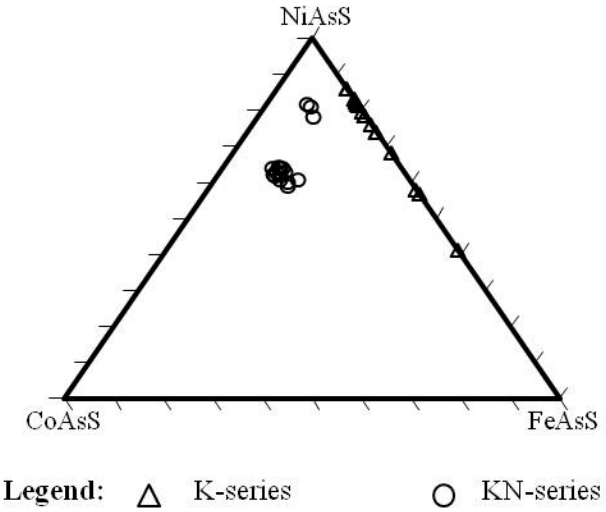

Figure 17. Composition of gersdorffite-cobaltite group minerals observed in run products. Cobalt was added only to the experiments of the KN-series.

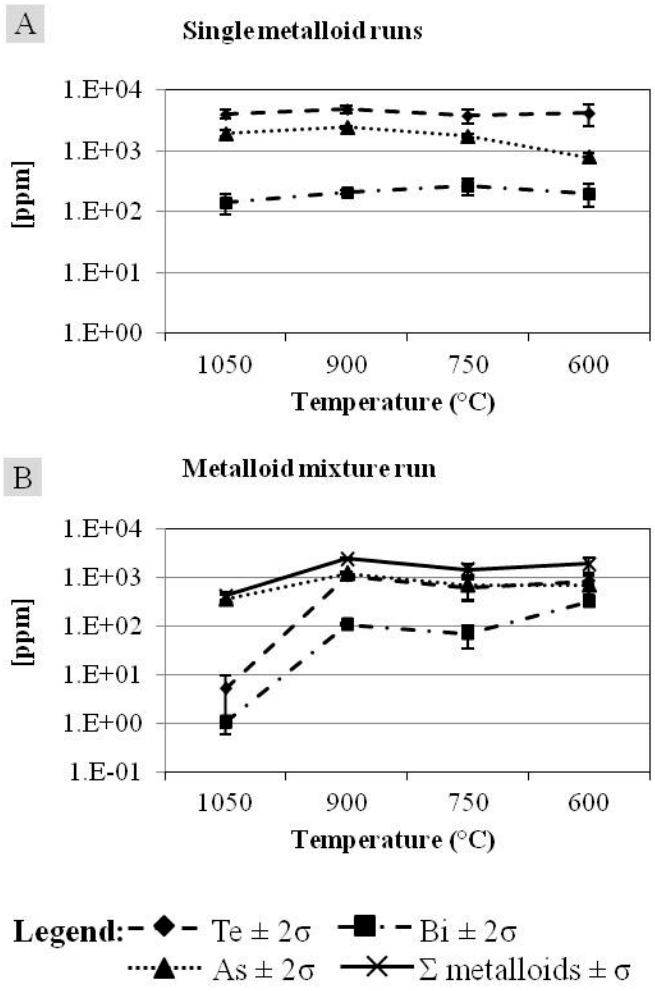

Figure 18. Metalloid content in mss (by LA-ICP-MS) equilibrated at different temperatures from experiments of the K-series.
A. From experiments containing a single metalloids
B. From experiments containing a mixture of metalloids.

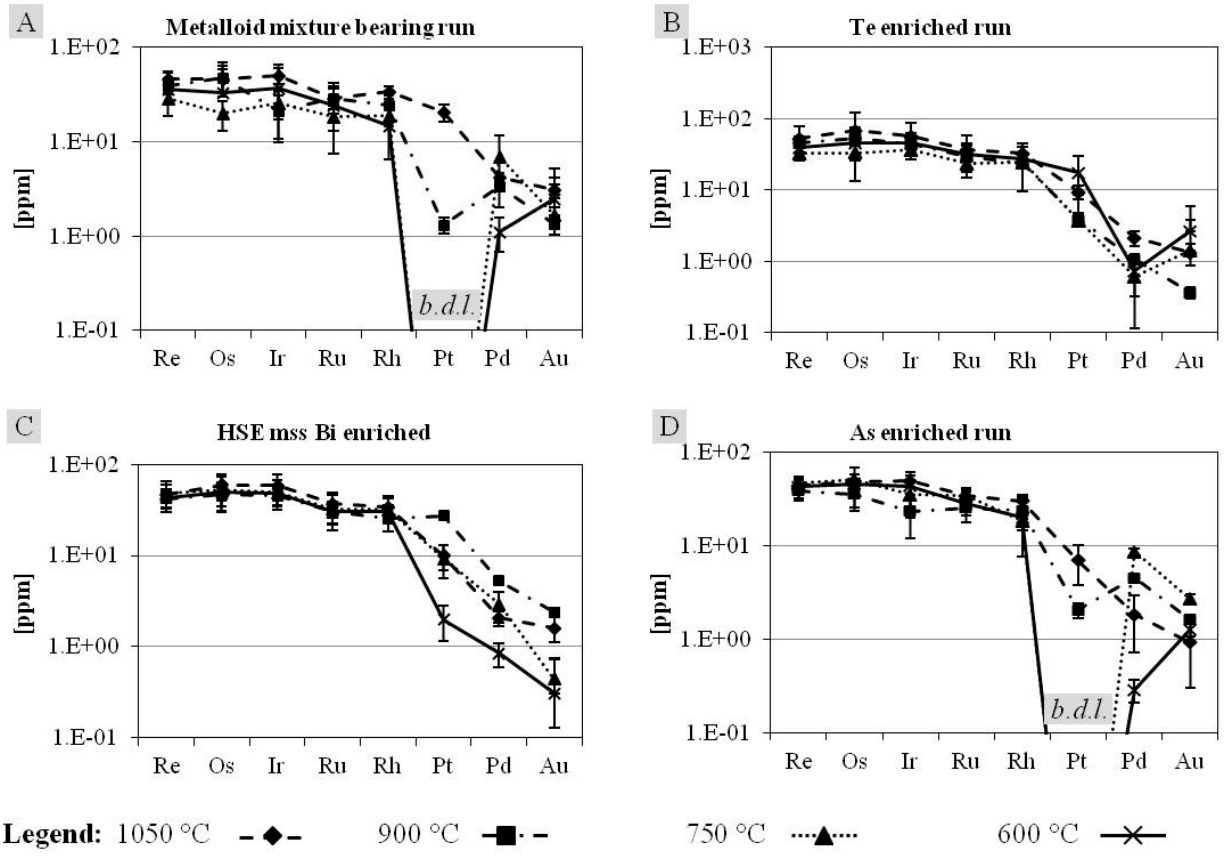

Figure 19. Concentration of HSE in mss (by LA-ICP-MS) from experiments of the K-series. A. Experiments containing mixtures of As, Bi, and Te. B. Experiments with only Te added. C. Experiments with only Bi added. D. Experiments with only As added.

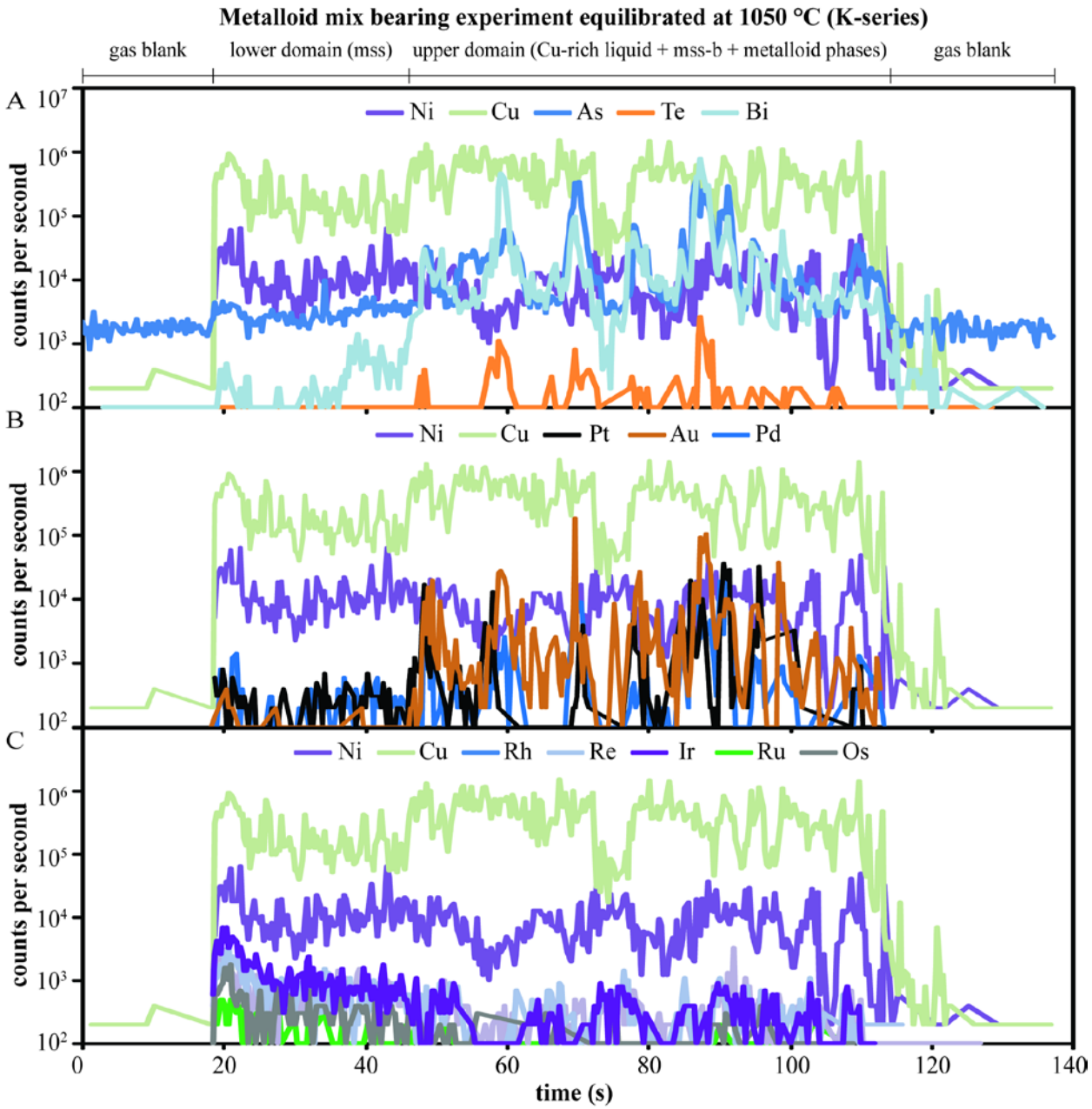

Figure 20. Time resolved spectra obtained from a line scan ablation through the part of the lower (mss) and the upper (mss-b, Cu-rich liquid and metalloid phases) domains of the metalloid mixture-bearing experiment equilibrated at 1050 °C. A. Metalloid spectra showing spikes corresponding to the ablation of metalloid-rich phases. B. Spectra belonging to Au, Pd and Pt. Positive spikes correspond to the metalloid spikes in A, indicating that the high concentrations are detected in the same phase. C. Spectra belonging to the other HSE. The intensity of the signal decreases from mss into the upper domain phase. No outstanding spikes are detected throughout the upper domain.

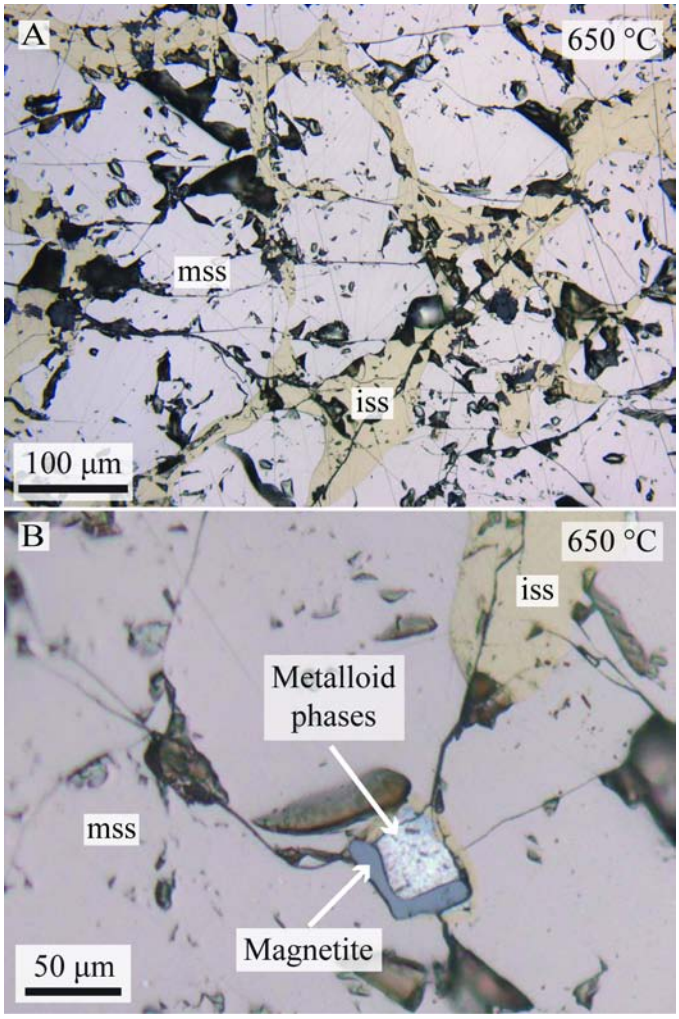

Figure 21. Example of run products from experiments of the KN-series. The experiments contained a higher proportion of Cu and Ni than the K-series, were doped with a mixture of As, Se, Sb, Te and Bi. Capsules were slowly cooled from 750 °C to 650 °C, then quenched. A. Reflected light image. Rounded grains of dominant mss (light pink) are separated by interstitial iss (yellow). B. Detail showing magnetite wrapping around a cluster of metalloid-bearing phases surrounded by a small patch of iss.

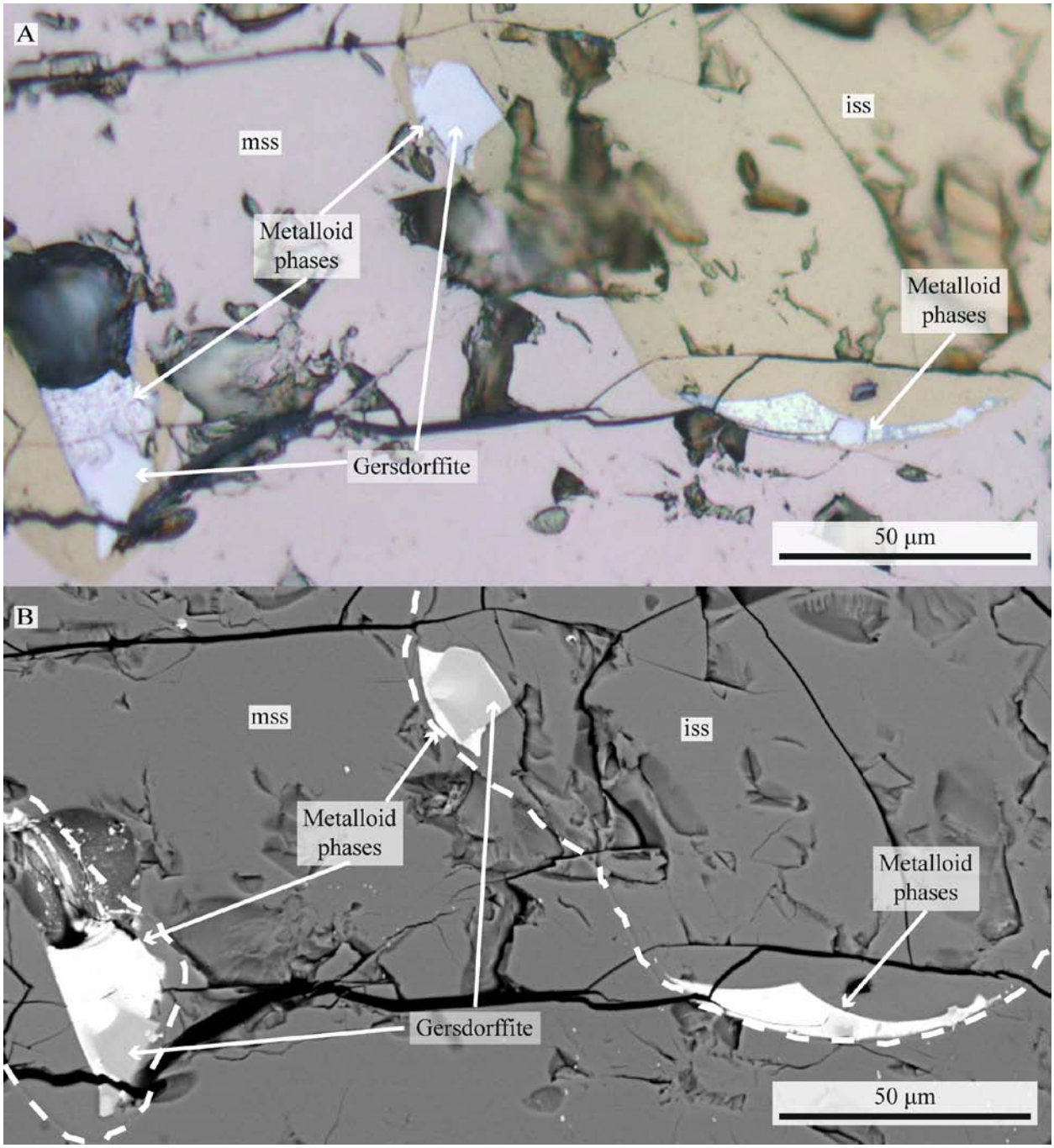

Figure 22. Examples of synthesized phases from experiments of the KN-series that contained 2 wt.% of a mixture of metalloids. A. Reflected light image showing mss (pinkish grey), iss (yellow), and metalloid-bearing phases occurring mainly within the iss and at near the boundary between mss and iss. Two metalloid domains can be seen: smooth uniform crystals of gersdorffite (medium grey) and a granular aggregate of metalloid-bearing phases (lighter grey). B. BSE image showing gersdorffite-cobaltite forming relatively large and most euhedral grain (medium grey) and how the other metalloids (white) wrap around the gersdorffite-cobaltite crystals. Relatively small nuggets were also included in mss (white specks).

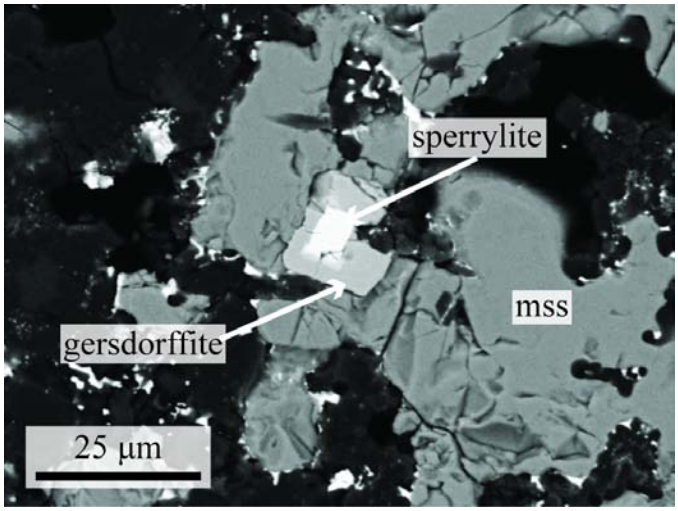

Figure 23. BSE image showing details of the run products obtained from experiments of the KN-series bearing 2 wt.% metalloid mixture and quenched at 650 °C. Euhedral crystal of sperrylite (white at the center of the picture) overgrown by gersdorffite-cobaltite (light gray) in a background of mss.

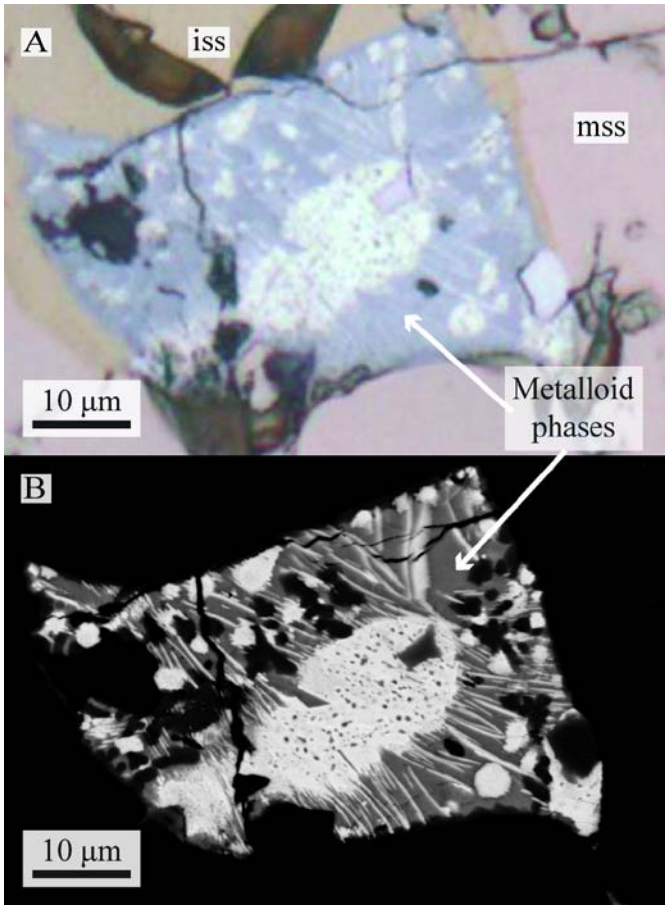

Figure 24. Images showing details of a metalloid-rich domain obtained from an experiment containing 2 wt.% of a metalloid mixture and quenched at 650 °C. A. Reflected light image showing the complex intergrowth of different phases within the domain. BSE image with brightness and contrast adjusted to highlight the different phases. The metalloid domain is composed of several different very small phases. Arsenic is concentrated in relatively larger gersdorffite crystals (darker grey), Bi is concentrated in the in center of the domain and in needle-like crystals likely formed upon quenching (brighter, lighter grey-white).

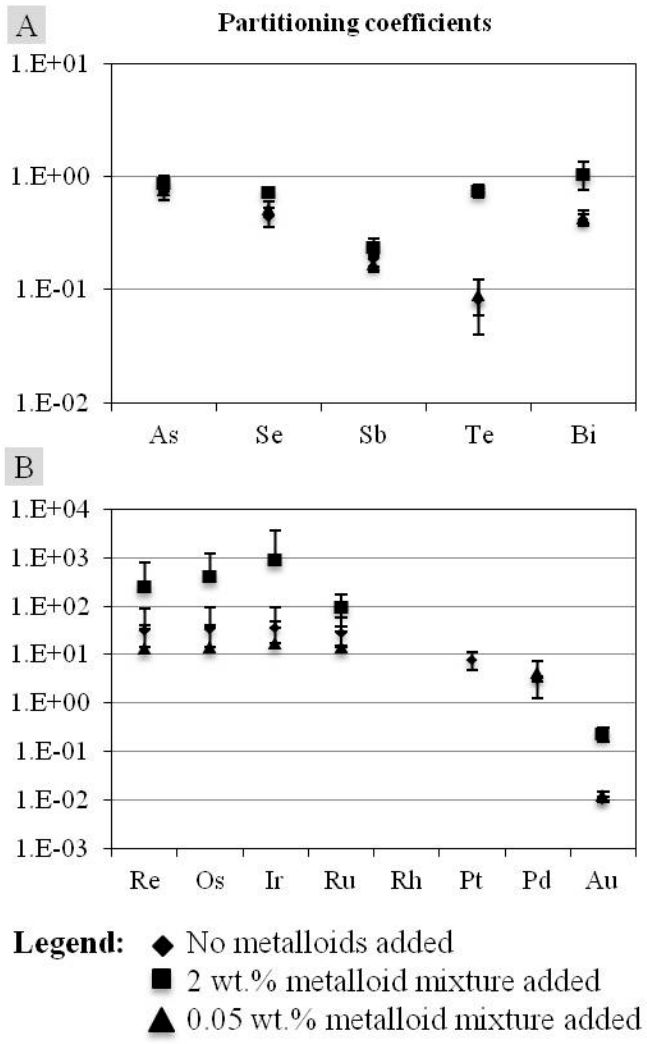

Figure 25. Partition coefficients between mss and iss obtained from experiments of the KN-series, equilibrated at 650 °C.
A. Partition coefficients of metalloids between mss and iss.
B. Partition coefficients of HSE between mss and iss.

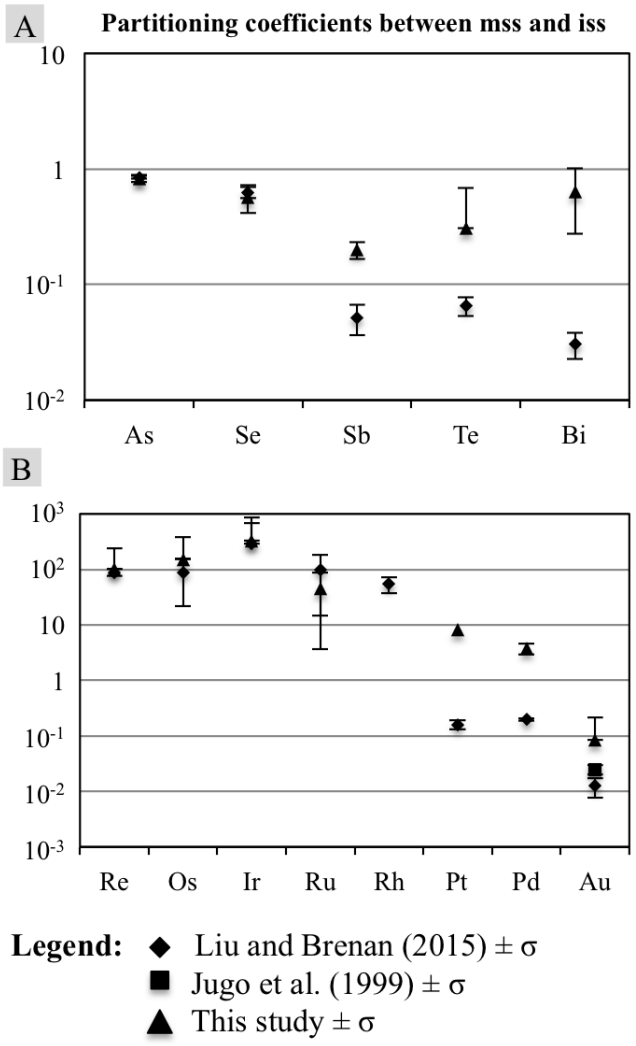

Figure 26. Comparison of partitioning coefficients of metalloids and HSE between mss and iss.

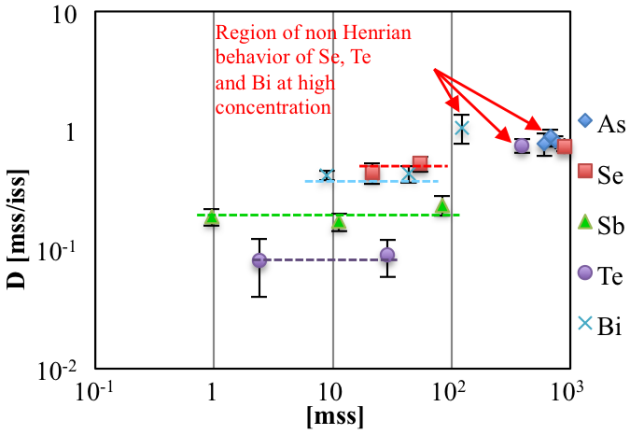

Figure 27. Partitioning coefficients of metalloids between mss and iss from KN-series plotted against the concentration of metalloids in mss to evaluate the Henryan behavior of metalloids at different concentrations. The error bar is 1σ. In the red circles the data showing non-Henryan behavior of Se, Te and Bi from the highly enriched experiments.

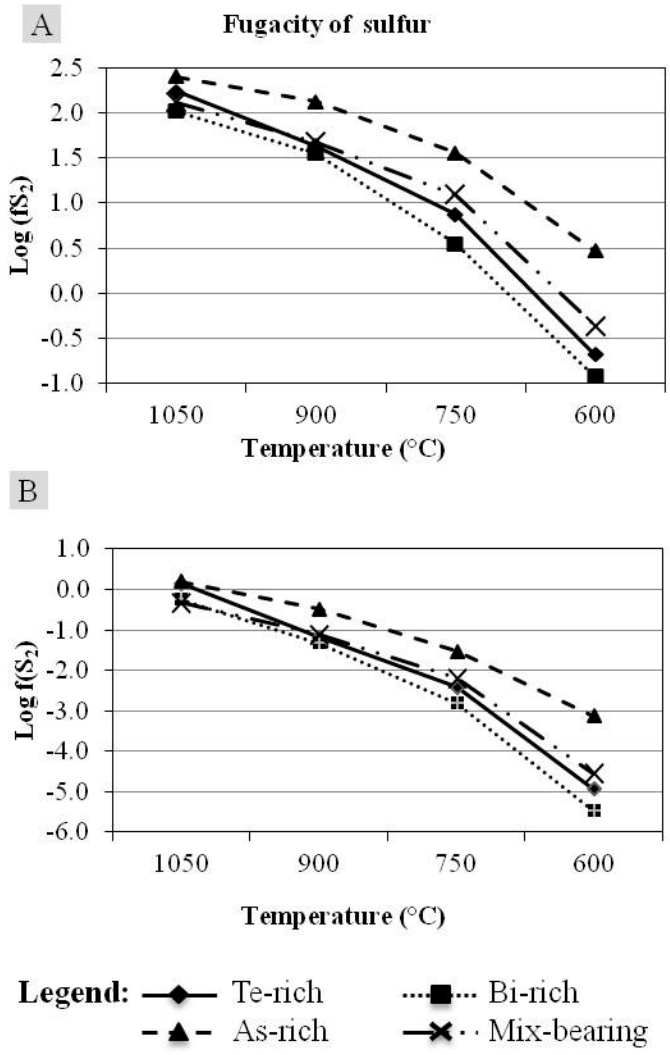

Figure 28. Fugacity of S (fS_2) estimated for the experiments of the K-series as a function of temperature. A. Using the equation from Toulmin and Barton (1964), which does not account for substitution in pyrrhotite. B. Using the modified Toulmin-Barton equation (Mengason et al., 2010) that accounts for other metals (Co, Zn, Mn, Ni, Cu, Ag, Au) in pyrrhotite.

Chapter 4

Magmatic Origin of Co-rich, PGE-bearing Pyrite: An Experimental Study on the Geochemical Behavior of Highly Siderophile Elements (HSE) and Metalloids in a mss-iss-pyrite System at 650 °C

Abstract

Pyrite is the most abundant sulfide on the Earth's crust and is a common accessory mineral in several magmatic sulfide deposits. Although most pyrite is hydrothermal, previous experimental studies have shown that pyrite can also have a primary magmatic origin, for example by exsolving from monosulfide solid solution (mss) after protracted cooling of a sulfide melt. Pyrite from some localities has significant amounts of Co, low-melting-point chalcophile elements (LMCE, such as As, Se, Sb, Te, Bi) and some platinum group elements (PGE: Ru, Rh, Pd, Os, Ir, Pt). The distribution of some of these elements is not homogeneous and seems to be developed in concentric zones, indicating different growth stages. The origin of such pyrite and the causes of element zonation are not clear. Better constraints on the origin of Co-rich, PGE-bearing pyrite can help unravel the geochemical processes affecting the sulfide assemblages in which it is found. An experimental study was undertaken to characterize pyrite formation in magmatic sulfide environments and its relationship with LMCE and highly siderophile elements (HSE: PGE, Re, Au). These two groups of elements were studied simultaneously using natural sulfides (pyrrhotite, chalcopyrite, and pentlandite) and elemental S. The sulfides were mixed and doped with approximately 50 ppm of each HSE. A mixture of metalloids was added in the concentration of 0.2 wt. % or 3 wt. % to aliquots of sulfide mixtures. Starting materials were sealed in evacuated silica tubes and fused at 1200 °C for four hours. Temperature was subsequently reduced to 750 °C at a rate of 60 °C/h, then to 650 °C at a rate of 0.5 °C/h to produce relatively large euhedral pyrite crystals; the experiments were then quenched. Experimental products contained euhedral pyrite, mss, interstitial intermediate solid solution (iss) and LMCE-bearing phases (interpreted as quench product of an immiscible

LMCE-bearing liquid). The sulfides were analyzed with EMPA-WDS for major elements, whereas LA-ICP-MS was used for trace elements and to construct element distribution maps in pyrite. The results show that Co-Ni-rich, HSE-bearing pyrite can form during cooling of a sulfide melt and can therefore be considered a magmatic phase. Among the HSE, Ru, Rh, Os, Re, Ir partition equally between mss and pyrite, Pt and Pd show overall preference for mss and Au partitions strongly into iss. The presence of LMCE-bearing phases affected only the concentration and partitioning of Au, Pt and Pd in sulfides. In some experiments, Co, Ni, Ru, Rh, Os, and Ir concentrated in the core of pyrite grains, indicating that the element zonation documented in some naturally occurring pyrite may also be produced during cooling of a sulfide melt.

4.1. Introduction

Pyrite is the most abundant sulfide in the Earth's crust (Craig et al., 1998) and commonly occurs as a minor or accessory mineral in the sulfide assemblage of several magmatic ore deposits, such as the Sudbury district, Canada (Hawley, 1962; Craig and Solberg, 1999; Dare et al., 2011), the Great Dike, Zimbabwe (Oberthür et al., 1997), the Imandra complex, Russia (Barkov et al., 1997), the Platreef, South Africa (Armitage et al., 2002), Aguablanca, Spain (Piña et al., 2012), Lac-des-Îles, Canada (Djon et al., 2012) and Thompson, Canada (Franchuk et al., 2013). Most pyrite is hydrothermal and without any significant trace elements of interest, but some hydrothermal pyrite has been shown to contain Au (e.g., Large et al., 2009; Deditius et al., 2014). Typically, studies of sulfide assemblages from magmatic Ni-Cu-PGE deposits tend to ignore pyrite and focus on other sulfides, such as pyrrhotite, pentlandite and chalcopyrite. Nevertheless, several studies have documented relatively high concentration (generally tens to thousands ppm, but up to few wt. % level) of Rh and IPGE (IPGE: Ir-like platinum-group elements: Os, Ir, Ru, Barnes et al., 1985) in pyrite from different deposits (Barkov et al., 1997; Dare et al., 2011; Piña et al., 2012; Djon et al., 2012) and Lorand and Alard (2010) documented high IPGE content in pyrite from Pyrenean peridotites. With exception of the relatively high Pt content in idiomorphic pyrite from Aguablanca, Spain (Piña et al., 2012), pyrite in magmatic ore deposits is reported to be generally poor in Pt, Pd and Au, a significant contrast to Au-rich pyrite of metamorphic or hydrothermal origin, such as orogenic gold deposits or Carlin-type deposits (Large et al., 2009; Deditius et al., 2014). Another aspect of interest is that pyrite can show concentric zonation in Co, Ni and some HSE (Craig and Solberg, 1999; Large et al., 2009; Dare et al., 2011).

Other trace elements of interests are also present in Co-rich PGE-bearing pyrite, in particular some of the low-melting point chalcophile elements (LMCE), a term introduced by Frost et al.

(2002) to refer to a group of chalcophile elements that have melting points below 1000 °C (Ag, As, Bi, Hg, Se, Sb, Sn, Tl and Te). The term 'LCME' is convenient because many of those elements are grouped under various names ('pnictogens' for As and Sb; 'chalcogens' for Se and Te; 'post-transition metal' or simply 'metal' for Bi, etc.; Westland, 1981). Among the LMCE, As, Bi and Te are of particular interest because they form platinum-group minerals (PGM) with some of the HSE. Because As and Te (along with Sb and sometimes Se) are commonly known as metalloids and Bi substitutes for Te in most PGM, we will refer to this subset of the LMCE (i.e. As, Se, Sb, Te, Bi) as metalloids henceforth, to distinguish them from the rest of the LMCE. Fleet et al. (1993) showed that metalloid-rich liquids coexist with mss at high temperature (~ 1000 °C) if the total metalloid content is about 1 wt.%. Experimental results of Helmy et al. (2010) showed that if As is added in percentage concentrations, the system will stabilize sperrylite (if Pt is present) or contain an immiscible Pd-Ni-As-bearing immiscible melt (when Pd is present instead of Pt). Helmy et al. (2007) highlighted the potential role of immiscible metalloid-bearing melts as possible carriers of some HSE (in particular Pd and Pt) and estimated that a mss-iss system will be saturated in Te-bearing phases when the Te content in mss and iss is approximately 3000 ppm. However, there is still little data regarding the amount of other metalloids and the effect of metalloids on the rest of the HSE in sulfide systems.

Few experimental studies have been conducted on magmatic pyrite. Kullerud et al. (1969) established that pyrite would only be stable below 743 °C in the Fe-S system and defined the phase assemblages in the Fe-Ni-Cu-S system. They showed that pyrite coexists with mss and iss below 739 °C if the total metal content to S (ΣM/S in at. %) is slightly higher that one. Craig (1973) obtained pyrite coexisting with pentlandite after experiments conducted at 400 °C and 200 °C and similar results are documented in Misra and Fleet (1973). Ueno et al. (2000) refined

the Fe-Ni-S system at 500 °C and 400 °C and obtained pyrite coexisting with mss and vaesite. To our knowledge, no experimental studies considering the incorporation of HSE and LMCE into pyrite and coexisting iss and mss have been published.

Experiments in the mss-iss-pyrite section of the Fe-Ni-Cu-Co-S system were conducted in the presence of the complete suite of HSE and the metalloid subset of the LMCE (As, Se, Sb, Te, Bi). The results obtained in this study show that Co-rich HSE-bearing pyrite can form from cooling of sulfide melts. Experiments aiming to reproduce this type of pyrite via hydrothermal processes are still needed; however, this study emphasizes the potential of pyrite as a phase that keeps a record in trace element content and element distribution, which is meaningful to interpret the paragenesis of the sulfide assemblages in which it is found. The fact that pyrite can host significant amounts of HSE (e.g., Piña et al. 2012) is also relevant for mineral processing, as some of the HSE in the whole rock may be trapped inside Co-bearing pyrite; thus, proper characterization of pyrite may be required in some ores to assess and optimize HSE recovery.

4.2. Experimental methods and analytical techniques

The starting materials used for the experiments were divided in three groups: sulfides, HSE and metalloids. Each group contained a mixture of materials. The sulfide mixture contained natural pyrrhotite (from North Bend, USA), pentlandite (from Morrison Mine, Sudbury), chalcopyrite (from Messina, South Africa), as well as synthetic elemental S and CoS (99.5 %, from Alfa Aesar). Natural pyrite (from Navajún, Spain) was used in some of the preliminary experiments. The natural sulfides were characterized with electron probe microanalysis using wavelength dispersive spectrometry (EPMA-WDS) for major elements and with laser ablation-inductively

coupled-mass spectrometry (LA-ICP-MS) for trace elements. The composition of the natural sulfides used for the experiments are listed in Table 14, which shows very low concentration of HSE, Sb, Te and Bi; significant amounts of As, Se and Co; and minor amounts of other chalcophile elements (e.g., Mn, Zn, Cd and Sn).

Preliminary experiments (Table 15) aimed to obtain the desired run products (mss, iss, pyrite) and were conducted without added metalloids or HSE, following previous experimental studies in pyrite-bearing sulfide systems (Kullerud et al., 1969; Misra and Fleet, 1973; Craig, 1973). Vaesite (NiS_2) was a ubiquitous product in many of the preliminary experiments and the proportion of the starting sulfides was modified to produce Ni-bearing assemblages without stabilizing vaesite.

Approximately 50 ppm of each HSE (Ru, Rh, Pd, Re, Os, Ir, Pt, Au) were diluted in pyrrhotite, following a two-step dilution protocol. First, 1 mg of each HSE were mixed to 492 mg of pyrrhotite, fused at 1200 °C and quenched, thus obtaining a pyrrhotite nominally doped with 0.2 wt.% HSE (although in fact, is composed of HSE-saturated pyrrhotite and excess HSE). Second, small amounts of the doped pyrrhotite were added to the starting sulfide mixture (Table 16), to reach the nominal concentration of 50 ppm per HSE in the mixture. This protocol is a modification of the protocol used by Sylvester et al. (2005) and Wohlgemuth-Ueberwasser et al. (2007) to prepare HSE-bearing sulfide standards for LA-ICP-MS.

Metalloids were added as a mixture of As, Se, Sb, Te and Bi in a 1:1 molar proportion (Table 16). Three experiments with different metalloid concentrations were prepared:

- 3.0 wt.% metalloid mix

- 0.2 wt.% metalloid mix

- No added metalloids ("control" run with natural concentrations of metalloids).

Approximately 250 mg of starting materials were placed at the bottom of silica tubes (GE Type 214, 6.0 mm outside diameter and 1.5 mm wall thickness and a total length between 6.5 and 7 cm). The materials occupied roughly the bottom 15-20 mm of the capsules and were overlain by silica wool (3-5 mm thickness) and a silica rod spacer (approximately 5 cm long, occupying the uppermost part of the capsules). Silica tubes were evacuated and flushed with Ar several times then welded with a hydrogen-oxygen torch under vacuum (10^{-2} torr). The obtained capsules were attached with a Pt-wire to a multi-sample holder and run simultaneously in a 1-atm vertical furnace. Prior to conducting experiments, the profile of the thermal gradient in the tube furnace was measured by placing the tip of an external thermocouple at different heights in the tube. The hot spot of the furnace is approximately 7 cm long and is located in correspondence of the two type R thermocouples that are connected to a programmable temperature controller with multi-segment capability. Care was taken to place the bottom part of the capsules, where the starting materials are located, as close as possible to center of the hot spot of the furnace.

Temperature was slowly increased to 200 ℃, 300 ℃ and 400 ℃ and left at each of those temperatures for 2 hours, to consume the elemental sulfur and avoid explosive exothermic reactions (Wohlgemuth-Ueberwasser et al., 2007). Subsequently, temperature was raised to 1200 ℃ at a rate of 60 ℃/h, to completely melt the sulfides and kept at 1200 ℃ for four hours. Temperature was then lowered to 750 ℃ at a rate of 60 ℃/h. This temperature was chosen because it is only few degrees above the upper stability limit of pyrite (743 ℃ in the Fe-Cu-S system, Kullerud et al., 1969). The cooling rate was then lowered to 0.5 ℃/h to promote the

crystallization of pyrite and the system was cooled to 650 ℃, then quenched in cold water. Some preliminary experiments (FS-13 to FS-19) were not quenched at 650 ℃, but, after the slow cooling step, they were allowed to cool to 240 ℃ at a rate of 60 ℃/h, at which point the cooling rate was reduced to 1 ℃/h until the experiments reached 200 ℃ and then quenched. These two extra steps were added to try to stabilize pentlandite and have it coexist with pyrite (cf. Misra and Fleet, 1973; Craig, 1973). However, the experiments did not produce pentlandite-bearing assemblages and longer equilibration times may be needed.

After quenching, capsules were sectioned longitudinally, the synthesized products mounted in epoxy and polished manually. Reflected light images were taken before carbon coating for SEM. Back scattered electron images were taken with a Zeiss EVO 50 SEM at the Ontario Geoscience Laboratories in Sudbury (GeoLabs), with an accelerating voltage of 20 kV and 750 pA beam current. Major elements were analyzed with a WDS using a Cameca SX100 electron microprobe at GeoLabs, at 20 kV accelerating voltage. Iron, Ni, Cu and S were analyzed for 15 s at 20 nA current, whereas Mn, Co, Zn, As, Se, Te, Sb, Pb and Bi for 20 s at 200 nA. Iron, Mn, Co and Zn were analyzed using a LiF crystal; Cu, Ni (Kα2), As and Se with a LLiF crystal; Te (Lα) with a PET crystal; Sb, Pb and Bi with a LPET crystal. Trace elements were analyzed with LA-ICP-MS (Resonetics RESOlution M50 laser probe and a Thermo-Fisher XSeriesII ICP-MS) at Laurentian University. The analyzed isotopes are: ^{33}S, ^{55}Mn, ^{57}Fe (used as internal standard), ^{59}Co, ^{60}Ni, ^{61}Ni, ^{63}Cu, ^{65}Cu, ^{68}Zn, ^{75}As, ^{77}Se, ^{99}Ru, ^{101}Ru, ^{103}Rh, ^{105}Pd, ^{108}Pd, ^{111}Cd, ^{118}Sn, ^{130}Te, ^{121}Sb, ^{185}Re, ^{189}Os, ^{193}Ir, ^{195}Pt, ^{197}Au, ^{208}Pb, ^{209}Bi. Dwell time was 10 ms on Fe, 5 ms on major elements and 15 ms on trace elements. Five line-scan analyses were performed on each phase. The laser beam was set at 26 μm in diameter and moved at a speed of 10 μm/s. The laser energy was 90 mJ, the fluence 5 J/cm^2 and the repetition rate 5 Hz. Po725 sulfide was the standard reference

material used for ^{99}Ru, ^{101}Ru, ^{103}Rh, ^{189}Os, ^{193}Ir, ^{195}Pt, whereas NIST610 glass was used for all other elements. There are some elements that are present in both reference materials. The concentrations of overlapping elements, obtained with both reference materials, were confronted and gave similar results. To account for the interference of ^{40}Ar argides with ^{59}Co, ^{61}Ni, ^{63}Cu and ^{68}Zn on ^{99}Ru, ^{101}Ru, ^{103}Rh and ^{108}Pd, a set of natural samples (gersdorffite-cobaltite, millerite, chalcopyrite, and sphalerite) with HSE content below detection limit were analyzed at the beginning and at the end of each session. The calculated argide production was then subtracted from the analyses. Trace element distribution maps were performed on one selected pyrite grain and surrounding mss and iss in each of the three run products. Relatively large grains with sections that passed close to the center of the crystal were used. The sections chosen were those that best approximated a regular hexagon because only hexagonal sections unequivocally pass through the center of a cube (as they are produced by planes perpendicular to the maximum diagonal on a cube). In contrast, square and trapezoidal sections are roughly parallel to a face (but not necessarily pass through the center of a cube) and triangular sections pass closer to a vertex than to the center of the solid. For the maps, the laser beam size was reduced to 10 μm in diameter. This decreases sensitivity, but increases resolution (good-resolution maps required approximately 50 parallel ablation lines). All analyses were processed using Iolite 2.5 for IgorPro 6.34A. Each time resolved spectra obtained from the ablations was inspected to assess the presence of nuggets, which appeared as isolated spikes emerging from uniform spectra. To obtain the element concentration in sulfides, only the nugget-free parts of signal were integrated. Examples of time resolved spectra on a pyrite grain are shown in Figure 29.

4.3. Results

Early preliminary experiments did not produce pyrite (FS-13 and FS-14). In FS-13 (ΣM/S = 1.08) only mss and pentlandite were present, whereas FS-14 (ΣM/S = 0.92) was composed only of mss. Pyrite was first obtained in the Cu-free FS-15 run. The crystals that formed were small and anhedral, completely surrounded by the dominant mss and often associated with abundant vaesite (Figure 30A). Subsequent experiments used progressively less Ni/(Fe+Ni), until vaesite was absent from the run products (composition P-04). This composition also resulted in larger pyrite crystals and was used as the base for HSE and metalloid-bearing experiments. With the introduction of Cu through chalcopyrite among the starting materials, iss appeared in the run products (Figure 30B). The compositions of the preliminary experiments and the final experiments are plotted in Figure 31.

The run products of the three main experiments are composed of dominant mss, followed by pyrite crystals, iss, metalloid phases and some PGM (Figure 32). Monosulfide solid solution is the most abundant phase. It occurs as relatively large, rounded and texturally homogeneous crystals. The mss crystals are often physically separated from each other and the interstices are filled by anhedral iss. Intermediate solid solution is not homogeneous, but is associated in most cases with metalloid phases and pyrite crystals. Pyrite crystals are relatively large (up to 500 μm) and euhedral to subhedral. Pyrite is always surrounded, partially or totally, by iss and was never found surrounded only by mss (Figure 32A and Figure 32B). In contrast, pyrite was often surrounded entirely by iss or contained inclusions of iss (Figure 32E). When present, metalloid domains composed of aggregates of several different metalloid-bearing phases were found mostly within iss (Figure 32C and Figure 32D), but were found also as inclusions in pyrite and, rarely, in mss.

Figure 33 shows reflected light and BSE images of the metalloid-rich domain in experiment P-13 The metalloid-domain is a fine intergrowth of several phases, which likely exsolved from a metalloid-rich immiscible melt during quenching. The composition of the metalloid phases was assessed only with semi-quantitative EDS (Appendix 2) and mainly to determine if PGM where present. However, no PGM (e.g., sperrylite) or sulfarsenides (e.g., gersdorffite) were recognized and the HSE were below detection limit.

The sulfides of the three main experiments have the same major element composition regardless of the concentration of metalloid mixture added. The major and trace element concentration in each sulfide is listed in Table 17 and plotted in Figure 34. Calculated Nernst partition coefficients (with propagated uncertainties) for each sulfide pair are listed in Table 18 and plotted in Figure 35 and Figure 36. The partitioning coefficients (between mss and iss) here obtained were compared with those obtained for the KN-series experiments (chapter 3). All the values are in very good agreement (Figure 37). Also, because metalloids were added at different concentrations, it was possible to evaluate whether metalloids respected the Henry's Law (e.g. Prowatke and Klemme, 2006). The large uncertainties shown in Figure 38 for Te and Sb, do not allow a reliable evaluation. The other metalloids (Se, As, Bi) showed Henrian behavior (all partitioning values are in agreement within uncertainty regardless of concentration in mss). In this case, the behavior of metalloids from these experiments is different relative to the KN-series experiments of chapter 3. In chapter 3, in fact, Te, Se and Bi showed a dependence of partitioning coefficients from initial metalloid concentrations.

The major element composition relationship between the three sulfides is shown in a modified Fe-Ni-S ternary diagram (Figure 39A) and in a modified Cu-Fe-S diagram (Figure 39B) that account for other components (Co, Mn, Zn). Monosulfide solid solution contains significant

amounts of Ni (3.5 wt.% to 4.3 wt.%), Cu (2.9 wt.% to 3.0 wt.%), Co (6000 to 7150 ppm) and Mn (6300 to 6980 ppm). The concentrations of metalloids and HSE in all sulfide phases are also shown in Figure 34. In the two runs in which metalloids had been added, Se and As are most abundant in mss. Among the HSE, Re, Ru, Os, Ir, Rh and Pt have comparable and very similar concentration in all three runs, within uncertainty, ranging as a group between 27.3 ± 3.1 ppm (Ru) and 85 ± 19 ppm (Re). Palladium also shows roughly uniform concentration in mss (9.22 ± 0.25 ppm to 11.13 ± 0.85) among the three experiments. Gold is the HSE that showed the greatest variation within mss. When metalloids were not added, Au content in mss reached 7.5 ± 1.1 ppm, whereas it was 4.01 ± 0.58 ppm and 0.85 ± 0.36 ppm in the mildly enriched and the highly enriched experiments, respectively.

The synthesized iss (25.53 ± 0.23 Cu; 36.05 ± 0.05 Fe, 35.05 ± 0.18 S, 0.53 ± 0.05 Ni; in wt.% ± 2σ) has a major element composition intermediate between those of cubanite (23.4 Cu, 41.2 Fe, 35.4 S) and chalcopyrite (34.6 Cu, 30.4 Fe, 34.9 S), contains high amounts of Mn (1.3 wt.% to 1.4 wt.%) and Zn (7900 ppm to 1.4 wt.%) and was significantly enriched in Au (containing between 89 ppm and 690 ppm of Au). The synthesized pyrite was rich in Co and Ni, containing between 3.4 wt.% and 5.3 wt.% Co and 1.9 wt.% to 2.4 wt.% Ni. Metalloid and Re, Ru, Os, Ir, Rh, Pt content in pyrite were similarly to those recorded for mss and ranged from 16 ppm Pt to 70 ppm Ir. In contrast, Pd and Au content in pyrite were very low, ranging from 0.10 ppm Pd to 2 ppm Au (Table 17).

The composition of mss was used to calculate the fugacity of S_2, using the formula derived by Toulmin and Barton (1964) for the Fe-S systems, but with the modification introduced by Mengason et al. (2010) to account for the presence of other metals in pyrrhotite. The fS_2 obtained range between -0.55 log units (experiment P-07 with 0.2 metalloid mixture) and -1.00

log units (high metalloid concentration, P-13). The experiments in which no metalloids were added (P-12) returned a fS_2 of -0.88 log units. Our results plot closely to the pyrrhotite-pyrite boundary defined in the Fe-S system by Toulmin and Burton (1964).

Element distribution maps for each of the 3 main experiments are shown in Figure 40 to Figure 43 (Figure 42 shows time-resolved spectra of one of the ablation lines used to create Figure 41). The maps show the element distribution in pyrite and coexisting mss and iss and are centered on pyrite because only pyrite showed complex zonation. Reflected light and back-scattered electron (BSE) images are included for reference and to show the presence of PGM detectable under the SEM. Figure 40 shows element distribution maps for the sulfide assemblage obtained in experiment P-12 (with no metalloids added). The distribution of key major elements outline each major phase: highest S is pyrite, highest Cu is iss; all that remain is mss (except when PGM of metalloids phases are present). Comparison with the Cu distribution map shows that Zn, Cd, Sn, and Au have preference for and partition strongly into iss. In contrast, the Pd distribution map shows that mss dominates the Pd budget in the system (at the conditions of the experiment). In fact, the Pd distribution map is the best of the set to outline the presence of mss; Mn CPS (counts per second) are slightly lower than in iss; Ni and Pt have comparable intensities in mss and pyrite, but are uniformly distributed in mss and zoned in pyrite. Pyrite is the most complex phase. The Co distribution map outlines pyrite best and shows that Co content is relatively uniform, whereas Ni content is higher towards the center and significantly low towards the edge of the grain. Arsenic, Sb, Te, Bi and Pb behave very similarly. They are generally present in very low concentration in pyrite, but have higher content along the edge of the py grain, at the grain boundary with the iss and mss. In addition, As, Sb, Te, Bi and Pb maps show localized spikes corresponding to small metalloid nuggets included in the pyrite grain. Two metalloid nuggets can

be seen in the BSE image, but the maps shows others that were either below the surface or too small to be detected by the SEM. In contrast to the other metalloids, Se shows no preference for any other sulfides present and is evenly distributed. Among the HSE, Ru, Rh, Re, Os and Ir show the same behavior. In the grain mapped, they occupy evenly the majority of the pyrite crystal; however there are irregular, sub-rounded patches with very low concentration that seem to have a random distribution in the grain. There are no discernible features in reflected light, the BSE image, or other element maps (such as S, Fe, Co and Se) indicating variable thickness, holes or other features that could explain the low intensity patches. The distribution of Pt is very asymmetrical: Pt concentrates mainly on one side of the grain, it has some similarities with the distribution of Ni but is completely different than the distribution of the other HSE. A comparison of the Ir and Pt maps shows that the almost circular 'patch' with very low Ir content on the lower right of the map has a high Pt content. Gold and Pd are mostly absent and can be seen only within spikes that emphasize the presence of metalloid-bearing phases trapped within pyrite.

Figure 41 shows element distribution maps for the sulfide assemblage obtained in experiment P-07 (0.2 wt.% metalloid mixture added). The time-resolved spectra resulting from an ablation line roughly at the middle of the mapped area is shown in Figure 42. In general, the results are consistent with the experiment described above: Zn, Cd, Sn and Au have strong preference for iss, Pd is dominantly in mss and pyrite shows complex distribution of elements. Based on the distribution of the IPGE (Ru, Rh, Os and Ir) and metalloids, this particular grain can be divided in three zones: a core with high IPGE content, a middle region with very low IPGE content and a rim, outlined mainly by the metalloids and Pb. In contrast to the pyrite grain shown in Figure 40, Co distribution is less uniform, with higher intensities (which translate proportionally to higher

content) towards the region shown in the lower left. The distribution of Se is also different. In the assemblage shown in Figure 40, Se was uniformly distributed among all sulfides present; however, in P-07 the core of the analyzed pyrite grain has an inner core with higher Se content, the edge of the pyrite grain is also outlined by Se and the rest of the crystal has relatively low Se content. The Re distribution is similar to that of the IPGE, although the intensity contrast is more subtle. Although Pt is also more abundant in the core, its distribution is similar to that of Co and different than the distribution of the IPGE. Two other aspects are significant. First, in addition to outlining the edge of the pyrite grain, the metalloids also mark clusters within the pyrite grain (e.g., lower center-left that contains some Pd, Pt and Au). Second, the IPGE formed their own clusters (e.g., brightest area towards top center of the core in Ru, Rh, Os, Ir maps), but those clusters are not associated with any of the metalloids or any of the mapped elements.

Figure 43 shows element distribution maps for the sulfide assemblage and metalloid phases obtained in experiment P-13 (3 wt.% metalloid mixture added). The mapped area includes an intergrowth of two pyrite grains that contain numerous inclusions of metalloid phases. The grain on the left side has rectangular section; thus, there is no real control on whether the section mapped is close to center of the grain. The exposed section of the grain on the right side is roughly hexagonal and expected to intersect the crystal close to its center. In general, the behavior of elements in iss and mss is similar to that observed in the previously discussed experiments and only the exceptions are discussed. In contrast to the two experiments discussed previously, metalloid-rich phases are abundant, clearly highlighted as the brightest (white) areas in the BSE image, both enclosed and surrounding the pyrite grains. These metalloids phases incorporate Pd, Pt and Au (as well as Cd and Sn), emphasizing the role of metalloids on the behavior of those three HSE. The IPGE are not associated with the metalloids, they are

dominantly in pyrite, but their distribution appears more chaotic and scattered. However, there are two features that deserve attention: (a) a sharp discontinuity that runs diagonally and, towards the right, from the upper corner of the grain with rectangular section; (b) the variations in intensity on the pyrite grain with roughly hexagonal section are consistent with growth zoning (best seen on the Rh and Ir maps). The last HSE to consider is the Re map, which shows small spikes that do not match the distribution of metalloids (plus Au, Pd, Pt) or the distribution of the IPGE.

4.4. Discussion

Although this is not first experimental study documenting the synthesis of pyrite from sulfide melts (cf. Kullerud et al., 1969; Craig, 1973; Misra and Fleet, 1973; Ueno et al., 2000), to our knowledge this is the first documented study of a pyrite-bearing system that contains the HSE and metalloids. The results confirm that pyrite will form during cooling of a sulfide melt if the bulk S content is sufficiently high and show that such pyrite is Co-Ni-rich and contains significant amounts of Ru, Rh, Os, Ir and Pt, as well as some amount of metalloids. Textural relations, with pyrite typically at the boundary between iss and mss, often surrounded totally or partially by iss and in some cases including iss (Figure 32), indicate that, in Cu-bearing sulfide systems, pyrite is not simply the product of exsolution from mss (as shown for Ni-Fe-S but Cu-free systems; e.g., Craig, 1973). We suggest that pyrite formed by a reaction between mss and iss, possibly extracting Fe and S from both phases.

Even if a hydrothermal origin for high-Co, IPGE-bearing pyrite cannot be discarded, there are no experimental results supporting such origin and detailed analyses of pyrite with clear

hydrothermal origin mostly document enrichment in Au, but no other HSE (e.g., Large et al., 2009; Deditius et al., 2014). Furthermore, Deditius et al. (2014) indicated that Au solubility in pyrite is retrograde and decreases exponentially with increasing temperature (~ 300 ppm at 200 °C vs. ~ 0.1 ppm at 500 °C). Therefore, naturally occurring pyrite with similar characteristics is consistent with a primary (magmatic) origin. This includes, among others, Ru-rich pyrite in the Imandra layered intrusion, Russia (Barkov et al., 1997); pyrite with Ni-Co zonation in Craig Mine, Sudbury (Craig and Solberg, 1999); unzoned IPGE-enriched pyrite in Pyrenean peridotites (Lorand and Alard, 2010); Co-Ni-IPGE rich pyrite from McCreedy East, Sudbury (Dare et al., 2011); euhedral pyrite with high Rh, Co, As and Pt content from Aguablanca, Spain (Piña et al., 2012); Co-IPGE rich pyrite from the Morrison-Levack ore system, Sudbury (Adibpour et al., 2015). Moreover, because pyrite is more robust than other sulfides to re-equilibration (Craig et al., 1998), occurrences of IPGE-rich pyrite may serve as indicator of a magmatic origin for the sulfide assemblages in which it is found.

Although the experiments were cooled slowly from temperatures above the stability field of pyrite and quenched soon after reaching 650 ºC, the pyrite crystals that formed in the experiments show complex element zonation (Figure 40 to Figure 43). Thus, such zonation (e.g., as shown in pyrite from Morrison, Adibpour et al. 2015) does not necessarily imply secondary stages of growth (i.e. by later metamorphic or hydrothermal processes). Brenan et al. (2000) measured diffusion of Os in pyrrhotite and pyrite. They observed that the diffusion of Os is much higher in pyrrhotite than in pyrite and that the rate of diffusion in pyrite decreases with decreasing temperature. In our experiments, therefore, when pyrite nucleated, elements started diffusing from mss and iss into the new forming crystals. However, the rate of growth of the pyrite crystals was likely faster than the rate of element diffusion; thus, preserving chemical

zonation, much in the same way that oscillatory zoning is preserved in plagioclase. The absence from the experimental protocol of an equilibration step at 650 °C probably allowed the preservation of the zonation, although the existence of Co zonation in natural pyrite (Craig and Solberg, 1999) indicates that pyrite zonation is often preserved in nature. To confirm this hypothesis, further experiments equilibrated at various temperatures, and with longer duration, are needed to assess if such zonation can be annealed and erased.

Regarding element partitioning, there are several significant results. The first one pertains to the behavior of Pd. Although it is well documented that Pd partitions into a Cu-rich melt at high temperature (e.g., Ballhaus, et al. 2001) and into pentlandite at lower temperature (e.g., Barnes et al., 2006), there is little information to constrain Pd behavior at intermediate temperatures. The concentration of Pd in mss was always measurable and ranged between 9 ppm and 11 ppm, whereas it was below detection limit in iss in two of three experiments and barely above detection limits (0.2 ppm) in the third experiment. Therefore, even though the partitioning coefficient of Pd between mss and iss could be calculated only in one case and the uncertainties are relatively large (due to the error propagation of the uncertainties associated with the Pd content in iss) it is possible to state that Pd, at 650 ºC, is no longer dominantly into the Cu-rich phase and has diffused into mss. This implies that very little Pd is incorporated into iss when the residual Cu-rich liquid crystallized. Therefore, the temperature of iss crystallization determines when Pd is incorporated preferentially into mss. Gold was shown to partition strongly into iss relative to the other sulfides, as has been shown previously (e.g., Jugo et al. 1999). Platinum shows slight preference for mss over pyrite (roughly 3 times more Pt in mss than pyrite), despite the fact that pyrite grains have variable and zoned Pt content: some grains show high Pt domains toward the center of the grains, surrounded by areas that were Pt poor. The concentrations of

elements in pyrite used to calculate the partitioning coefficient are obtained from integrations that include both rim and core values. This was chosen to have an idea of the bulk partitioning between two phases. The rest of the HSE (Ru, Rh, Re, Os, Ir) showed a slight preference for pyrite over mss (Table 18) but these values reflect the average content in pyrite. Among the metalloids, As and Se partition roughly equally between the 3 sulfide phases present, with partition coefficients close to unity (Figure 35), whereas Sb and Bi have preference for iss and Te showed a slight preference for mss. However, the large uncertainties for Sb, Te and Bi (compared to As and Se) indicate some degree of heterogeneity in those elements. In addition, Table 17, 18 and Figure 36 include concentrations and partitioning when the core and the rim of the zoned pyrite crystal (in experiment P-07) are quantified separately. The results show that the Ru, Rh, Re, Os and Ir content is higher in the pyrite core than in the rim (Table 17) meaning that partitioning of these elements between mss and pyrite is different than when the concentration of these elements is integrated over the whole pyrite grain. Although the partitioning mss/pyrite rim likely reflects the partitioning at the equilibrium temperature (last contact between the two phases), the partitioning mss/pyrite core indicate that at the initial stages of pyrite growth Ru, Rh, Re, Os and Ir were incorporated into the pyrite structure at a relatively fast rate, depleting the mss in those elements. The last stages of py growth contained less of these HSE because the grew from an already depleted medium (mss and iss).

The presence of metalloids affected the behavior of Pd, Pt and Au, which were incorporated in metalloid-rich phases but did not affect the behavior of Ru, Rh, Re, Os and Ir in the system (Figure 29 and Figure 43). More significantly, only the concentration of Au in iss decreased significantly when a metalloid-bearing phase was present (from 676 ppm in the experiment with no metalloids added to 89 ppm in the experiment with 3 wt.% metalloids; Table 17). Although

some Pt and Pd were clearly incorporated in the metalloids-bearing phases, the Pd and Pt content in mss remained more of less constant (at ca. 10 ppm Pd) or varied little (between 49 and 66 ppm Pt) regardless of the amount of metalloids added in the experiments.

4.5. Conclusions

The results of this study show that:

1. Cobalt-rich, HSE-bearing pyrite can form from the cooling of a magmatic sulfide liquid.

2. Textural evidence (i.e. pyrite always in contact with iss) indicates that in Cu-bearing systems pyrite does not exsolve from mss (as documented in Cu-free systems) but forms at grain boundaries between mss and iss.

3. If the metalloid content is sufficiently high, an immiscible metalloid-rich liquid will be present in the system.

4. The presence of such metalloid-rich melt does not strongly affect the behavior of Ru, Rh, Re, Os and Ir in the coexisting sulfide assemblage. Only Au content in iss is moderately affected by the presence of metalloid-rich liquids and although both Pt, Pd are taken by metalloid phases their content in mss remained largely unaffected.

5. Element distribution maps revealed the presence of PGM inclusions in pyrite. Such inclusions are not visible in BSE images and are likely caused by nano-scale inclusions. However, the distribution of such inclusions is not uniform across the

grain, which indicates that they did not formed as exsolution during quenching but likely were present at run conditions.

6. Experiments performed under the same conditions, but with different amounts of metalloids, produced pyrite with variable zonation of trace elements. In some experiments, zonation seems to mark two different stages of growth with Se, Ni, Ru, Rh, Re, Os and Ir initially concentrating in the core of pyrite grains. The zonation, however, is probably due to a rate of growth that is faster than the rate of diffusion of elements through the grain.

7. At 650 °C Pt partitions equally between mss and pyrite whereas Au partitions strongly into iss and Pd partitions strongly into mss.

8. The presence of Co-rich, HSE-bearing py in several localities worldwide is consistent with such pyrite being the primary product of the cooling of a sulfide melt.. However, further experimental work need to assess whether pyrite crystallization from hydrothermal fluids can also produce Co-rich, HSE-bearing pyrite.

Acknowledgements

This article contains results from part of the Ph.D. project of the first author. The project was funded by NSERC, CEMI, Vale, and Sudbury Integrated Nickel Operations as an NSERC-CRD project. We thank Edward Nelles for providing the pn used as starting material, Sandra Clarke (GeoLabs), Dave Crabtree (GeoLabs), and Joseph Petrus (Laurentian University) for their help with EDS, EMPA and LA-ICP-MS, respectively, as well as D. Tinkham, A.M. McDonald and P.

Lightfoot for feedback on many of the ideas presented here as well as valuable comments on earlier versions of the manuscript.

References

Adibpour, M., Jugo, P.J., and Ames, D.E., (in press, 2015). Trace element distribution in sulphide assemblages of the Levack-Morrison ore system, Sudbury, Ontario: Looking for chemical fingerprints of mineralization processes, In: Targeted Geoscience Initiative 4: Canadian Nickel-Copper-Platinum Group Elements-Chromium Ore Systems — Fertility, Pathfinders, New and Revised Models, (eds) D.E. Ames and M.G. Houlé; Geological Survey of Canada, Open File XXXX, p.

Armitage, P.E.B., McDonald, I., Edwards, S.J. and Manby, G.M., 2002, Platinum-group element mineralization in the Platreef and calc-silicate footwall at Sandsloot, Potgietersrus District, South Africa: Transactions of the Institution of Mining and Metallurgy. Section B-Applied Earth Science, v. 111, p. B36-B45.

Ballhaus, C., Tredoux, M. and Späth, A., 2001, Phase Relations in the Fe-Ni-Cu-PGE-S System at Magmatic Temperature and Application to Massive Sulphide ores of the Sudbury Igneous Complex: Journal of Petrology, v. 41, p. 1911-1926.

Barnes, S.-J., Cox, R.A. and Zientek, M.L., 2006, Platinum-group element, Gold, Silver and Base Metal distribution in compositionally zoned sulfide droplets from the Medvezky Creek Mine, Norl'sk, Russia: Contributions to Mineralogy and Petrology, v. 152, p. 187-200.

Barnes, S.J., Naldrett, A.J. and Gorton, M.P., 1985, The origin of the fractionation of the platinum-group elements in terrestrial magmas: Chemical Geology, v. 53, p. 303-323.

Barkov, A.Y., Halkoaho, T.A.A., Kauko, V.O., Alapieti, L., Alapieti, T.T. and Peura, R.A., 1997, Ruthenian Pyrite and Nickeloan Malanite from the Imandra Layered Complex, Northwestern Russia: Canadian Mineralogist, v. 35, p. 887-897.

Brenan, J.M., Cherniak, D.J. and Rose, L.A., 2000, Diffusion of osmium in pyrrhotite and pyrite: implications for closure of the Re-Os isotopic system: Earth and Planetary Science Letters, v. 180, p. 399-413.

Craig, J.R., 1973, Pyrite-Pentlandite Assemblages and Other Low Temperature Relations in the Fe-Ni-S System: American Journal of Science, Copper, v. 273-A, p. 496-510.

Craig, J.R. and Solberg, T.D., 1999, Compositional Zoning in Ore Minerals at the Craig Mine, Sudbury, Ontario, Canada: Canadian Mineralogist, v. 37, p. 1163-1176.

Craig, J.R., Vokes, F.M. and Solberg, T.D., 1998, Pyrite: physical and chemical textures: Mineralium Deposita, v. 34, p. 82-101.

Dare, S.A.S., Barnes, S.J., Prichard, H.M. and Fisher, P.C., 2011, Chalcophile and platinum-group element (PGE) concentrations in the sulfide minerals from the McCreedy East deposit, Sudbury, Canada, and the origin of PGE in pyrite: Mineralium Deposita, v. 46, p. 381-407.

Deditius, A.P., Reich, M., Kesler, S.E., Utsunomiya S., Chryssoulis, S.L., Walshe, J. and Ewing, R.C., 2014, The coupled geochemistry of Au and As in pyrite from hydrothermal ore deposits: Geochimica et Cosmochimica Acta, v. 140, p. 644-670.

Djon, M.L.N. and Barnes, S.J., 2012, Changes in sulfides and platinum-group minerals with the degree of alteration in the Roby, Twilight and High Grade Zones of the Lac-des-Iles Complex, Ontario, Canada: Mineralium Deposita, v. 47, p. 875-896.

Fleet, M.E., Chryssoulis, S., Stone, W.E. and Weisner, C.G., 1993, Partitioning of platinum-group elements and Au in the Fe-Ni-Cu-S system: experiments on the fractional crystallization of sulfide melt: Contributions to Mineralogy and Petrology, v. 115, p. 36-44.

Franchuk, A., Lightfoot, P.C. and Kontak, D.J., 2013, High tenor Ni-PGE sulfide mineralization in the South Manasan ultramafic intrusion, Thompson Nickel Belt: Abstract, GAC-MAC Annual Meeting, Manitoba, Winnipeg, 21-24 May 2013, Proceedings, Geological Association of Canada, p. 98.

Frost, B.R., Mavrogenes, J.A. and Tomkins, A.G., 2002, Partial melting of sulfide ore deposits during medium- and high-grade metamorphism: Canadian Mineralogist, v. 40, p. 1-18.

Hawley, J.E., 1962, The Sudbury Ores: Their Mineralogy and Origin. Part I, The Geological Setting: Canadian Mineralogist, v. 7, p. 1-29.

Helmy, H.M., Ballhaus, C., Berndt, J., Bockrath, C. and Wohlgemuth-Ueberwasser, C., 2007, Formation of Pt, Pd and Ni tellurides: experiments on sulphide-telluride systems: Contributions to Mineralogy and Petrology, v. 153, p. 577-591.

Helmy, H.M., Ballhaus, C., Wohlgemut-Ueberwasser, C., Fonseca, R.O.C. and Laurenz, V., 2010, Partitioning of Se, As, Sb, Te and Bi between monosulfide solid solution and sulfide melt – Application to magmatic sulfide deposits: Geochimica et Cosmochimica Acta, v. 74, p. 6174-6179.

Jugo, P.J., Candela, P.A. and Piccoli, P.M., 1999, Magmatic sulfides and Au:Cu ratios in porphyry deposits: an experimental study of copper and gold partitioning at 850 °C, 100 MPa in a haplogranitic melt-pyrrhotite-intermediate solid solution-gold metal assemblage, at gas saturation: Lithos, v. 46, p. 573-589.

Kullerud, G., Yund, R.A. and Moh, G.H., 1969, Phase Relations in the Cu-Fe-S, Cu-Ni-S, and Fe-Ni-S Systems: Economic Geology Monograph 4, p. 323-343.

Large, R.R., Danyushevsky, L., Hollit, C., Maslennikov, V., Meffre, S., Gilbert, S., Bull, S., Scott, R., Emsbo, P., Thomas, H., Singh, B. and Foster, J., 2009, Gold and Trace Element Zonation in Pyrite Using a Laser Imaging Technique: Implications for the Timing of Gold in Orogenic and Carlin-Style Sediment-Hosted Deposits: Economic Geology, v. 104, p. 635-668.

Lorand, J.P. and Alard, O., 2011, Pyrite tracks assimilation of crustal sulfur in Pyrenean peridotites: Mineralogy and Petrology, v. 101, p. 115-128.

Mengason, M.J., Piccoli, P.M. and Candela, P., 2010, An evaluation of the effect of copper on the estimation of sulfur fugacity (fS2) from pyrrhotite composition: Economic Geology, v. 105, p. 1163-1169

Misra, K.C. and Fleet, M.E., 1973, The Chemical Compositions of Synthetic and Natural Pentlandite Assemblages: Economic Geology, v. 68, p. 518-539.

Oberthür, T., Cabri, L.J., Weiser, T.W. and McMahon, G., 1997, Pt, Pd and other trace elements in sulfides of the main sulfide zone, Great Dike, Zimbabwe: a reconnaissance study: Canadian Mineralogist, v. 35, p. 597-609.

Piña, R., Gervilla, F., Barnes, S.J., Ortega, L. and Lunar, R., 2012, Distribution of platinum-group and chalcophile elements in the Aguablanca Ni–Cu sulfide deposit (SW Spain): Evidence from a LA-ICP-MS study: Chemical Geology, v. 302-303, p. 61-75.

Prowatke, S. and Klemme, S., Rare earth element partitioning between titanite and silicate melts: Henry's law revised: Geochimica et Cosmochimica Acta, v. 70, p. 4997-5012.

Sylvester, P.C., Cabri, L.J., Turbett, M.N., McMahon, G., Laflamme, J.G.H. and Peregoedova, A., 2005, Synthesis and evaluation of a fused pyrrhotite standard reference material for platinum-group element and gold analyses by laser ablation-ICPMS: Extended Abstract, X International Platinum Symposium: Platinum-group elements; from genesis to beneficiation and environmental impact, Oulu, Finland, 16-20 August, Geological Survey of Finland, Espoo, Proceedings, p. 16-20.

Toulmin, P. and Barton, P.B., 1964, A thermodynamic study of pyrite and pyrrhotite: Geochimica et Cosmochimica Acta, v. 28, p. 641-671.

Ueno, T., Shin-ichiro, I., Nakatsuka, S., Nakano, K., Harada, T. and Yamazaki, T., 2000, Phase equilibria in the system Fe-Ni-S at 500°C and 400 °C: Journal of Mineralogy and Petrological Sciences, v. 95, p. 145-161.

Westland, A.D., 1981, Inorganic Chemistry of the Platinum-Group Elements, *in* Cabri, L.J., ed., Platinum-Group Elements: Mineralogy, Geology, Recovery: Montreal, The Canadian Institute of Mining and Metallurgy, Special Volume 23, p. 5-18.

Wohlgemuth-Ueberwasser, C.C., Ballhaus, C., Berndt, J., Stotter Paliulionyte, V. and Meisel, T., 2007, Synthesis of PGE sulfide standards for laser ablation inductively coupled plasma mass spectrometry (LA-ICP-MS): Contributions to Mineralogy and Petrology, v. 154, p. 607-617.

Tables

Table 14. Composition of the natural sulfides used as starting material.

Mineral	n[3]	S[1] wt.%	Mn ppm	Fe wt.%	Co ppm	Ni ppm wt.%*	Cu ppm wt.%*	Zn ppm	As ppm	Se ppm	Ru[2] ppm	Rh[2] ppm	Pd[2] ppm	Cd ppm	Sn ppm	Sb ppm	Te ppm	Pb ppm	Bi ppm
Pyrrhotite	5 (10)	39.13	53	60.51	24	20.9	107	18	430	*b.d.l*[4].	*b.d.l.*	*b.d.l.*	*b.d.l.*	0.12	*b.d.l.*	2.0	*b.d.l.*	7	0.14
2σ		0.58	106	0.74	47	5.4	36	24	120					0.12		3.7		18	0.22
Pentlandite	5 (10)	33.41	*b.d.l.*	32.67	1850	33.7*	3300	16	1180	98.5	1.18	0.12	1.90	0.23	0.28	0.08	108	25	0.03
2σ		0.23		1.66	180	1.6	5700	19	210	8.9	0.10	0.13	0.35	0.16	0.27	0.05	16	13	0.01
Chalcopyrite	5 (10)	34.93	*b.d.l.*	30.26	3.0	*b.d.l.*	34.60*	*b.d.l.*	1064	43.3	0.22	10.75	*b.d.l.*	0.19	0.10	0.04	*b.d.l.*	9.5	0.08
2σ		0.24		0.17	1.2		0.39		75	4.8	0.03	0.57		0.17	0.03	0.02		5.5	0.04

[1]Data for S, Fe, Ni in pentlandite and Cu in Chalcopyrite from EMPA-WDS analyses (in wt.%). All other data from LA-ICP-MS analyses (in ppm). Limits of detection (ppm): S=170; Mn=2.35; Fe=220; Co=1.14; Ni=4.47 (LA-ICP-MS) and 230 (WDS); Cu=3.24 (LA-ICP-MS) and 280 (WDS); Zn=9.00; As=8.26; Se=3.19; Ru=0.08; Rh=0.02; Pd=0.01; Cd=0.18; Sn=0.08; Sb=0.03; Te=0.74; Re=0.01; Os=0.01; Ir=0.003; Pt=0.01; Au=0.05; Pb=0.07; Bi=0.01.

[2] Values for Ru, Rh and Pd corrected for argide interference.
[3]Number of analyses: LA-ICP-MS and (EMPA-WDS).
[4]Below detection limit. No data for Re, Os, Ir, Pt and Au is shown because these elements were below the detection limit in all minerals.

Table 15. Bulk composition (in wt.%) of preliminary experiments performed to obtain pyrite as a primary phase.

Run	S	Fe	Co	Ni	Cu	at. ΣM/S	Starting material (wt.%)[1]	Run products
FS-13	34.19	29.75		36.06		1.08	3.8 py, 96.2 pn	mss + pn
FS-14	37.77	32.91		29.31		0.92	21.8 py, 78.2 pn	mss
FS-15	40.66	35.46		23.88		0.82	36.3 py, 63.7 pn	mss + py + vs
FS-17	40.66	35.44		23.90		0.82	28.4 po, 63.2 pn, 8.4 S	mss + py + vs + mt
FS-19	40.50	35.31		19.06	5.13	0.82	34.3 py, 50.9 pn, 14.8 ccp	mss + iss + py + vs
P-01	40.55	37.64	1.02	15.85	4.94	0.82	1.6 CoS, 7.2 S, 35.6 po, 41.5 pn, 14.2 ccp	mss + iss + py + vs
P-02	40.65	41.73	1.01	12.20	4.40	0.79	1.6 CoS, 7.9 S, 45.0 po, 32.8 pn, 12.7 ccp	mss + iss + py + vs
P-03	40.73	45.70	1.02	8.15	4.41	0.82	1.6 CoS, 7.3 S, 57.0 po, 21.4 pn, 12.7 ccp	mss + iss + py + vs
P-04[2]	42.13	48.17	1.03	4.24	4.42	0.77	1.6 CoS, 6.7 S, 69.1 po, 9.9 pn, 12.7 ccp	mss + iss + py

[1]Natural pyrite (py), pentlandite (pn), chalcopyrite (ccp) and pyrrhotite (po) were used in all experiments. CoS (99.5 %) from Alfa Aesar.
[2]All subsequent experiments used this proportion of starting materials.

Table 16. Nominal composition of starting mixtures.

	wt.%	wt. ratio
Sulfide mixture		
CoS	1.58	
elemental S	6.67	
'0.2Po'	2.5	
Pyrrhotite	66.59	
Pentlandite	9.93	
Chalcopyrite	12.73	
Total	100.00	
S	42.13	
Fe	48.18	
Co	1.04	
Ni	4.23	
Cu	4.42	
Total	100.00	
Metalloid mixture[1]		
As (As_2S_3)	17.37	1.56
Se	11.15	1.00
Sb (Sb_2S_3)	23.98	2.15
Te	18.00	1.62
Bi	29.50	2.65
Total	100.00	
"0.2Po"[2]		
Ru	0.2	
Rh	0.2	
Pd	0.2	
Re	0.2	
Os	0.2	
Ir	0.2	
Pt	0.2	
Au	0.2	
Pyrrhotite	98.4	
Total	100.0	

[1]Metalloids from Alfa Aesar: Bi (99.5%), As_2S_3 (99.999%), Sb_2S_3 (99.999%), Te (99.99%), Se (99.5%).
[2]HSE from Alfa Aesar: Ru (99.9%), Rh (99.95%), Pd (99.95%), Re (99.99%), Os (99.8%), Ir (99.9%), Pt (99.9+%), Au (99.95%).

Table 17. Composition of run products.

Phase	**n**[1]	**S**[2]	**Mn**	**Fe**	**Co**	**Ni**	**Cu**	**Zn**	**As**	**Se**	**Ru**[3]	**Rh**	**Pd**
	isotope	-	*55*	-	*59*	-	-	*68*	*75*	*77*	*101*	*103*	*108*
No metalloid added (P-12)													
mss	5 (10)	40.08	6980	52.42	6950	3.47	2.96	100	472	21.4	27.3	40.6	9.22
2σ		0.26	180	0.25	590	0.09	0.14	28	49	5.7	3.1	3.6	0.25
iss	7 (10)	35.14	14630	36.11	1950	0.48	25.38	13900	720	30	0.42	b.d.l.[4]	b.d.l.
2σ		0.83	740	0.25	510	0.03	0.48	2100	110	11	0.64		
py	12 (10)	53.09	1300	40.7	33000	1.98	0.04	34	402	20.4	32	45	1.8
2σ		0.33	4900	1.7	37000	0.46	0.01	71	84	8.7	21	28	6.1
0.2 wt.% metalloid mixture (P-07)													
mss	5 (10)	40.26	6930	51.46	6000	4.26	3.01	57	460	205	39.1	59.8	11.13
2σ		0.31	390	0.48	3600	0.22	0.25	14	110	33	4.7	6.1	0.85
iss	12 (10)	35.18	13400	36.02	1800	0.59	25.79	7900	670	243	5	b.d.l.	0.2
2σ		0.42	1600	0.25	1200	0.02	0.28	3100	460	43	30		1.4
py	15 (10)	53.21	5	40.2	51000	2.44	0.04	b.d.l.	340	89	42	48	0.14
2σ		0.31	14	2.1	19000	0.64	0.02		200	33	22	26	0.06
Pyrite core vs. rim concentrations													
Rim	3		19		35400	1.88	0.04	75	404	102.0	18.1	26	0.12
2σ			27		10294	0.36	0.02	11	84	6.9	2.6	23	0.06
Core	3		4.2		44833	2.61	0.025	21	262	124.1	55.9	48.5	0.13
2σ			2.5		1301	0.15	0.001	39	19	7.5	2.4	2.7	0.02
3 wt.% metalloid mixture (P-13)													
mss	10 (10)	39.9	6300	52.08	7150	3.83	2.93	88	261	1070	36.4	38.9	10
2σ		0.22	480	0.32	310	0.14	0.06	40	46	110	4	1.8	1
iss	6 (10)	34.84	13050	36.03	2280	0.52	25.42	13200	322	1030	0.26	b.d.l.	b.d.l.
2σ		0.3	550	0.26	180	0.02	0.39	1300	19	380	0.22		
py	14 (10)	52.94	22	40.2	53000	1.93	0.04	21	300	580	35	44	0.1
2σ		0.34	85	2.1	14000	0.48	0.07	81	240	180	25	35	0.08

Table 17 (*cont.)* Composition of run products.

Phase	n[1]	Cd	Sn	Sb	Te	Re	Os	Ir	Pt	Au	Pb	Bi
	isotope	*111*	*118*	*121*	*130*	*185*	*189*	*193*	*195*	*197*	*208*	*209*
No metalloid added (P-12)												
mss	5 (10)	0.7	0.48	4.17	2.4	44.9	35	38	66	7.5	188	1.27
2σ		0.27	0.14	0.66	1.5	7.7	11	11	13	1.1	31	0.35
iss	7 (10)	88	31	10.7	1.7	0.5	0.27	0.4	0.5	676	86	4.7
2σ		21	7.2	1.9	1.8	1.5	0.78	1.1	1.2	124	33	0.85
py	12 (10)	*b.d.l.*	0.18	1	*b.d.l.*	51	44	51	27	2.1	40	0.34
2σ			0.36	2.6		41	28	35	20	5.5	100	0.69
0.2 wt.% metalloid mixture (P-07)												
mss	5 (10)	0.37	0.68	27.2	229	85	50	52.9	49.2	4.01	146	24.7
2σ		0.13	0.13	4.2	53	19	8	9	5.3	0.58	19	4.7
iss	12 (10)	32	56	160	220	9	14	11	2.2	370	500	320
2σ		15	20	250	420	47	78	68	8.4	100	1200	620
py	15 (10)	*b.d.l.*	*b.d.l.*	15	20	32	57	58	20	1.4	70	30
2σ				108	140	31	33	32	7	9.9	490	230
Pyrite core vs. rim concentrations												
Rim	3	0.3	0.25	34	48	13.9	28	66	14.6	1.9	116	59
2σ		0.5	0.43	82	80	3.4	19	61	4.3	3.5	180	90
Core	3	0.1	0.08	0.9	2.51	51.8	75.3	79.5	22	0.08	5.8	2.2
2σ		0.3	0.04	1.0	2.48	2.5	1.9	1.5	2	0.12	6.4	2.1
3 wt.% metalloid mixture (P-13)												
mss	10 (10)	*b.d.l.*	0.8	50	173	52.3	49	56	58.9	0.85	4.8	26
2σ			0.27	15	70	4.7	13	14	4.6	0.36	1.8	13
iss	6 (10)	64.2	79.4	142	51	0.14	0.07	0.14	0.3	89	2.1	108
2σ		5.7	7.3	13	11	0.26	0.22	0.31	0.3	4.5	0.45	12
py	14 (10)	*b.d.l.*	0.2	4.3	9	32	54	69	16.1	0.19	0.58	6
2σ			0.57	9.8	19	24	31	78	9.6	0.53	0.68	15

[1]n indicates the number of analyses performed. The number in parentheses indicates WDS analyses, the number out of parentheses indicates the LA-ICP-MS analyses.
[2]S, Fe, Ni and Cu concentration from EMPA-WDS analyses (Limits of detection in wt.%: S = 0.016; Fe = 0.022; Ni = 0.023; Cu = 0.027). All other data are from LA-ICP-MS analyses (L.O.D. in ppm: Mn = 4.97; Co = 1.08; Zn = 17.19; As = 6.7; Se = 6.50; Ru = 0.10; Rh = 0.04; Pd = 0.02; Cd = 0.29; Sn = 0.13; Sb = 0.09; Te = 1.36; Re = 0.03; Os = 0.01; Ir = 0.002; Pt = 0.02; Au = 0.03; Pb = 0.09; Bi = 0.08.
[3]Values for Ru, Rh and Pd corrected for argide interference.
[4]b.d.l.: below detection limits.

Table 18. Calculated partition coefficients per indicated sulfide pairs.

D	Mn	Co	Zn	As	Se	Ru	Rh	Pd	Cd	Sn	Sb	Te	Re	Os	Ir	Pt	Au	Pb	Bi
No metalloid added (P-12)																			
mss/iss	0.48	3.6	0.0072	0.66	0.72	66			0.008	0.0154	0.39	1.4	100	130	110	140	0.0111	2.18	0.27
$\pm\sigma$[1]	0.08	1.3	0.0022	0.19	0.32	58			0.0032	0.0057	0.12	1.1	130	150	140	160	0.0035	0.97	0.09
mss/py	5.2	0.21	2.9	1.18	1.05	0.86	0.91	5.2		2.7	4		0.89	0.8	0.75	2.46	3.5	4.8	3.7
$\pm\sigma$	9.5	0.12	3.1	0.14	0.26	0.29	0.29	8.8		2.8	4.9		0.37	0.29	0.28	0.97	4.6	6.4	3.7
iss/py	11	0.059	410	1.78	1.47	0.013				180	10		0.009	0.0063	0.007	0.018	320	2.2	14
$\pm\sigma$	20	0.034	430	0.23	0.41	0.011				180	13		0.015	0.0091	0.011	0.024	420	3	14
0.2 wt.% metalloid mixture (P-07)																			
mss/iss	0.52	3.4	0.0072	0.69	0.84	7		50	0.0114	0.0122	0.17	1.03	10	4	5	22	0.0109	0.3	0.08
$\pm\sigma$	0.03	1.6	0.0017	0.25	0.1	20		170	0.0033	0.0025	0.13	0.98	25	11	15	42	0.0017	0.36	0.08
mss/py	1300	0.118		1.37	2.30	0.93	1.25	81			1.8	11	2.7	0.88	0.91	2.45	3	2.1	0.8
$\pm\sigma$	1800	0.042		0.44	0.46	0.25	0.35	19			6.3	39	1.3	0.27	0.26	0.45	11	7.6	2.8
iss/py	2600	0.034		1.98	2.72	0.13		1.6			11	11	0.28	0.24	0.19	0.11	270	7	10
$\pm\sigma$	3400	0.014		0.90	0.55	0.36		5.1			39	40	0.74	0.69	0.59	0.21	970	27	37
mss/py-rim	370	0.17	0.76	1.14	2.01	2.16	2.32	93	1.4	2.7	0.81	4.8	6.1	1.76	0.81	3.4	2.1	1.3	0.42
±σ	266	0.06	0.11	0.18	0.18	0.20	1.07	25	1.3	2.3	0.98	4.1	1.0	0.60	0.38	0.5	2.0	1.0	0.32
mss/py-core	1637	0.13	2.7	1.75	1.65	0.70	1.23	82.8	3.3	8.1	29	91	1.64	0.66	0.67	2.22	49	25	11.1
±σ	493	0.04	2.5	0.22	0.14	0.04	0.07	5.9	4.5	2.2	16	46	0.19	0.05	0.06	0.16	35	14	5.4
iss/py-rim	715	0.05	105	1.66	2.38	0.28		1.7	123	221	4.8	4.6	0.6	0.49	0.17	0.15	198	4.3	5.4
±σ	516	0.02	22	0.59	0.23	0.83		5.8	118	191	6.9	5.9	1.7	1.38	0.52	0.29	186	6.1	6.7
iss/py-core	3165	0.04	370	2.55	1.96	0.09		1.5	289	667	172	88	0.17	0.19	0.14	0.10	4512	86	144
±σ	968	0.01	345	0.88	0.18	0.27		5.2	389	208	164	94	0.45	0.52	0.43	0.19	3285	114	155

Table 18. ***(cont.)*** **Calculated partition coefficients per indicated sulfide pairs.**

D	Mn	Co	Zn	As	Se	Ru	Rh	Pd	Cd	Sn	Sb	Te	Re	Os	Ir	Pt	Au	Pb	Bi
3 wt.% metalloid mixture (P-13)																			
mss/iss	0.48	3.1	0.0066	0.81	1.04	139				0.01	0.35	3.4	380	700	400	190	0.0096	2.3	0.24
±σ	0.03	1.5	0.0015	0.3	0.12	391				0.0021	0.27	3.2	990	1900	1200	360	0.0015	2.8	0.23
mss/py	290	0.136	4.2	0.87	1.83	1.05	0.89	99		4	12	19	1.63	0.91	0.81	3.7	4.6	8.3	4.2
±σ	507	0.018	8.1	0.35	0.3	0.39	0.35	40		5.9	13	22	0.62	0.29	0.47	1.1	6.7	5.1	5.1
iss/py	600	0.043	600	1.07	1.76	0.0076				400	33	5.8	0.0043	0.0013	0.0021	0.019	480	3.6	18
±σ	1200	0.006	1200	0.42	0.43	0.0042				580	38	6.3	0.0044	0.0021	0.0026	0.011	690	2.1	21

[1]Uncertainties calculated using a formula for error propagation. See text for details. Empty cells indicate that the partitioning coefficient could not be calculated because one of the two concentrations is below detection limit.

Figures

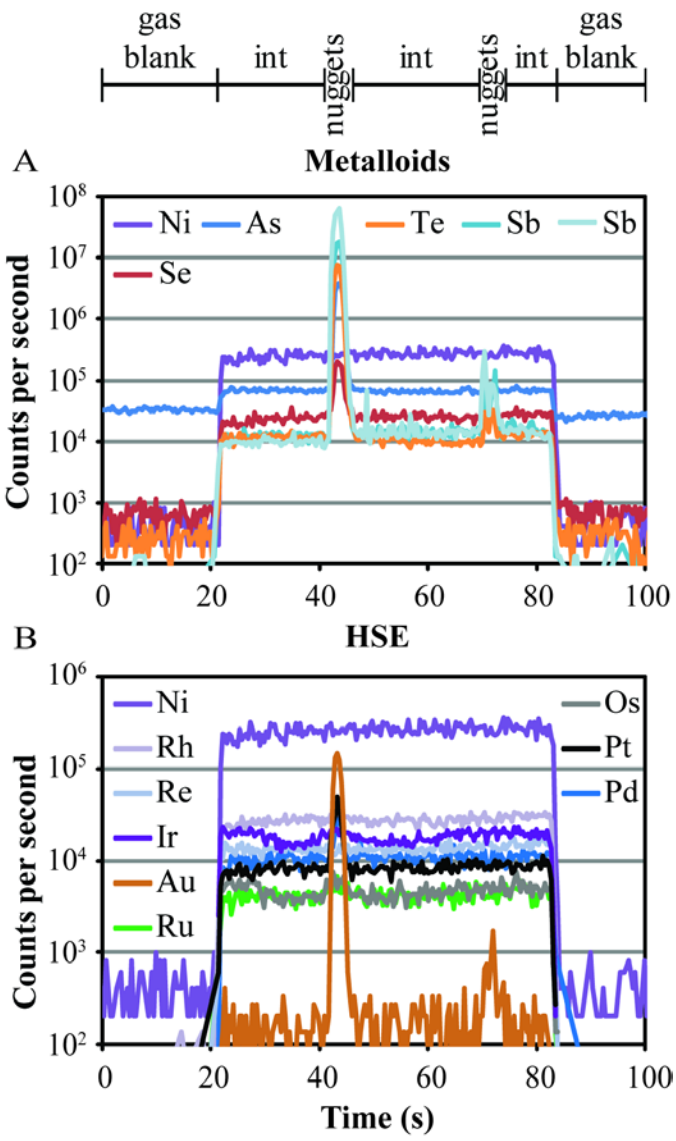

Figure 29. Example of time resolved spectra of the metalloids (A) and the HSE (B) in the mss of the highly enriched run. The isolated spikes show the presence of nuggets composed of all metalloids that were eliminated from the integration.

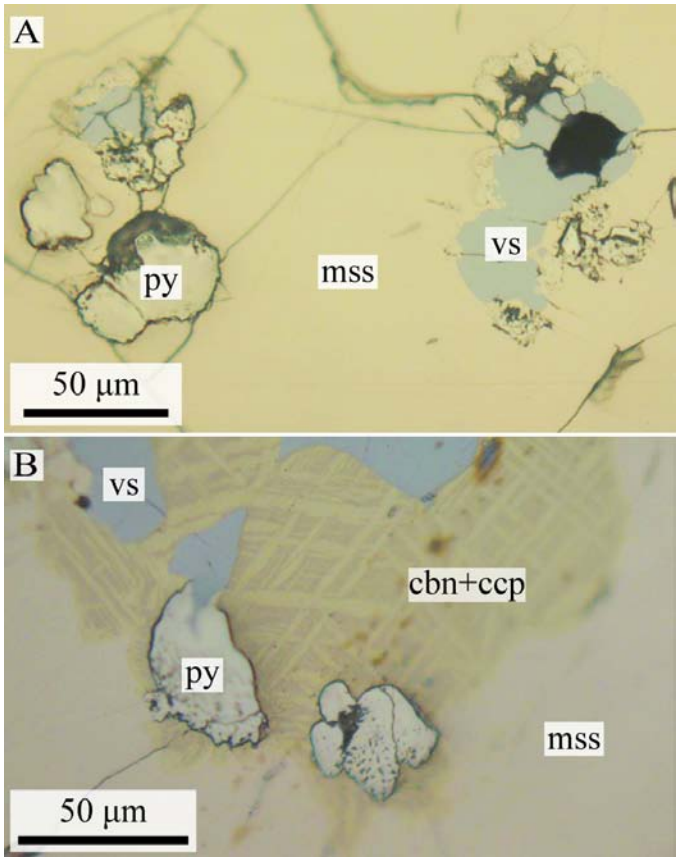

Figure 30. Reflected light images of preliminary run products. A. Small anhedral pyrite crystals (py), associated with dominant mss and abundant vaesite (vs) (run FS-15). B. Vaesite (light gray) is surrounded by cubanite (cbn) and chalcopyrite (ccp, two shades of yellow). The anhedral crystals in relief are pyrite and the background dominant mineral is mss (run FS-19).

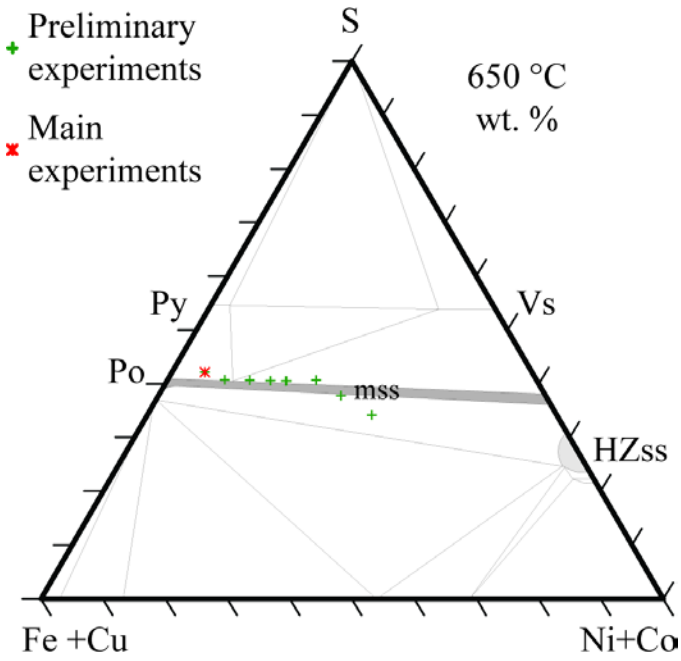

Figure 31. Composition of preliminary and main experiments on a modified phase diagram of the Fe-Ni-S system, based on Kullerud et al. (1969).

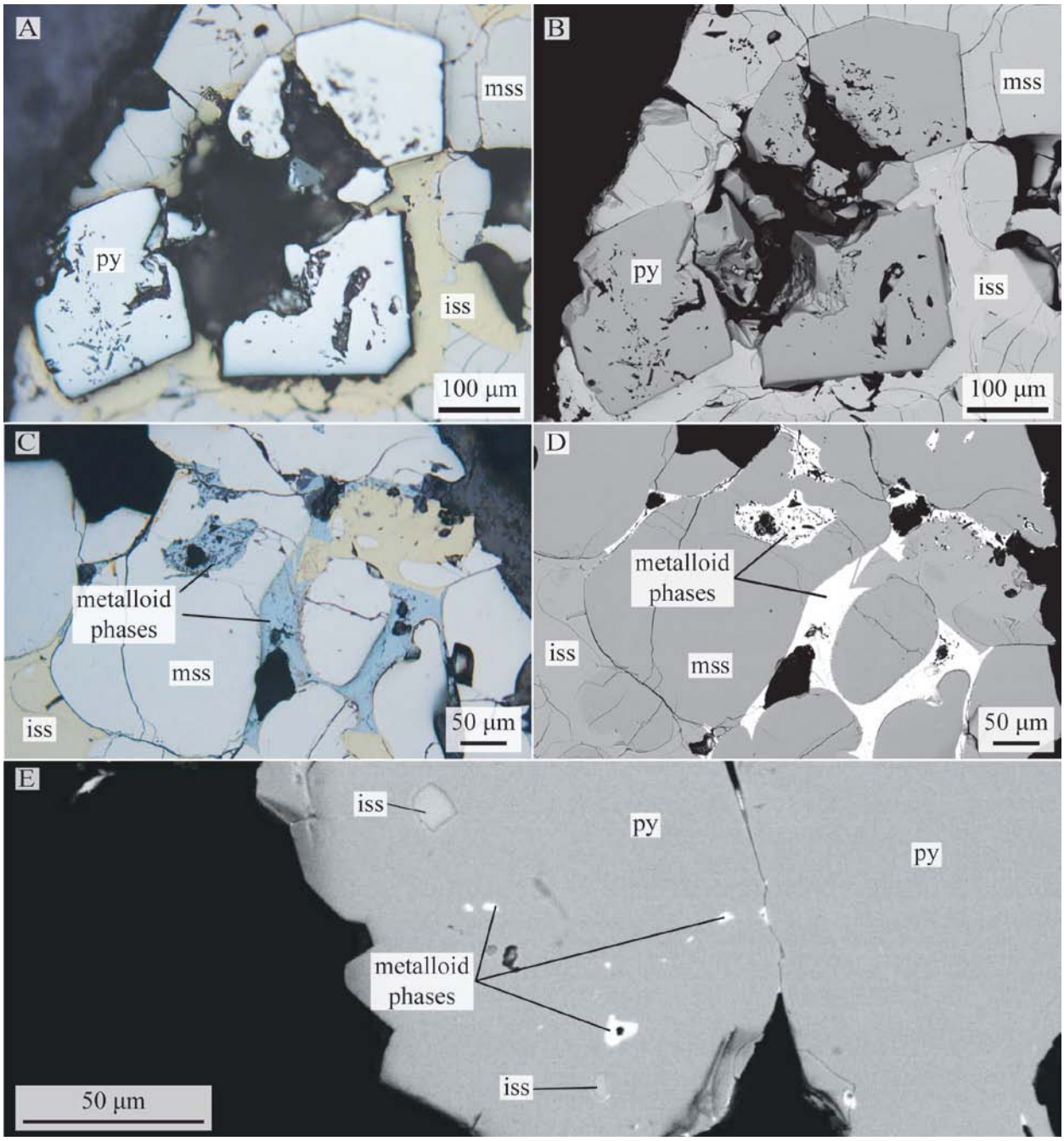

Figure 32. Reflected light and back-scattered electron images of run products. A. Reflected light image and B. BSE image of P-12 (no metalloid added). Big pyrite euhedral crystals (py) totally or partially surrounded by iss (yellow in A, lighter gray in B). Both are included in dominant mss (light pink in A, in the background). C. Reflected light image and D. BSE image of P-13 (3 wt.% metalloid mixture added): dominant rounded mss with interstitial iss (yellow in C). Metalloid phase aggregates (blue in C, white in D) are mainly associated with iss, but can occasionally be embedded in mss. E. Detail of a pyrite grain showing inclusions of iss, along with inclusions of metalloid phases.

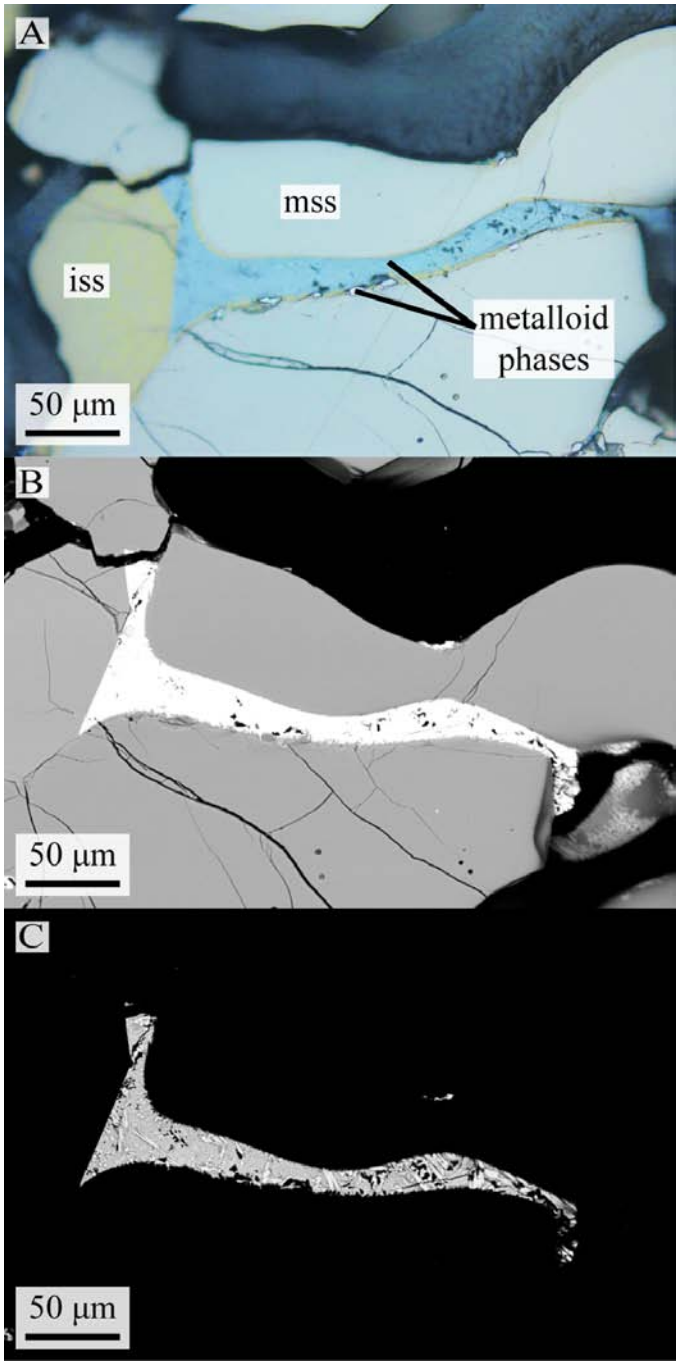

Figure 33. Detailed images of the metalloid-rich domain in experiment P-13. A. Reflected light image showing separate metalloid phases filling the space between two mss grains. A thin veneer of iss separates the mss from the metalloids B. BSE image of A using typical contrast and brightness for sample inspection. C. BSE image with brightness and contrast adjusted to highlight the presence of several distinct phases

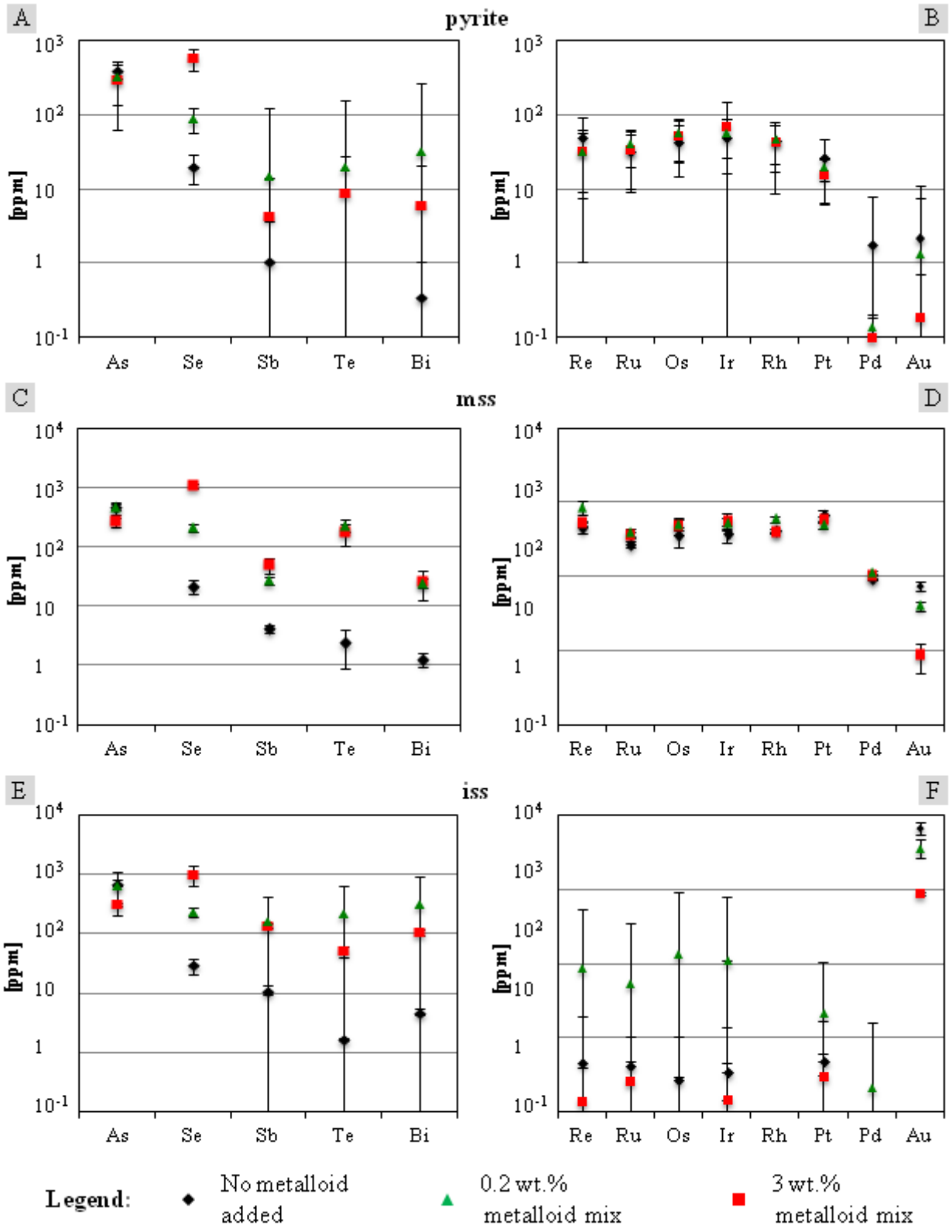

Figure 34. Concentration of metalloids and HSE in each sulfide phase. A, C, and E. Concentration of metalloids in pyrite, mss and iss, respectively. B, D and F. Concentration of HSE in pyrite, mss and iss. The error bars are 2σ.

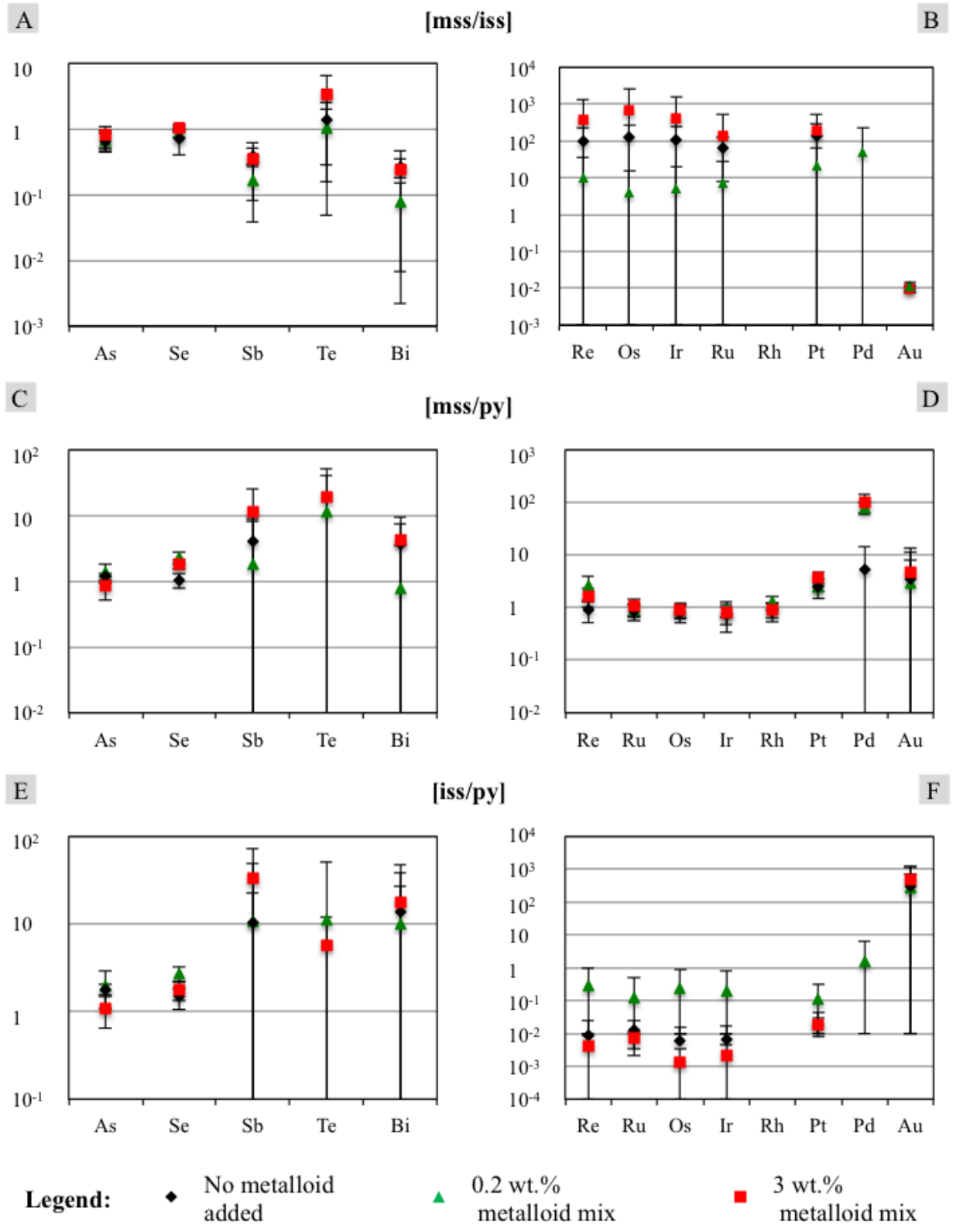

Figure 35 Nernst partitioning coefficients of metalloids and HSE. A and B show the coefficients between mss and iss. B and C show the coefficients between mss and pyrite. E and F show the coefficients between iss and pyrite. The error bars are ± 1σ of the propagated uncertainties.

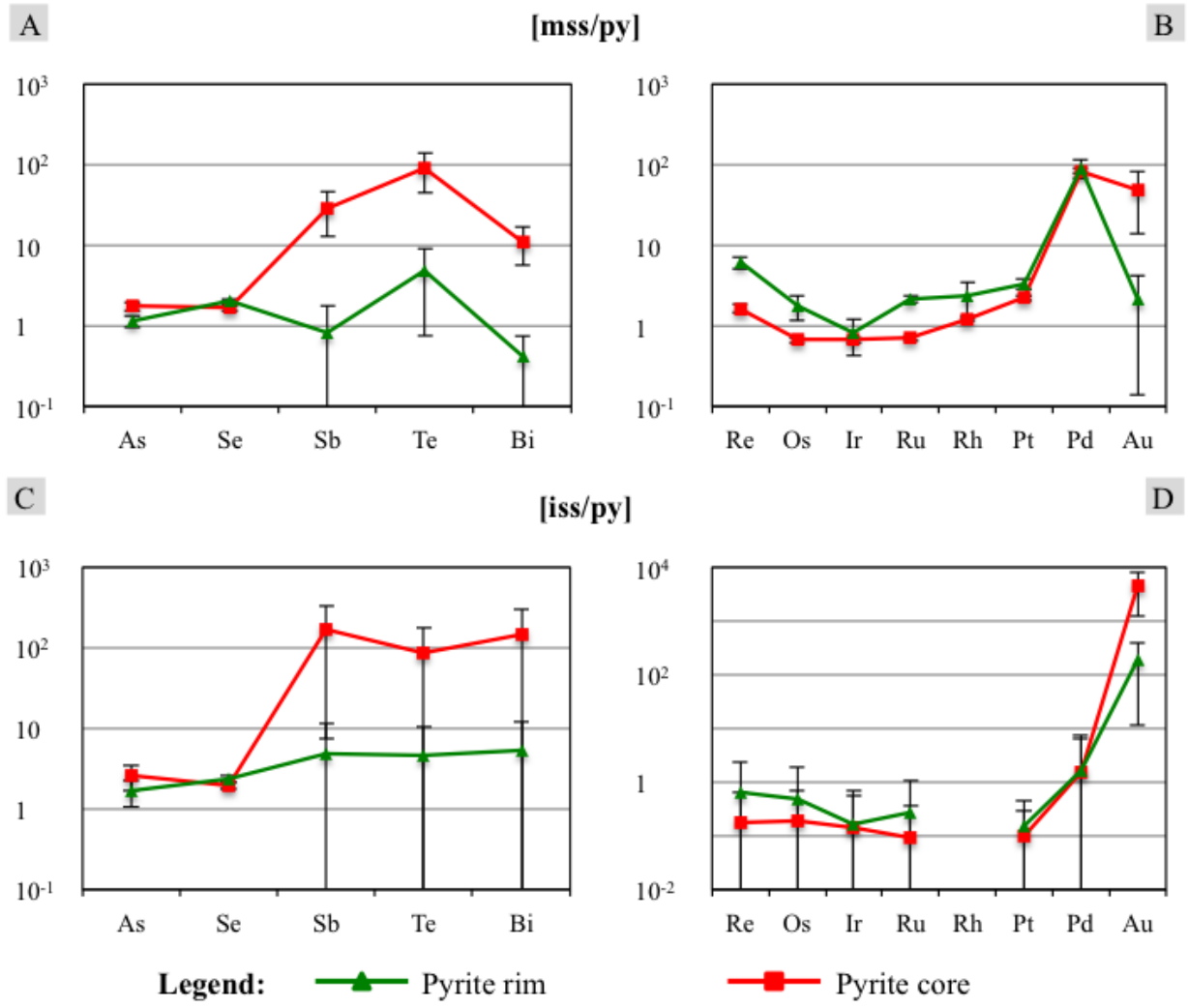

Figure 36. Nernst partitioning coefficients of metalloid and HSE between sulfides and the core or the rim of pyrite from experiment P-07 (0.2 wt.% metalloid added). A and B show the coefficients between mss and pyrite. C and D show the coefficients between iss and pyrite. The error bars are ± 1σ of the propagated uncertainties.

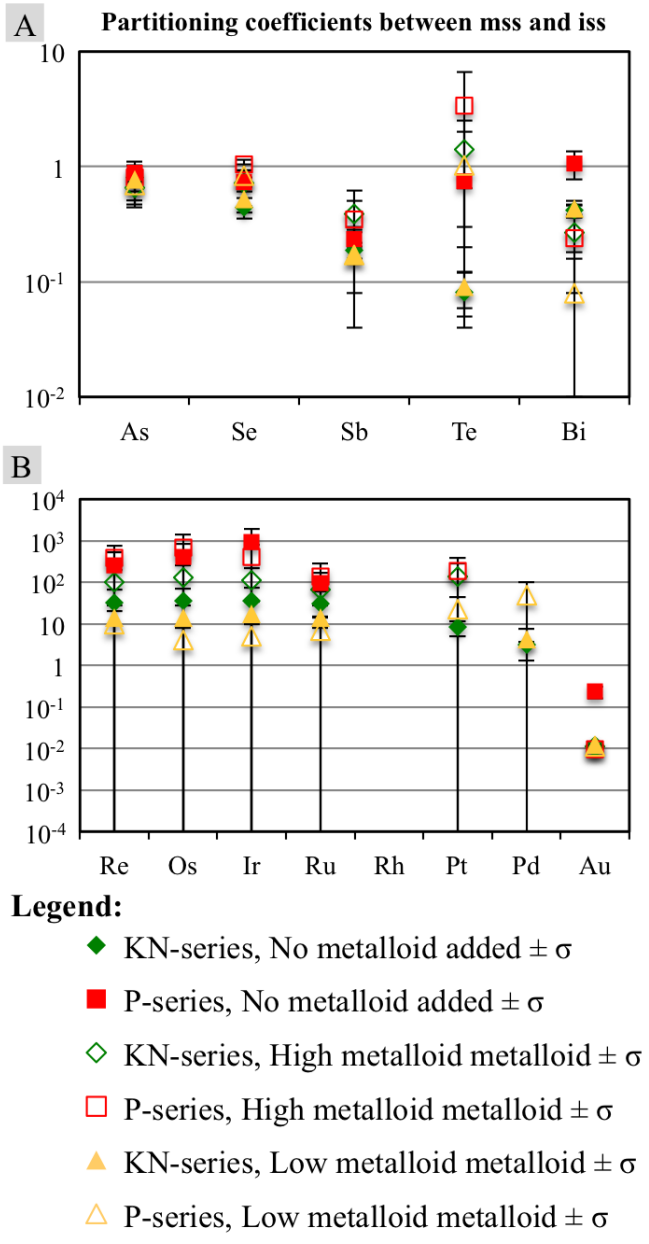

Figure 37. Confrontation of the partitioning coefficients of metalloids and HSE between mss and iss obtained from the KN-series and the P-series experiments.

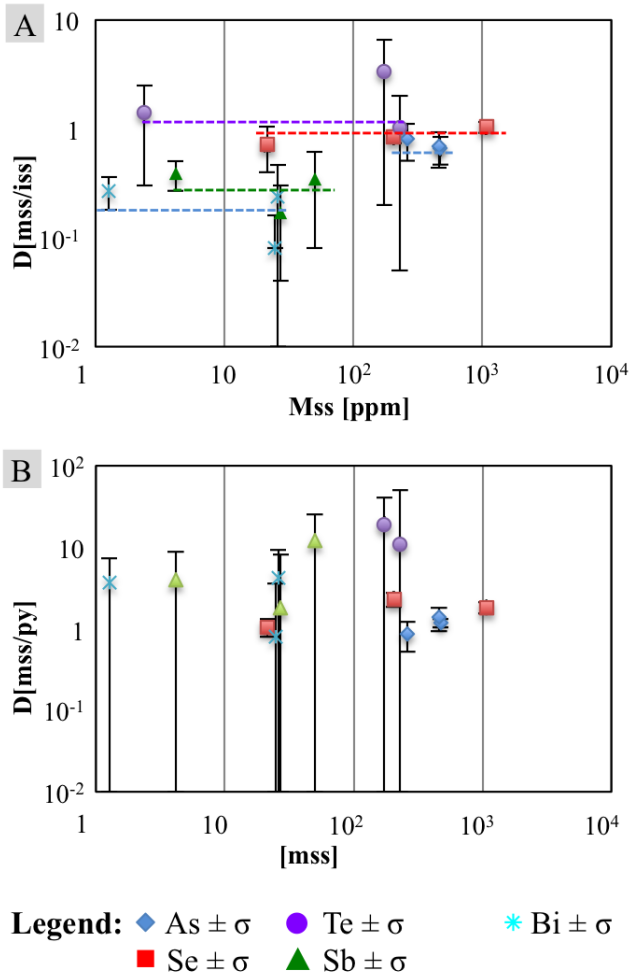

Figure 38. Evaluation of Henryan behavior of metalloids. A. Partitioning coefficients of metalloids between mss and iss against metalloid concentration in mss. B. Partitioning coefficients of metalloids between mss and pyrite against concentration of metalloids in mss. The error bars are 1σ

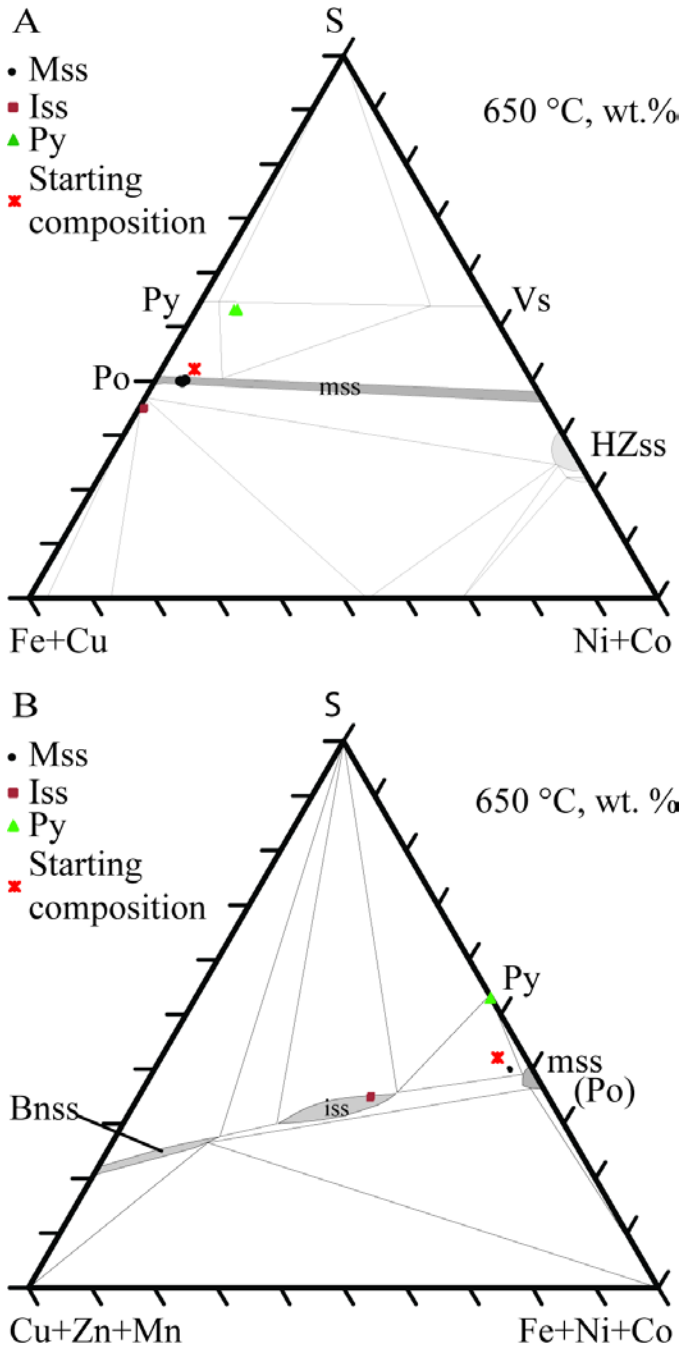

Figure 39. Ternary diagrams showing the bulk composition of the starting materials and of the experimental products. The stability fields shown for reference are from Kullerud et al. (1969) in Fe-Ni-Cu-S systems. A. Modified Fe-Ni-S system to account for Cu and Co. The composition of pyrite highlights the significant amount of Co that can be incorporated in magmatic pyrite. B. Modified Fe-Cu-S system to account for Zn and Mn which partition strongly into iss.

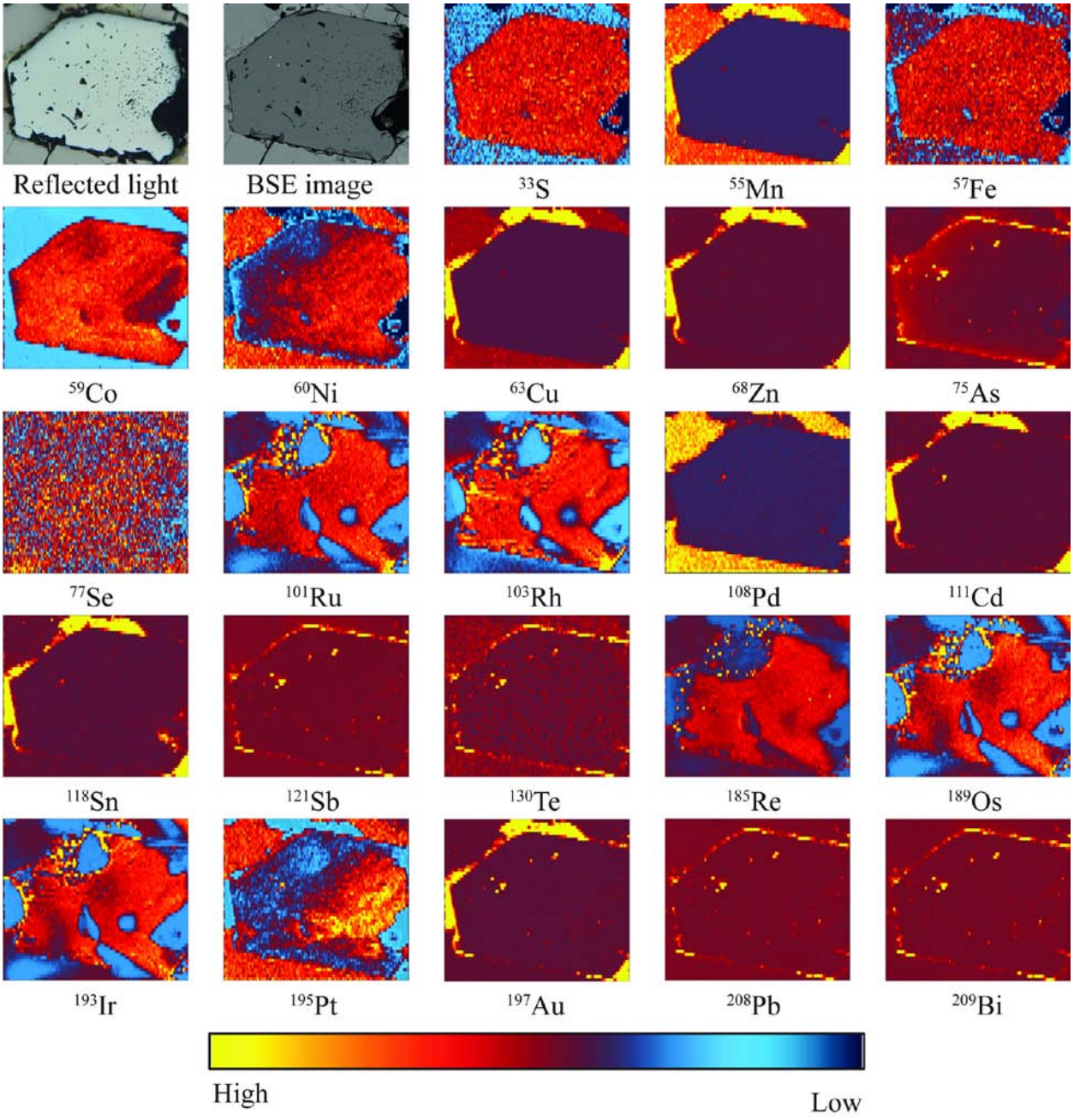

Figure 40. Element distribution maps of the sulfide assemblage from experiment P-12 (no metalloid mixture added) showing an euhedral pyrite grain surrounded by iss and mss. The pyrite grain is approximately 370 µm across. Each map shows relative abundance (in CPS) in a 'warm-cold' scale, where the highest count for each element is assigned the highest value in the scale.

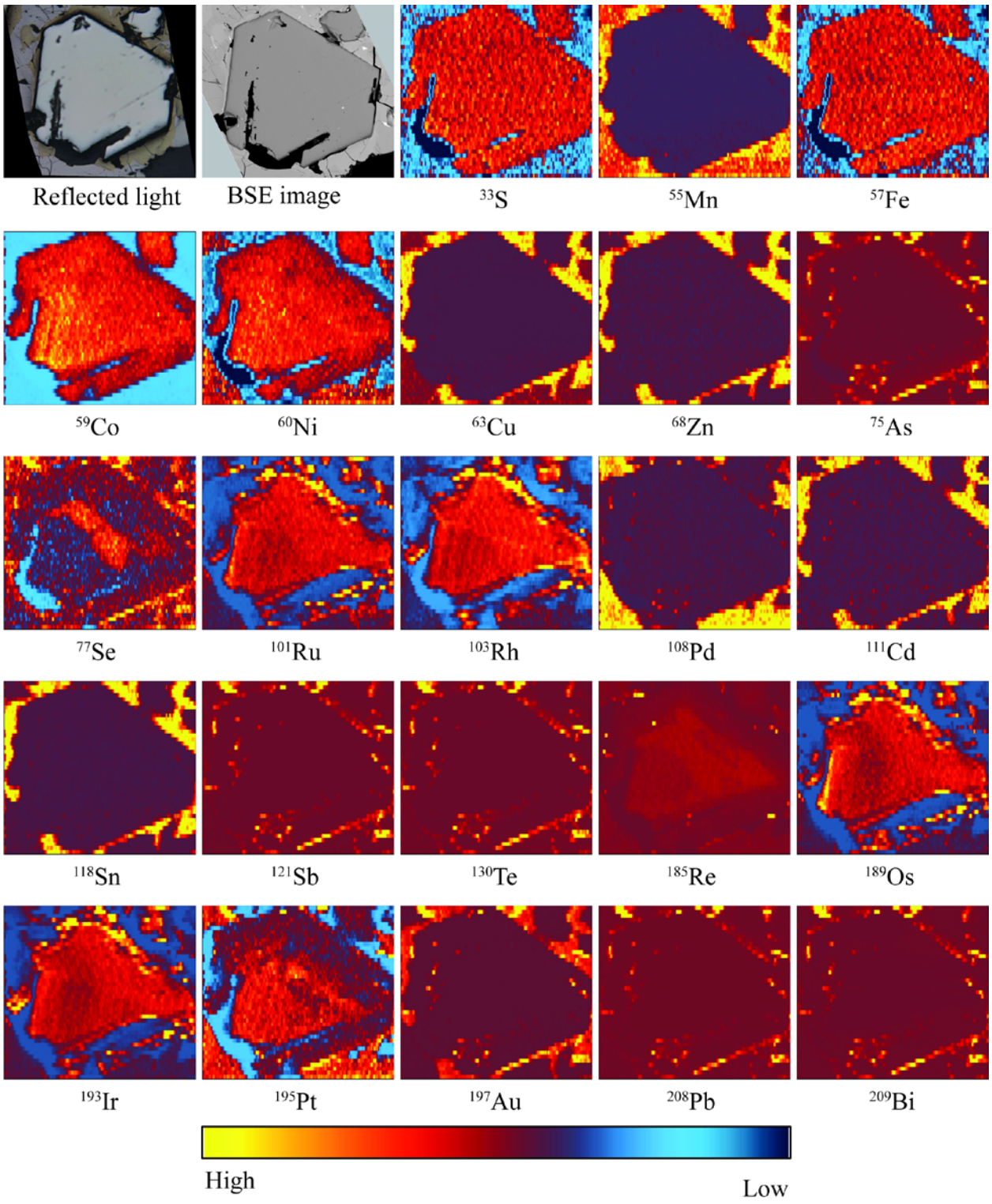

Figure 41. Element distribution maps of a euhedral pyrite grain surrounded by iss and mss from P-07 run (0.2 wt.% metalloid mix), showing relative abundance of elements. The pyrite grain is approximately 380 µm across. The first two images showing the reflected light and BSE images show the correct aspect ratio of the grain.

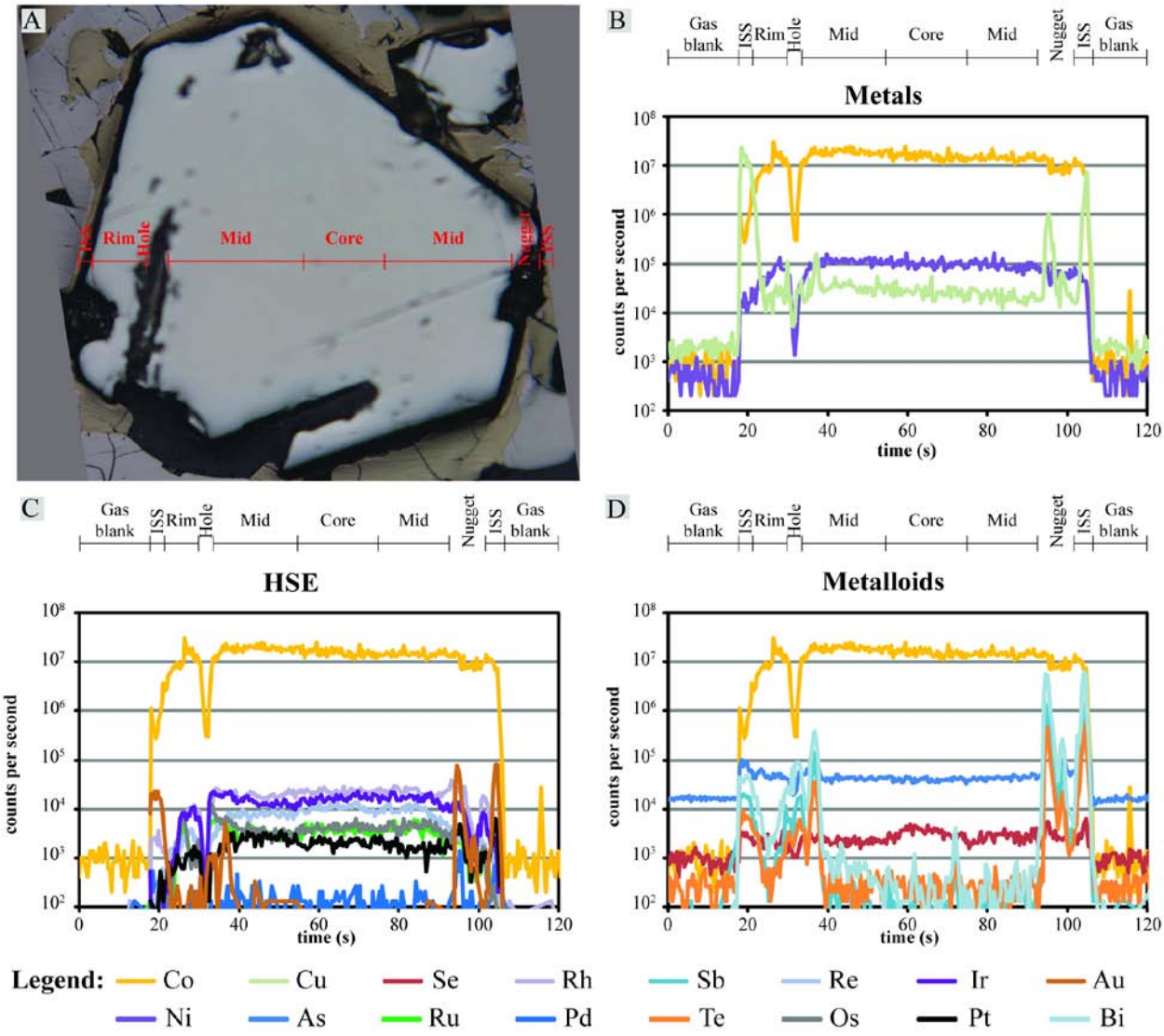

Figure 42. Time-resolved spectra of one laser ablation line across the pyrite grain shown in Figure 41. A. Reflected light image showing the position of the ablation line, which is approximately 0.4 mm long. B. Spatial distribution of Co, Ni and Cu. C. HSE distribution; the Pd signal is almost invisible at the baseline (together with Au). D. Distribution of metalloids.

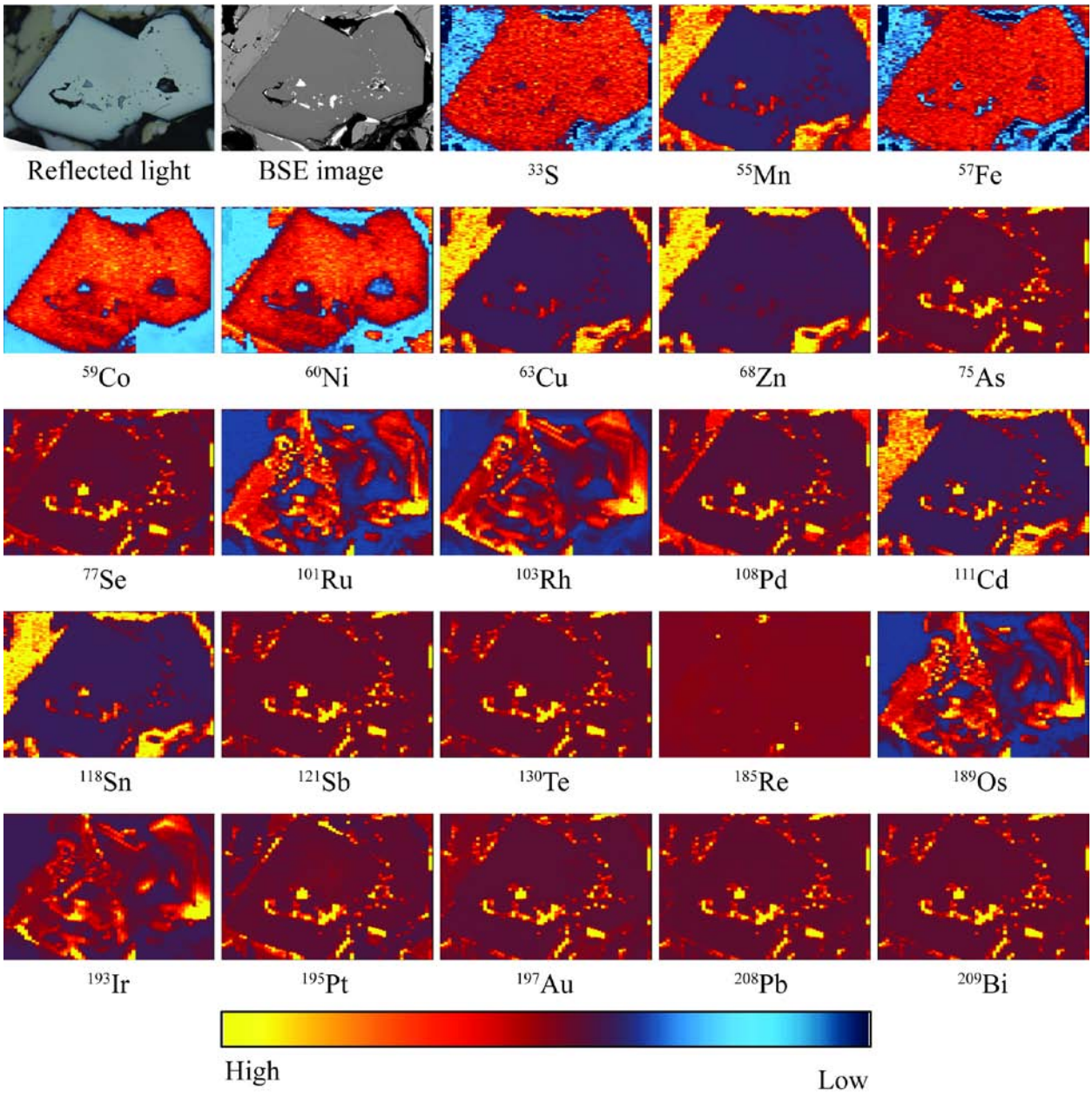

Figure 43. Element distribution maps of two euhedral pyrite grains surrounded by iss and mss from experiment P-13 (3 wt.% metalloid mixture). The width of the areas mapped is about 1 mm.

.

Chapter 5

General conclusions

The results obtained from the three experimental studies documented in this dissertation provide valuable constraints regarding the behavior of metalloids, in particular As, Te, and Bi and their effects on the HSE in sulfide systems. These results are significant as they help understand the origin of PGM during the formation and evolution of a magmatic sulfide ore deposit.

The first experimental study showed that Au, Pd, Pt (and to a lesser extent Rh) can be efficiently fractionated from the other HSE (Ru, Re, Os, Ir) and mobilized along fractures and grain boundaries without the need to involve hydrothermal fluids. The results showed that this phenomenon occurred at temperatures below the solidus of a typical sulfide assemblage (down to ~ 600 °C) and that the metalloids were not the transport agents because control experiments (anhydrous and metalloid-free) produced similar results. The presence of graphite in the experiments and previous studies (e.g., Hanley et al. 2005) suggesting a role of simple hydrocarbons in the mobilization of HSE indicate the carbon-bearing compounds (e.g., a S-C gas phase) may be responsible for the observed behavior (but future studies will need to investigate that possibility further).

The second study showed that mss can dissolve a considerable amount of metalloids, especially if they were added individually to the starting materials. Tellurium is the most soluble (~ 4800 ± 600 ppm at 900 ℃), followed by As (~ 2100 ± 200 ppm at 900 ℃) and Bi (~ 260 ± 15 ppm at 900 ℃). Conversely, when metalloids are present as a group (with also Sb and Se added in the starting materials), the concentration that can be detected in mss is significantly lower, meaning than less amounts of metalloids is needed to saturate metalloid phases than has been previously estimated. However, the metalloid content in mss and iss at saturation is still relatively high (hundreds of ppm) implying that it is unlikely that sulfide melt exsolve metalloid phases under

normal conditions. The results also showed that only Pt, Pd and Au were affected by the metalloids and that the HSE partitioned preferentially into mss and were not affected by the presence of metalloids.

The results of the third study show that Co-rich HSE-bearing pyrite can be obtained during cooling of a sulfide liquid. The association with iss indicates that pyrite does not originate from mss as concluded from Cu-free studies. In general, pyrite inherits the same HSE than mss, particularly Ru, Rh, Re, Os, Ir and Pt. whereas Pd is hosted preferentially into mss and Au is hosted into iss. However, the rate of pyrite growth is faster than the rate of element diffusion through the pyrite crystals. This generates a zonation of some elements, such as the IPGE, Pt and Se. To our knowledge these are the first documented experiments showing that Co-rich, HSE bearing pyrite is can be formed from a sulfide melt and are not necessary of hydrothermal origin.

Appendices

Appendix 1. Approximate composition of PGM and metalloid minerals detected in K-series and KN-series experiments (semi-quantitative EDS analyses; in at.%).

Run and mineral phases	O	S	Fe	Co	Ni	Cu	As	Se	Rh	Pd	Sb	Te	Ir	Pt	Au	Pb	Bi
K-series 1050 °C																	
Mixture-bearing run																	
		28.25	6.95		25.1	1.87	37.83										
		27.13	6.92		24.71	1.78	38.91					0.56					
		31.49	8.54		23.01	2.28	34.68										
		12.23	9.83		1.61	3.47						34.38					38.48
	18.66		14.18			6.39						25.43					35.35
	16.63		9.64			3.96						28.01					41.77
Te-rich run																	
	17.7	5.16	6.59		22.46	0.95						47.13					
		1.83	5.3		29.45							63.42					
Bi-rich run																	
	43		11.46		1.45	5.23											38.85
	44.75		4.49			1.95											48.82
	43.01		2.08														54.91
metalloid liquid	37.6		2.17														60.23
	35.43											1.49					63.09
	32.31																67.69
	37.46																62.54
	7.07	44.65	2.87			15.88										5.28	24.25
	6.28	46.05	2.29			10.68										7.84	26.86
elongated mineral in metalloid liquid	9.58	44.09	3.21			10.67										6.6	25.85
	24.4	38.2	1.71			12.09											23.61
		52.92	3.95			11.78											31.34
	6.99	49.04	5.14			10.57											28.26
		48.28	2.69			15.69										6.7	26.65
Te-liquid		1.99	2.62		29.67	1.35						64.39					
As-rich run																	
Te-liquid		2.27	2.61		29.91	1.32						63.89					
		37.5	10.43		19.3	3.63	29.13										
go-co		41.25	14.44		14.24	5.95	24.12										
		39.86	10.83		17.73	2.68	28.91										
K-series 900 °C																	
Mixture-bearing run																	
Bi-Te liquid		28.5	1.54		1.85	8.93	1.89					24.66					32.64
		28.12	1.24			7.06	1.67					27.02					34.88
		29.76	2.81		26.51	1.47	38.1					1.36					
gf-co		31.89	3.51		27.45	1.04	36.12										
		34.74	5.6		24.42	2.15	33.1										
Te-rich run																	

Appendix 1 (*cont.*) Approximate composition of PGM and metalloid minerals detected in K-series and KN-series experiments (semi-quantitative EDS analyses; in at.%).

Run and mineral phases	O	S	Fe	Co	Ni	Cu	As	Se	Rh	Pd	Sb	Te	Ir	Pt	Au	Pb	Bi
			3.46		5.19	2.28						86.74				2.33	
		2.06	4.38									93.56					
		16.25	12.02		21.36	3.73						45.86				0.77	
		21.68	14.85		15.96	4.53						42.98					
Liq			4.51			3.94	0.94					87.73				2.88	
Sticks		4.15	6.31		27.68							61.85					
Bi-rich run																	
			10.81			3.15						1.93					84.12
			8.03		4.82	2.9											84.25
Liq			15.12		6.44							3.18					75.27
		51.95	14.7		0.9	12.2										5.13	15.13
Dark		53.13	4.81		11.11												30.94
As-rich run																	
		48.28	4.86			33.17	13.69										
		47.78	4.67			22.57	16.37					1.56				7.06	
irarsite-platarsite		30.06	7.83		1.76	1.42	34.57		2.44				13.7	8.22			
	7.5	1.8	3.47				58.3							28.93			
K-series 750 °C Te-rich run																	
Light colored		28.08	23.89		12.71	4.15						28.97				2.2	
Dark colored		45.83	37.51		6.83	2.93						6.89					
Light colored	21.94	1.04	3.59		22.6							50.82					
Dark colored	8.01	35.16	30.6		8.91	3.51						13.82					
						14.54	0.25					82.86				2.35	
	8.25	1.88				18.96						70.91					
						10.77						87.3				1.92	
Bi-rich run																	
	40.54											2.03					57.43
	7.13	49.4				13.55											29.92
	38.49		1.12			2.61											57.78
As-rich run																	
Nuggets		48.70	25.09		3.15	12.19	9.16		1.70								
Nuggets		49.58	24.38		2.62	12.27	9.35		1.80								
	9.89	38.89	15.83		5.26	7.12	19.08		3.92								
K-series 600 °C Mixture-bearing run		31.72	5.27		26.3		36.71										

Appendix 1 (*cont.*) Approximate composition of PGM and metalloid minerals detected in K-series and KN-series experiments (semi-quantitative EDS analyses; in at.%).

Run and mineral phases	O	S	Fe	Co	Ni	Cu	As	Se	Rh	Pd	Sb	Te	Ir	Pt	Au	Pb	Bi
			3.81									50.88					45.3
			5.43									43.89					50.67
			8.59			4.12	0.14					45.03					42.12
		49.25	33.8		4.55	1.85	3.42					3.65					3.47
		28.53	6.75		24.58		39.41			0.73							
		31.23	5.84		26.05		36.89										
		31.68	5.36		26.29		36.67										
		26.18	6.08			9.31	3.78					25.08					29.56
Te-rich run																	
			3.31		30.99							65.70					
			2.08		31.37							66.55					
Melonite					32.86							67.14					
					32.45							67.55					
			0.97		32.62							66.41					
			3.70		31.55							64.75					
Bi-rich run																	
																	100
			6.69			3.46						4.56					85.29
																	100
			2.26														97.74
As-rich run																	100
		33.40	5.90		25.74		34.16			0.80							
		36.14	5.39		25.35		33.11										
		35.70	6.45		25.02		32.83										
		48.70	5.48		0.76	10.90	19.89					3.66				10.60	
		31.72	5.27		26.3		36.71										
			3.81									50.88					45.3
			5.43									43.89					50.67
			8.59			4.12	0.14					45.03					42.12
		49.25	33.8		4.55	1.85	3.42					3.65					3.47
		28.53	6.75		24.58		39.41			0.73							
		31.23	5.84		26.05		36.89										
		31.68	5.36		26.29		36.67										
		26.18	6.08			9.31	3.78					25.08					29.56

Appendix 1 (*cont.*) Approximate composition of PGM and metalloid minerals detected in K-series and KN-series experiments (semi-quantitative EDS analyses; in at.%).

Run and mineral phases		O	S	Fe	Co	Ni	Cu	As	Se	Rh	Pd	Sb	Te	Ir	Pt	Au	Pb	Bi
No metalloid added (KN-01)																		
Pt-bearing gf-co(?)		25.86	21.52	10.64		0.65	5.67	24.42							11.24			
2 wt.% metalloid mixture (KN-02)																		
nugget		22.69		10.91		1.85	4.17		3.8			5.16	25.91					25.51
gf-co	rim			4.91		1.74	5.62		2.23			12.12	38.09					35.29
	core		27.98	3.96	9.29	21.8	0.8	35.22				0.94						
gf-co	rim		28	4.28	8.37	19.46		38.28				0.49						
	core		30.87	4.44	7.11	16.55	1.21	39.08				0.74						
metalloid aggregate		15.28		4.68		9.06	3.19		1.53			17.21	26.55					22.5
				6.34		2.42	3.63		3.02			11.1	38.71					34.78
				8.28			3.7		2.7			9.12	39.07					37.13
gf-co in metalloid	rim			4.2			2.78		2.78			12.8	36.43					41.01
	core		28.5	3.74	8.39	20.62		38.1				0.66						
metalloid aggregate		15.49		6.55			5.39		2.13			11.64	29.62					29.18
sperrylite in gf-co	rim		26.66	3.8	8.15	21.43		38.21				0.54			1.22			
	core		3.86	2.38		3.19		61.52							29.05			
gf-co			28.6	4.89	7.93	19.16		37.95				0.66			0.8			
metalloid aggregate				2.65					2.18			9.63	34.73					50.81
Pd-bearing metalloid aggregate		16.38		1.15		6.66	1.15	3.08			15.05	34.96	13.01					8.56
			27.21	3.19			6.91		3.24			16.83	21.94					20.68
metalloid aggregate			40.05	1.99			13.68	0.11	2.74			23.46	8.95					9.03
metalloid aggregate				2.51			2.82		2.31			9.4	42.71					40.25
			42.93	1.48			15.58		2.31			26.52	2.84				4.14	4.2
sperrylite in gf-co	rim		27.47	3.77	7.77	20.51		38.78				0.64			1.07			
	core		5.04	2.3		1.96		61.01							29.69			
Pt-bearing gf-co			27.87	3.9	7.64	20.47		39.03							1.09			
metalloid aggregate		18.66		4.54		3.8			1.73			13.05	29.35					28.88
metalloid aggregate				3.95		2.98	2.7					17.56	34.72					38.09

Appendix 1 (*cont.*) Approximate composition of PGM and metalloid minerals detected in K-series and KN-series experiments (semi-quantitative EDS analyses; in at.%).

Run and mineral phases		O	S	Fe	Co	Ni	Cu	As	Se	Rh	Pd	Sb	Te	Ir	Pt	Au	Pb	Bi
gf-co in metalloid aggregate	rim			3.63			2.51		2.88			10.95	44.82					35.2
	core		29.08	3.63	3.49	25.68		34.3				3.82						
	core		26.91	2.87	3.47	28.25		33.24				5.27						
Pt-Rh-bearing gf-co in metalloid	rim			6.9		2.77	1.92	0.35	2.44			9.6	43.3					32.73
	core		27.83	4.31	5.7	15.56		40.18		4.84					1.59			
	core		27.86	4.26	7.79	20.43		38.84							0.83			
gf-co			29.38	3.51	8.03	18.72		39.71				0.66						
gf-co in metalloid aggregate	rim	18.03		2.55			1.47		1.9			8.73	29.66					37.66
	core		28.27	3.16	3.24	27.13		31.82				6.38						
gf-co in metalloid aggregate	rim			6.17			4.02		2.57			10.58	40.43					36.23
	core		29.06	3.64	7.55	19.06		40.69										
gf-co in metalloid aggregate	rim			2.06			5		2.66			11	42.91					36.37
	core		28.31	3.28	8.32	20.58		38.90				0.62						
0.05 wt.% metalloid mixture (KN-03)																		
Sb-bearing sperrylite		2.9		4.58			2.49	51.99				7.94			30.09			
		2.53		4.6			2.3	53.92				6.46			30.19			
	host		13.04	16.77		1.83	5.92	37.41				5.01			20.02			
	inclusion		29.84	25.39		3.11	10.59	16			1.62	2.65	2.16		8.63			
	inclusion	21.69	24.82	23.15		4.82	1	13.81				2.3			8.43			
unknown		12.69	28.08	11.58		2.48	4.31					1.79	8.7				21.44	8.93
Au-bearing bismuthide		47.11	16.65	15.61		1.03	4.83									2.73		12.05

Appendix 2. Semi-quantitative analyses of the metalloid phases[1].

O	S	Mn	Fe	Co	Cu	As	Se	Sb	Te	Pb	Bi	total
No metalloid added (P-12)												
	55.14	0.87	2.40		5.97	22.56				13.07		100.01
	51.23	1.00	3.07		6.90	20.00		1.01		16.77		99.98
	51.74	0.75	3.83		6.47	20.41				16.80		100.00
0.2 wt.% metalloid mixture (P-07)												
	51.79	0.67	3.26		7.36	11.77		5.23	2.10	12.68	5.14	100.00
	52.83	1.06	3.99		9.08	9.97		4.69		12.60	5.80	100.02
	49.38	0.66	6.85	0.73	9.44	10.52		4.10	3.88	10.25	4.20	100.01
7.31	46.64		5.50	0.87	9.16	9.38		3.91	3.44	9.63	4.19	100.03
	58.57	0.53	10.03	1.41	8.52	9.61		3.59	3.37		4.38	100.01
9.13	45.92	0.69	4.43		9.37	9.37		3.79	3.17	10.04	4.10	100.01
	49.58	1.17	5.03		11.95	8.85		4.57	3.43	10.74	4.68	100.00
	50.86	0.94	3.00		7.09	13.45		5.08	2.99	11.44	5.14	99.99
12.41	41.9		3.35		5.58	11.64		4.45	4.77	11.18	4.72	100.00
9.63	51.88	0.81	8.51		9.04	10.5		3.38	1.73		4.52	100.00
7.30	43.51	0.72	6.78		8.91	8.74		4.39	3.51	11.45	4.68	99.99
3 wt.% metalloid mixture (P-13)												
	46.13		1.64		6.59	11.85	4.12	9.79	12.78		7.10	100.00
	45.69		1.28		6.84	10.54	3.46	9.74	14.49		7.97	100.01
	46.02		1.82		7.31	10.97	3.64	10.25	11.81		8.17	99.99
13.9	38.82	0.54	1.93		4.88	11.22	3.00	7.42	13.20		5.10	100.01
	46.81		1.36		7.45	10.03	3.20	10.76	11.29		9.08	99.98
7.53	48.49	1.11	2.06		1.78	4.56	3.49	13.96			17.03	100.01
	46.51	0.77	1.31		10.26	8.50	3.25	10.38	10.16		8.87	100.01
	46.75	0.63	1.92		8.60	7.80	3.18	10.47	10.61		10.03	99.99
	46.28	0.75	1.29		10.18	8.49	2.95	10.35	10.41		9.30	100.00
	46.86	0.71	2.49		9.41	8.61	3.28	10.08	9.83		8.73	100.00
	46.74		3.15		9.89	8.36	3.12	9.81	9.93		9.00	100.00
5.31	44.29	0.61	1.77		9.16	8.16	3.24	9.52	9.36		8.58	100.00
	55.39	1.91	3.11		4.24	3.15		12.12			20.07	99.99
	50.94		2.66		8.73	9.50		11.37	6.20		10.61	100.01
	47.72		1.55		7.29	8.99	3.41	10.56	10.50		9.98	100.00
	50.82	0.67	1.51		1.99	6.07	3.20	14.63	4.81		16.31	100.01

[1]Analyses obtained with EDS, expressed in at.% and normalized to 100 %.